

DOCTORAL THESIS

TiO₂ Thin Films by Ultrasonic
Spray Pyrolysis for
Photocatalytic Air-Cleaning
Applications

Ibrahim Dündar

TALLINN UNIVERSITY OF TECHNOLOGY
DOCTORAL THESIS
13/2021

**TiO₂ Thin Films by Ultrasonic Spray
Pyrolysis for Photocatalytic Air-Cleaning
Applications**

IBRAHIM DÜNDAR



TALLINN UNIVERSITY OF TECHNOLOGY

School of Engineering

Department of Materials and Environmental Technology

This dissertation was accepted for the defence of the degree 09/02/2021

Supervisor: Prof. Ilona Oja Acik
Department of Materials and Environmental Technology
Tallinn University of Technology
Tallinn, Estonia

Co-supervisors: Prof. Malle Krunk
Departments of Materials and Environmental Technology
Tallinn University of Technology
Tallinn, Estonia

Dr. Atanas Katerski
Department of Materials and Environmental Technology
Tallinn University of Technology
Tallinn, Estonia

Opponents: Prof. Smagul Karazhanov
Department for Solar Energy
Institute for Energy Technology
Kjeller, Norway

Prof. Sven Lange
Institute of Physics
University of Tartu
Tartu, Estonia

Defence of the thesis: 10/03/2021, at 13:00, seminar room U06-442/Zoom.

Declaration:

Hereby I declare that this doctoral thesis, my original investigation and achievement, submitted for the doctoral degree at Tallinn University of Technology has not been submitted for doctoral or equivalent academic degree.

Ibrahim Dündar

signature



European Union
European Regional
Development Fund



Investing
in your future

Copyright: Ibrahim Dündar, 2021

ISSN 2585-6898 (publication)

ISBN 978-9949-83-674-1 (publication)

ISSN 2585-6901 (PDF)

ISBN 978-9949-83-675-8 (PDF)

Printed by Koopia Niini & Rauam

TALLINNA TEHNIKAÜLIKOOL
DOKTORITÖÖ
13/2021

**TiO₂ õhukesed kiled ultraheli
pihustuspürolüüsi meetodil õhu
fotokatalüütiliseks puhastamiseks**

IBRAHIM DÜNDAR



Contents

List of Publications	7
Author's Contributions to the Publications.....	8
Introduction	9
Abbreviations, Terms, and Symbols.....	11
1 Literature Overview	12
1.1 Semiconductor photocatalysis – from fundamentals to applications	12
1.1.1 General view of semiconductor photocatalysis and materials	12
1.1.2 Basic principles of photocatalysis.....	13
1.1.3 Applications of semiconductor photocatalysis	15
1.2 Indoor air quality	17
1.2.1 Volatile organic compounds (VOCs) in indoor air	17
1.2.2 Currently available indoor air-cleaning technologies and challenges.....	18
1.3 TiO ₂ photocatalyst for air purification	18
1.3.1 TiO ₂ nanopowders for air cleaning.....	18
1.3.2 Nanocrystalline TiO ₂ thin films for air cleaning.....	19
1.4 Summary of literature overview and the aim of the study	22
2 Experimental method	23
2.1 Deposition of TiO ₂ thin films by ultrasonic spray pyrolysis	23
2.2 Characterization of TiO ₂ thin films.....	24
2.3 Evaluation of the photocatalytic activity of TiO ₂ thin films	24
2.3.1 Determination of gas-phase photooxidation of VOCs over TiO ₂ thin films....	24
2.3.2 Determination of stearic acid decomposition on TiO ₂ thin films	25
3 Results and Discussion	26
3.1 Effect of substrate and deposition temperature on photocatalytic activity of TiO ₂ thin films.....	26
3.1.1 Morphology, structural, and optical properties.....	26
3.1.2 Chemical composition and wettability.....	28
3.1.3 Photocatalytic activity	30
3.2 Investigating photocatalytic degradation of different VOCs over TiO ₂ thin films ...	32
3.2.1 Effect of air humidity.....	32
3.2.2 Effect of airflow rate	33
3.2.3 Effect of visible light	34
3.3 Influence of thickness on photocatalytic activity of TiO ₂ thin films	35
3.3.1 Surface morphology, structural and optical properties of TiO ₂ thin films	35
3.3.2. Photocatalytic activity	37
Conclusion.....	39
References	41
Acknowledgment	50
Abstract.....	51
Lühikokkuvõte.....	53

Appendix 1	55
Appendix 2	105
Curriculum vitae.....	108
Elulookirjeldus.....	110

List of Publications

The list of the author's publications, on the basis of which the thesis has been prepared:

- I **I. Dundar**, M. Krichevskaya, A. Katerski, I. Oja Acik. TiO₂ thin films by ultrasonic spray pyrolysis as photocatalytic material for air purification. Royal Society Open Science, 2019, 6, 181578.
- II **I. Dundar**, M. Krichevskaya, A. Katerski, M. Krunks, I. Oja Acik. Photocatalytic degradation of different VOCs in the gas-phase over TiO₂ thin films prepared by ultrasonic spray pyrolysis. Catalysts, 2019, 9, 915.
- III **I. Dundar**, A. Mere, V. Mikli, M. Krunks, I. Oja Acik. Thickness effect on photocatalytic activity of TiO₂ thin films fabricated by ultrasonic spray pyrolysis. Catalysts, 2020, 10, 1058.

Author's Contributions to the Publications

Contributions to the papers in this thesis are:

- I Deposition of TiO₂ thin films by ultrasonic spray pyrolysis, characterization of the films, participation in data collection for photocatalytic activity tests, analysis of results, and a major role in writing.
- II Deposition of TiO₂ thin films by ultrasonic spray pyrolysis, characterization of the films, analysis of results, and a major role in writing.
- III Deposition of TiO₂ thin films by ultrasonic spray pyrolysis, characterization of the films, performing photocatalytic activity tests, analysis of results and major role in writing.

Introduction

Photocatalytic technology has been applied for the removal of gaseous pollutants from air due to its excellent features such as low-cost operation and benign final products (CO_2 and H_2O).

Indoor air quality has become an increasing concern as people spend much of their time inside houses and offices. Indoor air can be contaminated by various factors, including significant emissions of volatile organic compounds (VOCs). The World Health Organisation (WHO) has used the term “Sick Building Syndrome” to describe the health concerns related to poor indoor air quality that building residents can experience.

Photocatalysis is a promising technique for indoor air purification because it can decompose VOCs and destroy bacteria, viruses, and fungi in air, unlike common indoor cleaning methods, such as high-efficiency particulate air (HEPA) filters. Photocatalytic air devices have been developed based on UV-C activated photocatalytic modules, which are coated with thick layers of commercial TiO_2 nanoparticles. However, the use of these air-cleaning devices is limited by several factors, such as their requirements for periodic maintenance and replacement of the photocatalyst module in the purifier, because less mechanically stable TiO_2 nanoparticles can become detached from the module and enter the indoor air. To overcome these limitations, the integration of large-area photocatalytic thin film coatings has been proposed as a future indoor air-cleaning solution. Photocatalytic coatings can be applied to building elements such as windowpanes. Therefore, transparent TiO_2 thin films on well-illuminated surfaces can benefit from their large area to remove VOCs while offering good mechanical stability and long-term photostability. The deposition method, as well as the preparation conditions, and annealing parameters determine the properties of TiO_2 thin films. The most common deposition methods for fabricating TiO_2 thin films for air purification are sputtering and sol-gel methods, which have the limitations of high fabrication costs and high precursor waste, respectively. However, ultrasonic spray pyrolysis, as a resource-saving technology, can reduce the fabrication cost. In addition, it is a rapid and robust method. Based on the literature survey, to the best of our knowledge, no publications on TiO_2 thin films deposited by ultrasonic spray pyrolysis for the degradation of air contaminants have been found.

This research aims to deposit TiO_2 thin films by ultrasonic spray pyrolysis and optimize the preparation parameters to obtain TiO_2 thin films with air-cleaning and self-cleaning features to be used, for example, as windowpane coatings. Ultrasonic spray pyrolysis offers the possibility of fabricating low-cost thin films with high scalability for industrial production. Therefore, this work extends the potential application of ultrasonic spray pyrolysis for photocatalytic air-cleaning applications. Moreover, in this study the gas-phase photocatalytic activity of TiO_2 films fabricated by ultrasonic spray pyrolysis was evaluated using a multi-section plug-flow reactor. The main advantage of the multi-section plug-flow reactor compared to other gas-phase photocatalytic activity evaluation methods is that the tested sample area can be gradually increased; in addition, the residence time can be extended by adding reactor sections.

To achieve the target of this thesis, some specific conditions and issues are addressed in this work; these serve as objectives of the study. First, the growth temperature of the TiO_2 thin film deposited by ultrasonic spray pyrolysis was optimized. Second, the performance of sprayed TiO_2 thin films towards the degradation of various VOCs was demonstrated under different operating conditions of a multi-section plug-flow reactor. Finally, the optimal thickness for TiO_2 thin films fabricated by ultrasonic spray pyrolysis

for photocatalytic applications was determined. From the perspective of applications, the influences of morphological, structural, and optical properties; surface chemical composition; wettability; and photocatalytic activity on the degradation of different gaseous VOCs and stearic acid on TiO₂ films were investigated.

This thesis is based on three published articles and sub-divided into three chapters. The first chapter provides a literature overview of the fundamentals of photocatalysis and indoor air purification solutions, including photocatalysis. In addition, the main fabrication methods and important parameters of photocatalytic TiO₂ thin films for air purification are addressed. The literature survey is concluded with the aim and objectives of this research work. In the second chapter, the experimental methods and processes are described. In the third chapter, the results and discussions of the thesis are divided into three sections. The first and second sections focus on the results obtained from papers I and II. These sections summarize the results of the deposition of TiO₂ films onto window and borosilicate glass substrates at different temperatures and the photocatalytic activity of these thin films towards the degradation of different VOCs degradation under different measurement conditions. The third section is based on the paper III, focusing on the effect of TiO₂ thin film thickness on photocatalytic activity.

This work is directly related to the ongoing research project in the Laboratory of Thin Film Chemical Technologies, which focus on the development TiO₂ thin films by wet-chemical process for environmental applications. This study was financially supported by the Estonian Ministry of Education and Research project IUT194, Estonian research council grant PRG627, Tallinn University of Technology based financing project B24, and the European Union through the European Regional Development Fund project TK141 "Advanced materials and high-technology devices for energy recuperation systems". This work has also been partially supported by ASTRA 'TUT Institutional Development Programme for 2016–2022' Graduate School of Functional Materials and Technologies.

Abbreviations, Terms, and Symbols

VOC	Volatile organic compound
WHO	World Health Organization
HEPA	High-efficiency particulate air (filter)
HVAC	Heating, ventilating, and air-conditioning
UV	Ultraviolet
VIS	Visible
MTBE	Methyl-tert-butylether
MEK	Methyl-ethyl-ketone
TBF	Tert-butyl formate
TTIP	Titanium tetraisopropoxide
Acach	Acetylacetone
BG	Borosilicate glass
WG	Window glass
SLG	Soda lime glass
ALD	Atomic layer deposition
RMS	Root mean square roughness
FTIR	Fourier-transform infrared spectroscopy
SEM	Scanning electron microscopy
AFM	Atomic force microscopy
XRD	X-ray diffraction
XPS	X-ray photoelectron spectroscopy
UV-VIS	Ultraviolet-Visible light spectroscopy
k	Reaction rate constant
BE	Binding energy
WCA	Water contact angle
RH	Relative humidity
M	Molarity
E _g	Bandgap

1 Literature Overview

Photocatalysis has been known since the early 20th century via the flaking of paints and the degradation of dyes over illuminated TiO₂ [1–2]. Significant research on photocatalysis was initiated in the 1970s, after Fujishima and Honda demonstrated the splitting of water into H₂ and O₂ under near-UV light using a TiO₂ photoanode and a Pt cathode [3–5]. After the discovery of this photocatalytic ability, interest in the scientific community has grown rapidly, particularly in the photocatalytic decomposition of environmental pollutants [6]. Thereafter, the scientific literature has increased rapidly since the '70s. Clear evidence of this attention is present in the large number of articles published in this area annually; more than 6000 such reports were published in 2019, according to the Institute for Scientific Information (ISI).

1.1 Semiconductor photocatalysis – from fundamentals to applications

1.1.1 General view of semiconductor photocatalysis and materials

Semiconductor photocatalysis is the initiation of photochemical reactions in the presence of a semiconductor catalyst activated by light radiation [7]. In heterogeneous photocatalysis, the catalyst can be in the form of nanoparticles (suspended or immobilized) or a polycrystalline thin film deposited on a substrate.

Nanoparticles are the most widely studied photocatalytic materials with broad use in industry, as they possess high specific surface areas, pore volumes, and pore sizes; they are expected to exhibit high photocatalytic activity due to the increasing mass transfer facilitating organic pollutant adsorption [8–9]. The idea of an immobilized photocatalyst onto supporting materials such as glass, ceramic tiles, and polymeric materials became accepted in the early '90s [10]. An immobilized form of photocatalyst has been prepared either with nanopowders or as thin films with thicknesses of a few nanometers up to a few micrometers.

Semiconductor photocatalysis has been used for air and water treatment [6]. Traditional remediation techniques for air are [11–12]:

- thermal and catalytic thermal oxidation,
- condensation of vapours,
- adsorption,
- absorption,
- bio-filtration.

The main advantages of photocatalysis compared to the technologies mentioned above are [11–12]:

- efficient for low concentration of pollutants,
- avoiding utilization of secondary wastes,
- relative low cost,
- reusability and environmental benignity.

Several metal oxides as semiconductor photocatalysts have been reported in the literature. The most studied photocatalysts are metal-oxide materials, for example, TiO₂, ZnO, WO₃, Fe₂O₃, SnO₂, and CeO₂ [13]. ZnO (bandgap energy $E_g = 3.4$ eV) has been widely examined as a photocatalyst for water treatment because of its suitable properties, including low cost, high redox potential, and environmentally friendly features [14]. However, it has been reported that ZnO has poor photostability and chemical instability [7, 14]. WO₃, which has the narrow optical bandgap of 2.7 eV, has received renewed

interest owing to its strong optical light absorption in the visible-light region. However, WO_3 remains far from becoming a practical semiconductor for photocatalysis applications owing to the high recombination rate of electron–hole pairs [15]. SnO_2 ($E_g = 3.6$ eV) has been mostly investigated for water treatment and shows relatively lower activity compared to TiO_2 and ZnO for decomposing dye molecules [16]. SnO_2 has been more widely employed as an additive to modify TiO_2 for improving its photocatalytic activity [16]. Fe_2O_3 is advantageous relative to TiO_2 and ZnO in using solar energy for photocatalytic applications owing to its lower bandgap of 2.2 eV. However, the photocatalytic performance of Fe_2O_3 is limited by certain factors such as the high recombination rate of charge carriers and the low diffusion lengths of holes (2–4 nm) [17]. Thus, Fe_2O_3 is used to form heterojunction nanocomposites with other semiconductors such as TiO_2 to overcome these factors [18]. CeO_2 ($E_g = 3.19$ eV) has attracted considerable interest as a photocatalyst for water and air treatment. It has strong stability under illumination and strong absorption of UV light [13]. However, this material is generally found to be less active than TiO_2 under UV irradiation [19–20].

TiO_2 ($E_g = 3.2$ eV) is one of the most studied photocatalytic materials and is considered one of the most promising photocatalytic materials owing to its excellent properties, such as photostability, nontoxicity, low cost, and chemical inertness [6, 21].

The ideal photocatalyst for environmental applications should fulfill the following conditions: suitability for visible or near-UV light energy harnessing, mechanical stability, biological and chemical inertness, low cost, easy production, and safety for both the environment and humans [22].

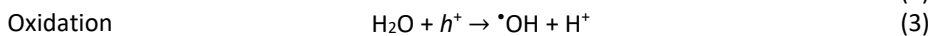
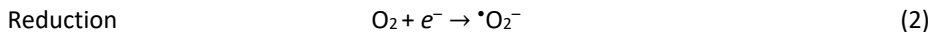
1.1.2 Basic principles of photocatalysis

Photocatalytic phenomena are observed once a photocatalytic material is exposed to light energy ($h\nu$). This involves the generation of valence-band holes (h^+_{VB}) and conduction-band electrons (e^-_{CB}) that are created when the photocatalyst absorbs an incoming photon has an energy greater than the bandgap energy E_g of the semiconductor (Eq. 1). The photon excites the electrons in the valence band, allowing them to jump into the conduction band, leaving behind an unfilled space in the valence band referred to as a hole. The generated electron–hole pair is responsible for the reduction or oxidation of environmental contaminants by the formation of radicals (Figure 1.1). Using TiO_2 ($E_g = 3.2$ eV) as an example, the photocatalytic mechanism is explained in detail [23]:



Figure 1.1 shows the charge carriers diffused towards the TiO_2 surface, where the initial photocatalytic reactions occur. After photogenerated electrons and holes reach the surface, they cause redox reactions with oxygen (O_2) or water (H_2O). The holes have a positive potential to generate hydroxyl radicals (OH^\bullet) from H_2O molecules adsorbed on the surface. The excited electrons react with O_2 to form the superoxide anion ($^{\bullet}\text{O}_2^-$) (Figure 1.1) [23].

The initial redox reactions for the formation of $^{\bullet}\text{O}_2^-$ and OH^\bullet are shown in Eqs. 2 and 3.



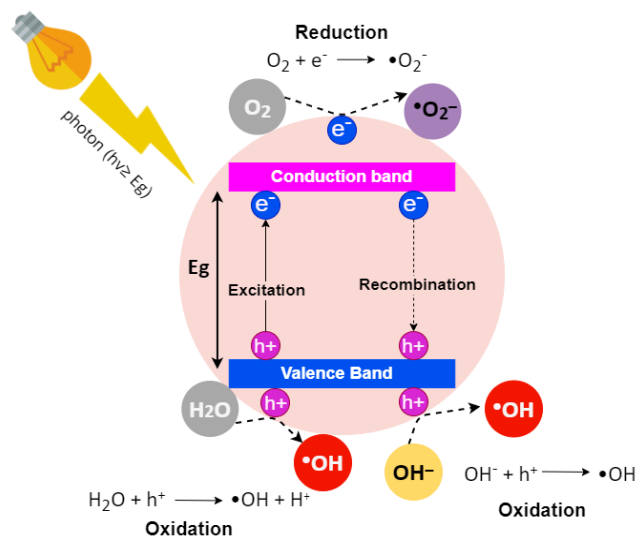
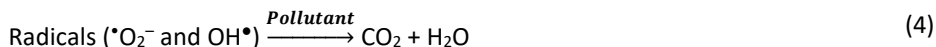


Figure 1.1. Schematic diagram of photocatalysis mechanism on an excited TiO_2 .

Thereafter, these radicals (typically $\bullet\text{O}_2^-$ and $\text{OH}\bullet$) can react with organic and inorganic pollutants converting them into CO_2 and H_2O (Eq. 4) [24].



However, the reactive oxygen species (ROS) are also key species in photocatalytic reactions. When the radicals ($\bullet\text{O}_2^-$ and $\text{OH}\bullet$) detach from the surface, they can form ROS, which are reactive due to their unsaturated bonds. At this point, the ROS can remain unchanged or they can react to form other ROS [24].

The following reaction pathways (Eqs. 6-8) show the formation of ROS, which are typically $\text{HO}_2\bullet$ and H_2O_2 :



Finally, the ROS can attack the pollutants and convert them into CO_2 and H_2O (Eq. 9) [24–25].



All the possible photocatalytic reactions in air are summarized in Table 1.1.

However, the high amount of the photogenerated electron-hole pairs spontaneously recombine either in the bulk or on the surface of TiO_2 , while less than 10% of the surviving survived charge carriers are utilized in redox reactions [25].

Table 1.1 Summary of the reactions during photocatalytic decomposition of organic compounds in air [24].

Incidents	Chemical reactions	Descriptions
Photoexcitation	$\text{TiO}_2 + h\nu \rightarrow h^+ + e^-$	Formation of charge carriers by radiation
Oxidation	$\text{H}_2\text{O} + h^+ \rightarrow \cdot\text{OH} + \text{H}^+$ $\text{OH}^- + h^+ \rightarrow \cdot\text{OH}$	H_2O or OH^- reacts with a photogenerated hole (h^+) and transforms to an oxidizing hydroxyl radical ($\cdot\text{OH}$)
Reduction	$\text{O}_2 + e^- \rightarrow \cdot\text{O}_2^-$	O_2 traps a photogenerated electron (e^-) and forms a superoxide radical ($\cdot\text{O}_2^-$)
ROS formation from radicals	$\cdot\text{O}_2^- + \text{H}^+ \rightarrow \text{HO}_2\cdot$ $\text{HO}_2\cdot + \text{H}_2\text{O} + e^- \rightarrow \text{H}_2\text{O}_2 + \text{OH}^-$ $\cdot\text{OH} + \cdot\text{OH} \rightarrow \text{H}_2\text{O}_2$ $\text{H}_2\text{O}_2 + e^- \rightarrow \cdot\text{OH} + \text{OH}^-$	Superoxide radical ($\cdot\text{O}_2^-$) creates a hydroperoxyl radical ROS ($\text{HO}_2\cdot$) Other reactions to create a hydrogen peroxide ROS (H_2O_2)
Decomposition of pollutants by radicals and ROS	$\cdot\text{OH}$, $\cdot\text{O}_2^-$, $\text{HO}_2\cdot$, H_2O_2 + Pollutant	Decomposition of pollutants after photocatalytic reactions $\text{Pollutant} \rightarrow \text{H}_2\text{O} + \text{CO}_2$

Considering the overall photocatalytic process, the photocatalytic efficiency mainly depends on the charge-carrier transfer rate and the recombination rate. Therefore, the main limitations to the use of photocatalysis are low charge-carrier transfer rate and high electron–hole recombination rate [26]. In addition, the intermediate products of gaseous pollutants may form on the surface of the photocatalyst, which can retard continuous reactions by blocking the active sites [27].

1.1.3 Applications of semiconductor photocatalysis

The main application areas of semiconductor photocatalysis based on TiO_2 are summarised in Figure 1.2.

One of the main applications of semiconductor photocatalysis is water and wastewater purification. Photocatalytic water treatment is used for cleaning industrial wastewater and natural water sources [21]. Small-scale photocatalytic systems with artificial UV light have been commercially available for several years [28–29].

Photocatalysis has been reported to destroy a wide range of organisms, including bacteria, fungi, algae, viruses, and microbial toxins [30–34].

The photoinduced superhydrophilic behavior of TiO_2 surfaces has been exploited commercially to develop antifogging and easy-to-clean surfaces for various applications. Self-cleaning windows and roof tiles are used worldwide. Pilkington Activ™ glass is the first example of a self-cleaning glass currently used in different commercial and private buildings. In recent years, several other self-cleaning glasses such as RadianceTi™, Sunclean™, and Bioclean™ have also been used in commercial applications [35].

Moreover, self-cleaning coatings with antifogging properties have been used in the automotive industry for self-cleaning windows, automotive mirrors, and headlights [36–38].

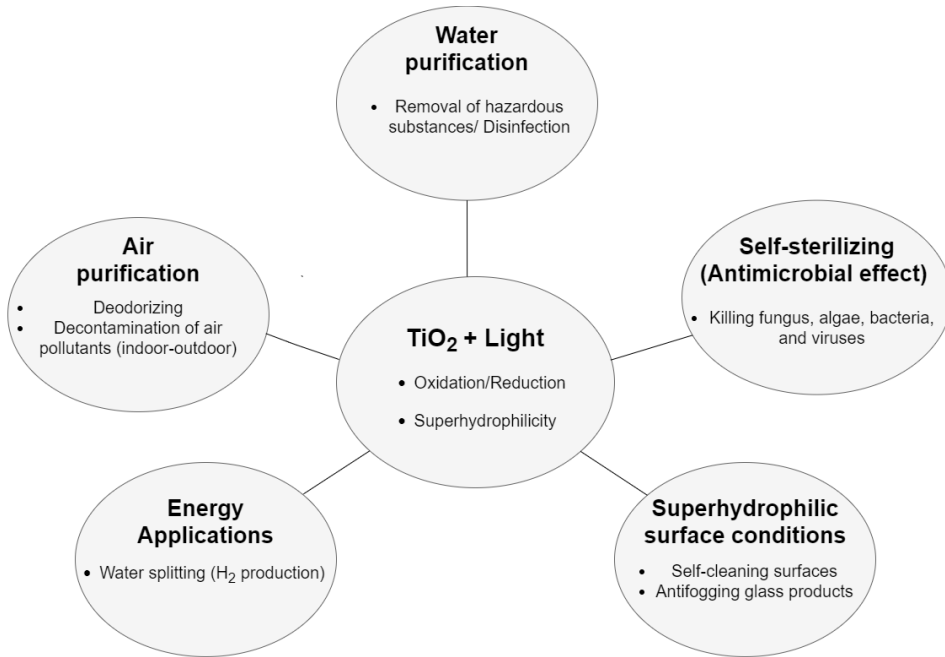


Figure 1.2. Overview of photocatalytic applications.

The photocatalytic decomposition of organic and inorganic contaminants in air has received much attention. Photocatalytic air purification, which is potentially suitable for outdoor and indoor environments, is the fastest-growing application field [39]. For outdoor air cleaning, photocatalysts can be used in cement bricks and concrete pavement surfaces; these are already available commercially [40–41]. For indoor air purification, some products as photocatalytic modules comprising TiO₂ nanoparticles on supporting plates [42] are available in the market [40]. Indoor air cleaning solutions are discussed in Section 1.2.

As a distinct application, hydrogen evolution by water splitting can be included as an energy application area for semiconductor photocatalysis [43].

Considering both the technological and economic importance of photocatalysis, the field has grown considerably over the past two decades. In 2020, the global market for photocatalytic products (e.g., self-cleaning industrial glass, concrete products, and air-water purifiers) was \$828.2 million. The expected global volume will reach \$1.54 billion by the end of 2025 [44]. Major factors driving the growth of the market are the rapidly growing demand for TiO₂ and increasing applications in water and air purification as well as self-cleaning technologies. TiO₂ has broad applicability, especially in self-cleaning technologies; therefore, it is widely used in building materials, which comprise more than 80% of the consumption worldwide. Further developments of TiO₂ are estimated to fuel the growth of the market. As the novel coronavirus SARS-CoV-2 (COVID-19) pandemic continues, the demand for photocatalytic antimicrobial coatings is expected to grow in the future [45].

1.2 Indoor air quality

Indoor air is defined as the air in non-industrial areas such as homes, offices, schools, and hospitals [46]. Air quality in transportation vehicles (car, bus, train, and aircraft) has also raised concern; these vehicles are also typical of indoor environments [47]. The population of the industrialized world spends more than 90% of their life indoors, with approximately 20% of the time spent in offices by working individuals [48–49].

The sources affecting indoor air quality are particulate matters, including particles associated with tiny organisms (dust, smoke, bacteria and viruses) and gaseous pollutants such as sulfur dioxide (SO₂), nitrogen oxides (NO_x), and volatile organic compounds (VOCs) [50].

The World Health Organisation (WHO) has used the term “Sick Building Syndrome” (SBS) to describe the health concerns relating to poor indoor air quality that building residents can experience [51]. SBS comprises various nonspecific symptoms that occur in humans, including headache, dizziness, and fatigue [51].

1.2.1 Volatile organic compounds (VOCs) in indoor air

VOCs are the most common air pollutants present in both indoor and outdoor air. These organic compounds are man-made and/or naturally originating hydrocarbons with high reactivity [52]. The United States Environmental Protection Agency (U.S. EPA) reported that VOC levels in indoor air are 2–5 times higher than in outdoor air [53]. VOCs, which can cause several diseases including cancer, have also been reported as a major factor in SBS [54].

The concentration of VOCs in indoor environments is significantly dependent on the sources and emissions. Common VOCs with approximate concentration ranges in indoor air and their origin sources are listed below [51, 55–57].

- Acetaldehyde (5–50 $\mu\text{g}\cdot\text{m}^{-3}$) – glues, deodorants, fuels, tobacco smoke, gas cookers, and building materials, such as particleboard and foam.
- Formaldehyde (8–66 $\mu\text{g}\cdot\text{m}^{-3}$) – wood products, gas cookers, perfumes, and building materials, including particleboard and foam.
- Toluene (6–320 $\mu\text{g}\cdot\text{m}^{-3}$) – gasoline, household products, including paints and paint thinners, glues, synthetic fragrances, and nail polish.
- Acetone (32–130 $\mu\text{g}\cdot\text{m}^{-3}$) – gasoline, tobacco smoke, household products, such as paints, paint thinners, insecticide spray, glues, and nail polish.
- Methyl *tert*-butyl ether (MTBE) (5.5–45 $\mu\text{g}\cdot\text{m}^{-3}$) – gasoline, combustion products.
- Heptane (4–87 $\mu\text{g}\cdot\text{m}^{-3}$) – gasoline, paints, glues, building materials, such as cement.

According to the international standard, the main VOCs such as acetone, acetaldehyde, toluene, and formaldehyde are the model air pollutants used for the international standard testing of potential air cleaners [58].

In summary, among VOCs, acetone and acetaldehyde are chemicals used extensively in a variety of industrial and domestic applications; they are found in appreciable concentrations in indoor air [58–59]. MTBE and heptane are released to the atmosphere from gasoline and motor vehicle exhaust and therefore considered as outdoor-generated VOCs that also affect indoor air quality, especially in buildings close to parking lots or streets [56, 60–62]. Therefore, it is essential to obtain healthy living environments in modern buildings using air-cleaning solutions.

1.2.2 Currently available indoor air-cleaning technologies and challenges

Air-cleaning systems are useful for minimizing the accumulation of contaminants in indoor air. There are two basic categories of indoor air cleaning, which are HVAC (heating, ventilating, and air-conditioning) systems and portable air cleaners [63].

Filtration is the most widely used method for indoor air cleaning. High-efficiency particulate air (HEPA) filters are the most common filtration technology. HEPA filters are used in ventilation systems and portable air cleaning devices. These filters can remove large particulate matter ($\geq 1 \mu\text{m}$), such as pet dander, pollen, and dust mites. However, they are ineffective in removing viruses, bacteria, and gaseous pollutants such as NO_x and VOCs. In addition, they must be replaced regularly because of inactivation, in which case they can become sources of pollution [63–65].

Photocatalysis is a promising technology for indoor air purification because it decomposes VOCs and destroys bacteria and fungi in the air [66–67].

Photocatalytic air-cleaning devices are on the market [68]. The majority of commercial photocatalytic air purifiers have UV-C lamps and photocatalytic modules, such as aluminum honeycomb meshes coated with thick layers of commercial TiO_2 nanoparticles (e.g., Evonik P25) [63, 69].

The application of air-cleaning devices using TiO_2 nanoparticles is limited due to several factors such as periodic maintenance and the replacement of photocatalyst modules in the purifiers [42, 66]. This is because TiO_2 nanoparticles immobilized with low adhesion can detach from the module and enter the indoor air over time [69–70]. The detached TiO_2 nanoparticles could contaminate indoor air; while TiO_2 is known as a nontoxic material, the hazardous effects of TiO_2 nanoparticles are still under examination in the ecosystem [71].

To overcome these drawbacks, the integration of large-area photocatalytic materials has been proposed as a future indoor air-cleaning solution in order to achieve maximum efficiency against indoor air pollutants by depositing photocatalysts onto building elements such as tiles or cementitious materials [69, 72]. Furthermore, photocatalytic coatings can be easily applied to large-area and well-illuminated surfaces, such as windowpanes [73]. However, the concept of a photocatalytic window for indoor air cleaning is yet to be developed.

1.3 TiO_2 photocatalyst for air purification

TiO_2 is one of the most widely used photocatalysts, which occurs in three polymorphic crystal forms: anatase (tetragonal), rutile (tetragonal), and brookite (orthorhombic) [8]. The anatase and rutile phases of TiO_2 are the most studied polymorphs for photocatalytic applications. Generally, the anatase phase of TiO_2 is more photocatalytically active than the rutile phase, which is because it shows better generation of electron–hole pairs, higher affinity towards O_2 because of the more negative redox potential of the conduction band, and a lower electron–hole recombination rate [25, 74–75].

The photocatalytic performance of TiO_2 depends on numerous factors such as crystal phase, crystallite size, bandgap energy, surface area, material amount, and surface chemical composition; these are mainly determined by the material type (powder vs. thin film) and deposition method [74].

1.3.1 TiO_2 nanopowders for air cleaning

The number of publications in the past two decades has indicated great interest in the application of commercial photocatalysts for the removal of VOCs from air. TiO_2 Aeroxide P25 from Evonik (formerly Degussa) is by far the most widely employed photocatalyst in

this field because of its high performance in the degradation of several VOCs, high availability, and relatively low cost [74–76]. Experimental results have shown that P25 contains 80% anatase and 20% rutile crystalline phases [76–77]. The other commercial TiO₂ nanopowders are the PC series (PC100, PC105, and PC500) from Cristal Global Companies and UV100 from Hombicat, possessing anatase phase with different mean crystal sizes in the range 10–25 nm [74].

Numerous studies have evaluated the photocatalytic performance of commercial TiO₂ powders [78–91]. In most of these studies, powder suspensions were dip-coated onto various type of support materials, such as activated carbon and fiberglass, which can potentially be used as a photocatalytic base (plate) in air-cleaning devices [80, 84], or the walls of photocatalytic reactors such as annular tubular and continuous reactors [86–87]. Generally, the effect of photocatalytic test parameters, such as the airflow rate [78], initial VOC concentration [79], relative humidity (RH) [80–81], and irradiation source [88] have been investigated.

Most of the studies have revealed that TiO₂ nanoparticles are highly effective in the photodegradation of several VOCs at high initial concentrations between 100 and 1000 ppm. Preis et al. reported a P25-coated reactor (640 cm²) with a specific quantity of ca. 1.4 mg·cm⁻² that achieved ca 75% conversion of *tert*-butyl alcohol (100 ppm) under UV light [89]. Galano et al. indicated that a coated reactor with the specific quantity of 3.5 mg·cm⁻² P25 in the coated reactor showed 90% conversion of 500 ppm MTBE [90]. Furthermore, several studies have been devoted to the comparison of the photocatalytic performance of P25 to other commercial powders or lab-synthesized powders [82, 87, 91]. Kirchnerova et al. [82] coated a 1200-cm² reactor with P25 and UV100 powders at 0.2 mg·cm⁻² and reported 95% and 89% conversion of *n*-butanol (580 ppm) over P25 and UV100, respectively [82]. Meanwhile, Krichevskaya et al. compared the flame aerosol-synthesized TiO₂ powders and P25 coated onto a reactor with a specific quantity of 1.2 mg·cm⁻². It was concluded that the synthesized TiO₂ powders were photocatalytically more active than P25; this was attributed to the primary particle size and specific surface area [91].

In summary, despite the high photocatalytic performance of powders or powdered coatings, their main limitations are poor adhesion and inapplicability in applications requiring high optical transparency [10, 92].

1.3.2 Nanocrystalline TiO₂ thin films for air cleaning

In contrast to TiO₂ powders, TiO₂ thin films have several advantages such as high mechanical resistivity, high transparency for window coatings, and cost-effectiveness due to reduced material amount [93]. Additionally, TiO₂ thin films can fulfill different physical surface functionalities such as exhibiting self-cleaning features with superhydrophilic surfaces while providing clean air [94].

The main techniques used to prepare TiO₂ thin films for air cleaning are magnetron sputtering, atomic layer deposition and sol-gel methods (dip and spin-coating) [23].

Magnetron sputtering

Several studies have reported on the gas-phase photodegradation of VOCs over TiO₂ thin films formed by the sputtering method [95–100]. Takahashi et al. [98] showed complete (5 μL) methanol oxidation on a 665-nm-thick TiO₂ film deposited on a glass substrate under UV light for 24 h. Gray et al. [95] and Österlund et al. [96] reported that the degradation of acetaldehyde depended on the crystallite orientation in sputtered TiO₂ films. Tomaszewski et al. investigated the influence of Na ions on the photocatalytic

activity of TiO₂ films deposited onto soda lime glass (SLG) and SLG coated with a SiO₂ barrier layer. The highest reaction rate for the photocatalytic decomposition of ethanol was found for the TiO₂ film deposited onto SLG coated with a SiO₂ barrier layer [97]. Moreover, Ho-Geun et al. [100] examined the effect of the irradiation source on the photocatalytic decomposition of methyl-ethyl-ketone (MEK) and acetaldehyde over TiO₂ films. It was reported that the TiO₂ films showed 25% and 60% conversion of MEK under UV-B and UV-C irradiation, respectively. However, no photocatalytic reaction was monitored over TiO₂ films under UV-A irradiation [100].

The limitations of the sputtering method for photocatalytic applications are high cost, substrate damage risk due to ionic bombardment and smaller grain sizes in the films compared to those obtained by chemical solution-based methods [66].

Atomic layer deposition (ALD)

The effects of film thickness and substrate type were investigated on TiO₂ thin films deposited by the ALD method for the photocatalytic degradation of toluene and acetaldehyde. Kim et al. [101] deposited TiO₂ thin films onto nano-diamond and reported about 50% conversion of toluene under UV-A light in 2000 min. Verbruggen et al. [102] deposited TiO₂ films with different thicknesses onto carbonaceous substrates for the photocatalytic decomposition of acetaldehyde under UV irradiation. The thickness of the TiO₂ layer was varied by using between 50 and 400 ALD cycles, where the optimal thickness (400 nm) was found after 200 ALD cycles; this coating showed an acetaldehyde conversion of ca. 50% in 20 min under UV-A light [102]. The major drawbacks of ALD are the low deposition rate and inapplicability of large-area coatings [103].

Sol-gel methods

The sol-gel methods (of dip-coating and spin-coating) are the most common deposition methods for fabricating TiO₂ thin films for the degradation of gaseous organic pollutants because these techniques are both simple and low in cost. Table 1.1 in Appendix 2 summarizes the photocatalytic decomposition of various VOCs on TiO₂ films prepared using sol-gel methods.

Many studies have focused only on the photocatalytic measurement parameters, such as VOC type [104, 106, 110], humidity level [110, 112, 115], and pollutant concentration [113, 115, 116] over TiO₂ films. However, some studies have focused on altering the parameters affecting both the characteristics of the photocatalyst and photocatalytic performance, such as the annealing temperature of TiO₂ films [116], stabilizing agents in precursor solutions [105], substrate types [111], and film thickness [122]. Biswas et al. [116] prepared TiO₂ films at various annealing temperatures (300, 400, and 500 °C) and reported that the highest photocatalytic activity (ca. 80% conversion of methanol) was obtained on a film annealed at 300 °C. This is explained by the effect of structural and morphological changes arising from the difference in annealing temperatures. Legrand et al. [105] used several stabilizing agents in TiO₂ sol. They concluded that the film prepared using an acetic acid-stabilized sol showed the highest initial reaction rate (0.006 min⁻¹), which was attributed to the higher crystallinity and prevalence of cracks on the film surface [105]. Ho et al. [111] reported that the ions diffused from the substrates of SLG, aluminum, and stainless steel during film preparation and heat treatment could have negative or positive effects on the photocatalytic activity of TiO₂ films. In their study, the samples prepared on quartz showed the highest reaction rate during acetone degradation (2.3 × 10⁻³ min⁻¹), which was ascribed to the high degree of purity of the TiO₂ film. Lee et al. [122] studied the film thickness effect on the photocatalytic

degradation of 2-propanol. They proposed that the photocatalytic activity increases with increasing film thickness because of the higher amount of photogenerated electron–hole pairs transferred from the bulk to the surface of the TiO₂ films. In addition, Watanabe et al. [107] investigated the effect of Na ion diffusion from the SLG substrate on the photocatalytic conversion of acetaldehyde over TiO₂ films as a function of film thickness. They reported an increase in reaction rate (0.1–0.4 μmol⁻¹ min⁻¹) with an increase in film thickness from 500 nm to 2.1 μm.

The major drawbacks of sol-gel methods are precursor wasting during film deposition and the necessity of annealing treatments at high temperatures to form the anatase phase [123].

Chemical spray pyrolysis

Spray pyrolysis is a robust, cost-effective, fast, easily scalable, and freely applicable chemical method of deposition for large-area coverage. In spray pyrolysis, aerosols are generated by atomizers, which are usually pneumatic, ultrasonic, or electrostatic [124]. The nebulization technique is often the most crucial parameter because it allows management of the scale and distribution of the droplets on the preheated substrates [124–125]. In the literature, most of the studies on photocatalytic TiO₂ thin films prepared by spray pyrolysis have focused on water treatment [126], and only a few studies have been conducted on the photocatalytic decomposition of VOCs over sprayed TiO₂ films (Table 1.1 in Appendix 2).

Watanabe et al. [107] sprayed 2.1-μm-thick TiO₂ films onto quartz and SLG substrates to show the detrimental effect of Na ions on the photocatalytic activity. They reported 48% and 33% conversion of acetaldehyde over TiO₂ films on quartz and SLG substrates, respectively, after 60 min under UV light [107]. Simonsen et al. [108] compared the photocatalytic activity for the degradation of acetone over commercially available coatings, such as Pilkington ActivTM, to that of sprayed TiO₂ films. They measured an almost negligible degradation (≤1%) of acetone on the 100-nm-thick TiO₂ thin film obtained by spray pyrolysis. Miki-Yoshida et al. [119] compared the photocatalytic efficiency of TiO₂ and ZnO films prepared by spray pyrolysis under the same deposition conditions. The TiO₂ film showed a 90% conversion of butane, which was 30% higher than that of the ZnO film. Kaneko et al. [120] sprayed TiO₂ films on glass fibers for the photocatalytic degradation of different VOCs. TiO₂ films showed complete conversion of 5 ppb of trimethylamine, methanethiol, and dimethyl sulfide under UV-A light in 120 min.

Despite the easy scale-up in industry and fast deposition process, no publications have been found on the photocatalytic removal of pollutants in air over TiO₂ thin films fabricated by ultrasonic spray pyrolysis.

In summary, the deposition method of thin films, as well as their deposition and annealing parameters, determine the thin-film properties such as phase composition, crystallite orientation, crystallite size, film thickness, and surface chemical composition, which in turn determine the photocatalytic activity. Moreover, it is difficult to compare the photocatalytic performances of thin films studied by different research groups because of the lack of standard test methods. According to the literature, different test conditions and different photocatalytic reactor configurations have been used, thus impairing comparisons of the results.

1.4 Summary of literature overview and the aim of the study

Photocatalysis is considered a promising technology for indoor air cleaning, possessing great advantages compared to filtration systems. Currently, it is used in some portable air devices comprising photocatalytic modules with UV lamps.

As stated in the literature, the selection criteria for choosing the ideal photocatalyst should fulfill several requirements such as easy production and low cost. Research in the development of efficient photocatalytic materials has achieved significant progress in recent years. Although many semiconductor materials have been studied, TiO_2 is considered to be the most effective photocatalyst. However, investigations on TiO_2 remain underway to extend its applicability.

Commercial TiO_2 powders are coated on photocatalytic modules for use in portable air purifiers. Therefore, most research has been conducted on thick TiO_2 powder coatings on different types of support materials; these have potential utility as photocatalytic modules in air-cleaning devices. However, there are several drawbacks that limit the use of powdered coatings, such as mechanical instability and low optical transparency. Meanwhile, the integration of large-area photocatalytic coatings on building elements comprising well-illuminated surfaces, such as windowpanes, has been proposed as a future indoor air-cleaning solution. In contrast to powder coatings, TiO_2 thin films have durable and functional features such as mechanical resistivity, high transparency, and superhydrophilicity. These features, however, strongly depend on the preparation technique and preparation conditions.

Among the various deposition methods, ultrasonic spray pyrolysis is simple, fast, and cost-effective, yielding smooth and durable films by the generation of small-sized initial droplets. Despite the many advantages, no comprehensive study has been reported on ultrasonically sprayed TiO_2 films as photocatalytic materials for air purification.

Moreover, in the field of photocatalytic air purification, the lack of standard evaluation methods and differences in reactor types can hinder readers' understanding of the performance of the photocatalyst and the correct comparison of photocatalytic materials.

Therefore, this thesis aims to deposit TiO_2 thin films by ultrasonic spray pyrolysis to achieve materials suitable as air-cleaning window coatings with self-cleaning properties. This will broaden the utility of the ultrasonic spray pyrolysis method in large-area photocatalytic applications for air cleaning. Thus, the objectives of this thesis are as follows:

1. To study the effect of the TiO_2 film deposition temperature on different glass substrates on the film morphology, structure, optical properties, and film surface properties such as chemical composition, wettability and photocatalytic activity toward the degradation of MBTE as a model pollutant.
2. To study the photocatalytic degradation of various indoor air pollutants such as MTBE, acetone, heptane, and acetaldehyde over the sprayed TiO_2 thin films and the effects of the operating parameters of the reactor such as humidity, airflow rate, and light source, on the photocatalytic performance of TiO_2 thin films.
3. To develop TiO_2 thin films with various thicknesses to determine the optimal thickness range for photocatalytic applications.

2 Experimental method

In this section, the experimental methods applied in this work are presented; the details of the experiments have also been published in papers I, II, and III.

2.1 Deposition of TiO₂ thin films by ultrasonic spray pyrolysis

In this work, TiO₂ thin films were deposited onto conventional industrial window glass [I] and borosilicate glass substrates [II, III]. Prior to film deposition, all substrates were washed with ethanol and subsequently sonicated in the deionized water for approximately 10 min using an ultrasonic bath.

TiO₂ thin films were prepared using titanium tetraisopropoxide (TTIP, C₁₂H₂₈O₄Ti, Merck, 98% purity) as the Ti source, acetylacetonate (AcacH, C₅H₈O₂, Merck, 98% purity) as a complexing agent, and ethanol (EtOH, C₂H₅OH; Estonian Sprit OU, 96%) as a solvent. The spray solution was composed of TTIP with a concentration of 0.1 mol·L⁻¹ [III] or 0.2 mol·L⁻¹ [I, II, III] and TTIP:AcacH with a molar ratio of 1:4 in ethanol. After the preparation of the precursor solution, TiO₂ thin films were deposited using the ultrasonic spray pyrolysis setup (Figure 2.1) onto the heated substrates at different temperatures (T_{dep}) of 250 °C, 350 °C, and 450 °C. All as-deposited samples were annealed at the temperature (T_{an}) of 500 °C for 1 h in air in a furnace; these are referred to as the as-prepared samples throughout the thesis.

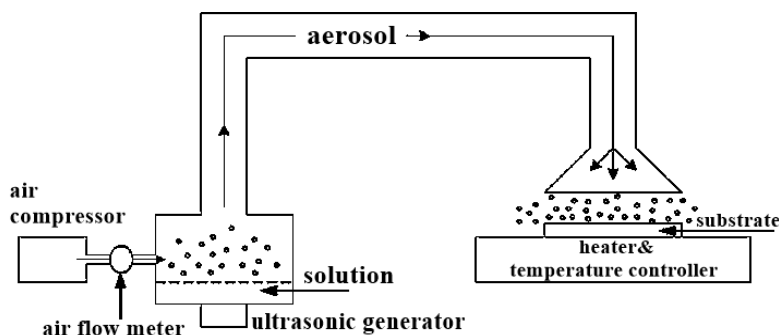


Figure 2.1. Schematic illustration of ultrasonic spray pyrolysis setup [128].

Table 2.1. Technological parameters for the deposition of TiO₂ thin films.

Precursors molar ratio	Substrate	T _{dep} , °C	T _{an} , °C	[TTIP], mol L ⁻¹	Number of spray cycles	Ref.
TTIP:AcacH (1:4)	Window glass	250, 350, 450	500 1h	0.2	6	[I]
	Borosilicate glass	350, 450	500 1h	0.2	6	[II]
	Borosilicate glass	350	500 1h	0.1, 0.2	1, 2, 3, 6,7, 9, 12, 15, 18, and 21	[III]

The details of the deposition of TiO₂ thin films have also been discussed in the papers I, II, and III, and also summarised in Table 2.1.

2.2 Characterization of TiO₂ thin films

The characterization methods used to determine the physical and chemical properties of TiO₂ thin films are summarized in Table 2.2. Detailed descriptions of each method used in this study can be found in the experimental sections of paper I, II, and III.

Table 2.2. Analytical techniques used for the characterization of TiO₂ thin films.

Properties	Characterization Methods	Apparatus	Ref.
Morphology; Film thickness	SEM	Zeiss EVO-MA15, Zeiss HR FESEM Ultra 55	[I, II, III]
Surface roughness	AFM	NT-MDT Solver 47	[I, II, III]
Phase composition; mean crystallite size	XRD	Rigaku Ultima IV	[I, II, III]
Phase composition	Raman	Horiba's LabRam HR800	[I]
Optical transmittance; optical bandgap	UV-VIS spectroscopy	Jasco V-670	[I, II, III]
Absorbance;	UV-VIS spectroscopy		[III]
Film thickness	UV-VIS spectroscopy		[III]
Wettability	Water contact angle measurement	DSA 25 (KRUS Instrument)	[I, II]
Chemical composition	XPS	Kratos Analytical Axis Ultra DLD	[I, II]

2.3 Evaluation of the photocatalytic activity of TiO₂ thin films

In this work, two in situ approaches were used to determine the photocatalytic performance of TiO₂ films; degradation of VOCs in gas-phase and destruction of stearic acid as a solid organic layer on TiO₂ films.

2.3.1 Determination of gas-phase photooxidation of VOCs over TiO₂ thin films

In papers I and II, the photocatalytic activity of thin films was tested in a multi-section plug-flow reactor [129]. The multi-section plug-flow reactor consisted of five sections, where the section volume was 130 mL and the surface area of the photocatalytic coating in one section of the reactor was 120 cm² with an overall surface area of 600 cm² for the entire reactor. The samples were placed inside each section of the reactor in the form of thin films on glass plates. The experimental setup consisted of two gas-flow controllers for measuring the diluent and polluted gas flow rates, a gas humidifier, and an INTERSPEC 200-X Fourier-transform infrared (FTIR) spectrometer with a Specac Tornado 8-m gas cell.

The photocatalytic activity was studied following the photocatalytic degradation of MTBE (C₅H₁₂O, Fluka, ≥99.5 purity), acetone (C₃H₆O, Sigma-Aldrich, ≥99.5 purity), acetaldehyde (C₂H₄O, Acros, >99.5 purity), and heptane (C₇H₁₆, Honeywell, ≥99 purity) in

the gas phase as model air pollutants (all reagents >99% purity). In the experimental setup, airflow rates of 0.5 [I] and 1.0 [I, II] L min⁻¹ were used, which gave residence times of 15.6 and 7.8 s per reactor section, respectively. The inlet concentrations of the gaseous pollutant were 5 and 10 ppm, respectively. The RH was maintained at 6 ± 1% [I] and 40 ± 5 % [I, II] under dry- and humid-air conditions, respectively. Two lamps were used: the UV Philips Actinic BL 15 W with an average irradiance of 3.5 mW·cm⁻² with reflector (maximum emission at 365 nm) or VIS Philips TL-D 15 W with an average irradiance of 3.3 mW·cm⁻² with reflector were used as the UV and visible (VIS) sources. The MTBE, acetone, acetaldehyde, and heptane peaks were quantified using an INTERSPEC 200-X FTIR spectrometer at the IR bands of 1063–1124, 1172–1245, 2630–2910, and 2825–3010 cm⁻¹, respectively. The gas-phase intermediate products of MTBE, heptane, TBF, and formic acid were also quantitatively monitored by FTIR at the IR bands from 1138 to 1190 and from 1103 to 1107 cm⁻¹, respectively.

Measurements were performed in the Laboratory of Environmental Technology at Tallinn University of Technology under the supervision Dr. Marina Kritševskaja.

2.3.2 Determination of stearic acid decomposition on TiO₂ thin films

In paper III, photocatalytic experiments were performed on the photodegradation of a stearic acid layer on TiO₂ films measuring 2 × 2 cm². Sol-gel spin-coating technique was applied to deposit a thin layer of stearic acid on the TiO₂ thin films. In a typical experiment, 100 μL of 8.8-mM stearic acid solution in methanol was cast onto the center of each TiO₂ thin film. The rotation speed was adjusted to 1000 rpm for 30 s for coating. The final coated film was dried at 80 °C for 10 min.

The degradation of stearic acid as a function of UV-A irradiation time was monitored by FTIR (Perkin Elmer, Beaconsfield, England). Stearic acid has strong absorption bands at 2958, 2923, and 2853 cm⁻¹. Therefore, the measurements were performed in the wavenumber region 3200–2500 cm⁻¹ in transmission mode. The details of other instrument parameters for the measurement can be found in the experimental part section of paper III. The decrease in the specific stearic acid band intensity was monitored using FT-IR spectroscopy as a function of irradiation time. FTIR spectra were measured before UV-A irradiation and after every 60 min for 3 h. The UV Philips Actinic BL 15 W lamp (Philips, Poland) with an irradiance of 3.5 mW·cm⁻² and maximum emission at 365 nm and UV-B/UV-A ratio of <0.2% was used as the irradiation source.

Stearic acid degradation under UV-A light is known to follow first-order kinetics that is the integrated band area (A) depends on time (t) as follow:

$$A(t) = A_0 e^{-k} \quad (1)$$

where k is the photodegradation rate constant. The photodegradation rate constant is the slope value of the linear fit of the plot ln (A/A₀) versus time [130].

3 Results and Discussion

This section presents the results and discussions of the effects of the deposition parameters and reactor operating parameters on the characteristics and photocatalytic activity of TiO₂ thin films. These results have been published in papers I, II, and III.

3.1 Effect of substrate and deposition temperature on photocatalytic activity of TiO₂ thin films

In this study, TiO₂ thin films were deposited at different temperatures onto window and borosilicate glass substrates.

3.1.1 Morphology, structural, and optical properties

Surface Morphology

According to the SEM surface images in papers I and II, compact TiO₂ thin films were observed on the window and borosilicate glass substrates. TiO₂ films deposited on window glass at 250 °C and 350 °C and on borosilicate glass at 350 °C showed planar surface structures; however, at the increased deposition temperature of 450 °C, the film surface showed well-distinguished grains [I, II].

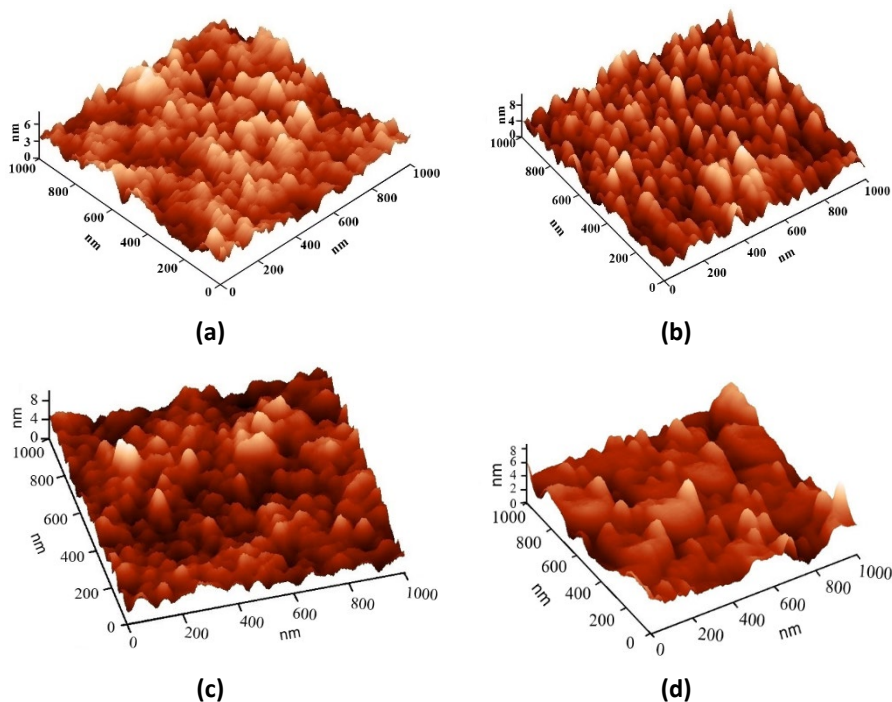


Figure 3.1. AFM images of TiO₂ thin films deposited on window glass at (a) 350 °C and (b) 450 °C and borosilicate glass at (c) 350 °C and (d) 450 °C.

Figure 3.1 shows the three-dimensional AFM deflection images of the as-prepared TiO₂ films deposited at 350 and 450 °C onto window and borosilicate glass substrates. The TiO₂ films sprayed at 350 °C show fine-grained structures compared to those deposited at 450 °C, which possess distinctive large grains. Further, the formation of

elliptical agglomerated clusters is observed in the TiO₂ thin film deposited onto borosilicate glass at 450 °C in Figure 3.1d.

The different surface topography of the films also resulted in a slight increase in the root mean square (RMS) roughness (Table 3.1). The higher RMS roughness of the TiO₂ films deposited at 450 °C could be due to the different topography of the film and the cavities formed between the well-distinguished grains.

The thicknesses of the TiO₂ films are presented in Table 3.1, as estimated from the cross-sectional SEM images [I, II]. The film thickness of the TiO₂ thin films was increased with increases in deposition temperature (Table 3.1). The increase in the film thickness with deposition temperature has also been found in other studies, for example, in the cases of ZrO₂ and TiO₂ deposition by spray pyrolysis [131–132].

Table 3.1 Summary of the morphological and structural properties of as-prepared TiO₂ thin films.

Deposition temperature, °C	TiO ₂ films on window glass			TiO ₂ films on borosilicate glass		
	Thickness, nm	RMS, nm	Mean crystallite size, nm	Thickness, nm	RMS, nm	Mean crystallite size, nm
250	110	NM	13	NM	NM	NM
350	180	0.8	35	190	0.6	26
450	240	1.2	32	330	1.0	22

*NM: Not measured

Structural and optical properties

The XRD patterns of the TiO₂ films deposited onto window glass and borosilicate glass at various temperatures are presented in Figure 3.2. The patterns exhibited reflection peaks at 2θ values of 25.3°, 37.9°, 48.1°, 54.1°, and 55.2°, corresponding to reflections from the (101), (004), (200), (105), and (211) crystal planes of the anatase TiO₂ structure (JCPDS 01-070-6826). No other crystalline phases of TiO₂ were detected. The mean crystallite size of TiO₂ was calculated using the main anatase peak (101) using the Scherrer formula.

The mean crystallite size of TiO₂ films on window glass was increased in from 13 to 32 nm with an increase in the deposition temperature from 250 to 450 °C, while similar mean crystallite sizes of 26 and 22 nm were found for the TiO₂ films deposited on borosilicate glass at 350 °C and 450 °C, respectively (Table 3.1). In addition, it was observed that TiO₂ films grown on borosilicate glass showed smaller crystallite sizes than those on window glass.

All TiO₂ films showed a total transmittance of ca. 80% in the visible spectral region. A similar optical bandgap was found for all samples of approximately 3.40 eV [I, II].

In summary, morphological studies have shown that TiO₂ films are compact. The increase in deposition temperature resulted in larger grains, higher surface roughness, and increased film thickness. XRD analyses revealed that the mean crystallite size varied depending on the deposition temperature and substrate type. All films showed high transparency (ca 80%) in the visible spectral range.

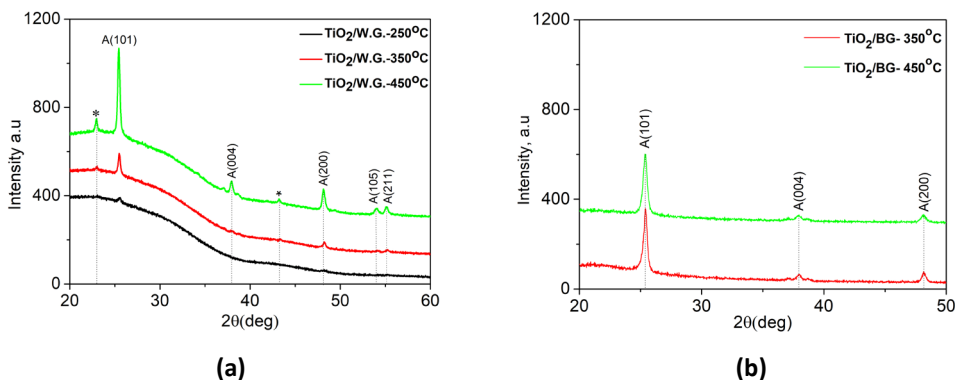


Figure 3.2. XRD patterns of TiO_2 films deposited onto (a) window and (b) borosilicate glass substrates. The peaks corresponding to SiO_2 from substrate are marked by "*" [1].

3.1.2 Chemical composition and wettability

X-ray photoelectron spectroscopy (XPS) measurements were performed on the as-prepared TiO_2 films deposited on window glass in paper I, while they were performed for the UV-treated TiO_2 films deposited on borosilicate glass in article II. The details of the data analysis of the XPS spectra can be found in papers I and II.

TiO_2 films on window glass substrate

Figure 3.3 shows the oxygen core level (O1s) spectra of as-prepared TiO_2 thin films fabricated on window glass substrates. The O1s core level spectrum of TiO_2 films deposited on window glass can be deconvoluted into three peaks. The peak observed at the binding energy (BE) value of 529.7 eV corresponds to the Me–O bond, and it is ascribed to the Ti–O. The peak observed at a BE value of 530.5 eV could be attributed to oxygen deficient region, revealing the presence of oxygen vacancies (V_o) [133]. Additionally, the peak at a BE value of 531.8 ± 0.3 eV reveals that the surface of the TiO_2 film involves surface hydroxyl groups (OH^-) [134].

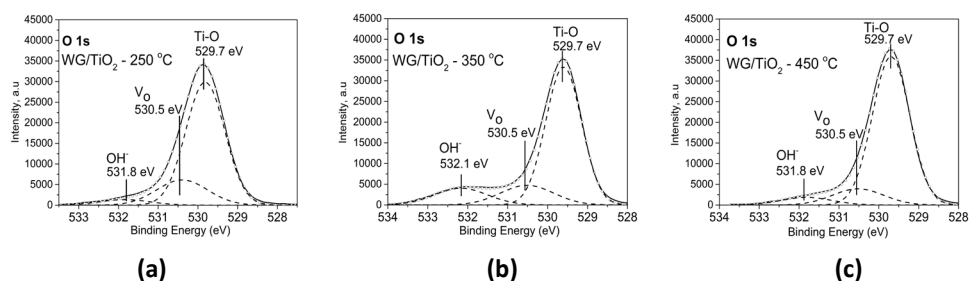


Figure 3.3. XPS spectra of O1s core level for as-prepared TiO_2 thin films on window glass deposited at (a) 250 °C, (b) 350 °C and (c) 450 °C.

The atomic concentrations of the components such as Ti–O, V_o , and OH^- were determined from the peak areas using sensitivity factors (Scofield's cross-section) provided by analysis software. The ratios of the components, $[\text{OH}^-]/[\text{Ti-O}]$ and $[\text{V}_\text{o}]/[\text{Ti-O}]$ are presented in Table 3.2.

As seen in Table 3.2, the ratios of $[\text{OH}^-]/[\text{Ti-O}]$ on the surfaces of the TiO_2 films on window glass is increasing from 0.06 up to 0.18 with the increasing of the deposition

temperature from 250 to 350 °C. However, a slight decrease in the $[\text{OH}^-]/[\text{Ti-O}]$ ratio was observed for the TiO_2 film deposited onto window glass at 450 °C. The surface OH^- groups can participate directly in the interfacial reactions by trapping photogenerated holes that diffuse to the TiO_2 surface and producing hydroxyl radicals ($\cdot\text{OH}$) (Figure 1.1) [135].

The $[\text{Vo}]/[\text{Ti-O}]$ ratio is recalculated for 250 °C deposited sample by fixing the V_o peak position at 530.5 eV. The recalculated $[\text{Vo}]/[\text{Ti-O}]$ value is 0.27 (Table 3.2). It can be seen that the $[\text{Vo}]/[\text{Ti-O}]$ ratio is decreasing with increasing the deposition temperature from 250 to 450 °C (Table 3.2). The presence of surface oxygen vacancies facilitates the adsorption of environmental species at the surface, where reactions occur. Thus, surface oxygen vacancies are called surface-active sites [136].

Table 3.2. Results of the XPS studies of as-prepared TiO_2 thin films deposited onto window and borosilicate glass at different deposition temperatures.

Glass substrate	T_{dep} , °C	As-prepared samples			After UV-treatment		
		[Na] at. %	$[\text{Vo}]/[\text{Ti-O}]$	$[\text{OH}^-]/[\text{Ti-O}]$	[Na] at. %	$[\text{Vo}]/[\text{Ti-O}]$	$[\text{OH}^-]/[\text{Ti-O}]$
Window	250	13.0	0.27	0.06	NM	NM	NM
Window	350	10.0	0.23	0.18	NM	NM	NM
Window	450	11.0	0.13	0.13	NM	NM	NM
Borosilicate	350	NM	NM	NM	3.0	0.12	0.11
Borosilicate	450	NM	NM	NM	1.0	0.09	0.05

* T_{dep} : Deposition temperature, **NM: Not measured

TiO_2 films on borosilicate glass substrate

XPS measurements were performed on the TiO_2 films on borosilicate glass after UV-A treatment in ambient air [II]. Similar to the TiO_2 films deposited on window glass substrates, the TiO_2 thin film deposited at 350 °C on the borosilicate glass substrate showed a higher level of oxygen vacancies and OH^- groups on the film surface than the sample deposited at 450 °C (Table 3.2). The lower number of oxygen vacancies on the TiO_2 thin films deposited at 450 °C can be attributed to the effect of the higher deposition temperature, which repairs surface oxygen defects.

Moreover, Na was detected on the surfaces of the TiO_2 thin films fabricated on window and borosilicate glass. According to the XPS data, a low average content (1–3 at.%) of Na was calculated for the TiO_2 films deposited on borosilicate glass, while that on the TiO_2 films deposited on window glass was 10–13 at. % (Table 3.2). Na diffusion probably occurs from the glass substrates into the TiO_2 film surface during the deposition and annealing processes. The Na content decreased with increases in the deposition temperature, which could be attributed to the higher film thickness inhibiting the diffusion of Na ions to the surface.

The detrimental effect of Na diffusion from soda lime glass to the film surface during the heat treatments has been investigated in several studies. In this regard, different negative influences of Na ions on the TiO_2 film properties have been proposed such as the production of recombination centers for photogenerated electron–hole pairs [137] and disrupting the crystallinity of TiO_2 [138].

Wettability

The wettability of the TiO₂ thin films was evaluated by measuring the average water contact angle (WCA) values [I, II]. According to the WCA results in paper I, the sample prepared at 250 °C exhibits a WCA value of ca. 33°, whereas TiO₂ films deposited at 350 °C and 450 °C show superhydrophilic surfaces (WCA < 10°). The sample deposited at 250 °C showed a superhydrophilic surface after exposure to UV light for 30 min. Moreover, the WCA values for the as-prepared TiO₂ films prepared on borosilicate glass at 350 °C and 450 °C were 12° and 17°, respectively [II].

Based on the XPS analysis and wettability test, TiO₂ thin films sprayed at 350 °C contain the highest surface ratios of OH⁻ groups on the surface irrespective of substrate type. In addition, the diffusion of Na ions from substrates were detected on the film surfaces. TiO₂ thin films prepared on window glass showed higher amounts of Na on the film surface compared to those deposited on borosilicate glass. The WCA measurements showed that all as-prepared TiO₂ films were hydrophilic and showed superhydrophilicity after 30 min of UV irradiation.

3.1.3 Photocatalytic activity

The photocatalytic performances of TiO₂ thin films were investigated through the photocatalytic decomposition of methyl *tert*-butyl ether (MTBE) using a multi-section plug-flow reactor. The photocatalytic decomposition of MTBE is characterized by its conversion, defined as $(C_{in}-C_{out})/C_{in}$ (%) as a function of residence time, which is increased by subsequent inclusion reactor sections. Here, C_{in} and C_{out} are the MTBE concentrations of the intake and output gases.

The photocatalytic conversion of MTBE was investigated at five residence times of 15.6, 31.2, 46.8, 62.4, and 78.0 s, employing one, two, three, four, and five sections of the reactor, respectively. The operating conditions were determined for the experimental runs as 15.6 s residence time per section, 6% RH, and the reactor temperature of 34 °C.

The photocatalytic activity of the TiO₂ thin films was first tested by using one section of the reactor (corresponding to a residence time of 15.6 s, as shown in Figure 3.4). The sample prepared at 250 °C showed only 4% conversion of MTBE (Figure 3.4), which could be attributed its low crystallinity (see Figure 3.2, Section 3.1.1). Thus, it was excluded from further experiments [I].

The photocatalytic activity of the TiO₂ films deposited at 350 °C and 450 °C were tested in all five sections, corresponding to a total coating area of 600 cm² (Figure 3.4).

As seen in Figure 3.4, TiO₂ thin films deposited at 350 °C irrespective of substrate type showed the highest MTBE conversions of 80% and 100% on window and borosilicate glass, respectively. Several factors could contribute to the higher photocatalytic performance of the TiO₂ thin films deposited at 350 °C compared to those deposited at 450 °C, including the surface morphology, higher level of oxygen vacancies, and OH⁻ groups. The presence of OH⁻ groups is known to benefit photocatalytic reactions; it has been reported that OH⁻ groups participate directly in the interface reactions by trapping photogenerated holes that diffuse to the TiO₂ surfaces and thereby producing reactive surface hydroxyl radicals ([•]OH) (see Figure 1.1, Section 1.1). OH⁻ groups can also act as active sites for the adsorption and reaction of reactant molecules on TiO₂ [139]. Additionally, it is well known that oxygen vacancies favor photocatalytic reactions because water dissociation occurs in the presence of surface oxygen vacancies, producing adsorbed OH⁻ groups. In addition, oxygen vacancies support O₂ adsorption, indicating that oxygen vacancies can facilitate the capture of photoinduced electrons by adsorbed O₂, simultaneously producing reactive oxygen species ([•]O₂⁻), and thus promoting the oxidation of organic pollutants [140].

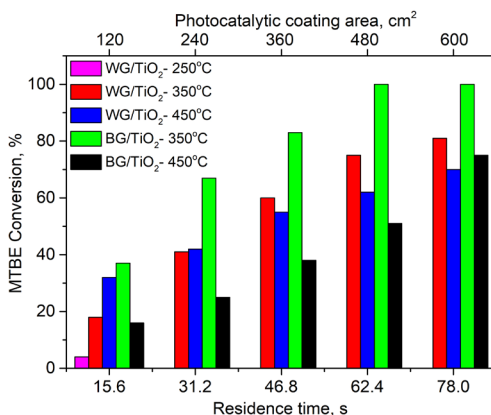


Figure 3.4. Photocatalytic conversion of MTBE on as-prepared TiO₂ thin films deposited onto window and borosilicate glass substrates at 250, 350 and 450 °C; MTBE inlet concentration 10 ppm; RH 6%.

Moreover, TiO₂ thin films deposited onto borosilicate glass at 350 °C showed higher photocatalytic activity (at 62.4 s, 100% degradation of MTBE) than those deposited on window glass (at 62.4 s, 75% degradation of MTBE) at the photocatalytic coating area of 480 cm². Considering the results given in the literature, this could be attributed to the high Na content detected on the surfaces of the samples fabricated on window glass (Table 3.1). It has been reported that high concentrations of Na ions can introduce surface and bulk recombination centers [141]. In addition, Nam et al. [142] and Krysa et al. [143] investigated the photocatalytic properties of TiO₂ thin films on different glass substrates. They claimed that the photocatalytic activity of the TiO₂ thin film depended greatly on the amount of Na because the Na concentration increased the TiO₂ crystallite size, which in turn decreased the photocatalytic activity of the TiO₂ films [143].

Before proceeding to the conclusion of Section 3.1, the main results of the selected studies regarding the conversion of common VOCs over TiO₂ powder coatings and as-deposited TiO₂ thin films were compared with the TiO₂ film deposited on borosilicate glass at 350 °C. However, comparison of the gas-phase photocatalytic efficiency of thin films is often difficult. Thus, the specific quantity of TiO₂, calculated as the mass (mg) of TiO₂ per unit of surface area (cm²), of the coating could permit comparison of some studies regarding the photocatalytic oxidation of VOCs. In the current work, the specific quantity of the 190-nm-thick TiO₂ film was 0.2 mg·cm⁻². This film achieved approximately 100%, 80%, and 70% conversion of MTBE, acetone, and acetaldehyde, respectively, over the photocatalytic coating area of 480 cm² (at 62.4 s) with the inlet concentration of 10 ppm under UV-A light (Figure 3.5a). For comparison, Preis et al. [89] reported the specific quantity of TiO₂ (P25) in the coated reactor as 1.4 mg·cm⁻², resulting in a 30% conversion of 100 ppm MTBE in 150 min under UV-A light. Krichevskaya et al. [91] indicated that the specific quantity of TiO₂ in the coated reactor was 1.2 mg·cm⁻²; this coating showed 100% conversion of 40 ppm toluene under UV-A irradiation for 60 min. Kluson et al. [109] detected a 45% conversion of acetone under UV-A light over a dip-coated TiO₂ film with a thickness of 675 nm. Ardizzone et al. [94] deposited TiO₂ films on glass substrates by an electrochemically assisted method with a thickness of ca. 450 nm; these achieved up to 87% conversion of acetaldehyde under UV-A light. Verbruggen et al. [102] reported 400-nm-thick TiO₂ films on carbonaceous substrates

fabricated by ALD; these showed 50% conversion of acetaldehyde with an inlet concentration of 50 ppmv under UV-A light in 20 min.

To summarize these findings, the TiO₂ thin films deposited on borosilicate glass at 350 °C demonstrated the highest photocatalytic activity. This could be attributed to the lower amount of Na ions, higher amounts of oxygen vacancies, and OH⁻ groups on the film surface. Therefore, the effect of the operating parameters of the photocatalytic reactor was investigated over TiO₂ films sprayed on borosilicate glass at 350 °C because they showed the highest photocatalytic performance among the TiO₂ samples.

3.2 Investigating photocatalytic degradation of different VOCs over TiO₂ thin films

TiO₂ films deposited on borosilicate glass at 350 °C were selected to investigate the gas-phase decomposition of different VOCs in a multi-section plug-flow reactor. VOCs of MTBE, acetone, acetaldehyde, and heptane were chosen as air pollutants for this study. Heptane, acetaldehyde, acetone, and MTBE were exposed to photocatalytic degradation tests under different conditions, that is, air humidity level (RH), airflow rate, and light source. The results have been published in paper II.

3.2.1 Effect of air humidity

The influence of the increase in RH from ca. 6 to 40% on the photocatalytic oxidation of acetaldehyde, acetone, heptane, and MTBE is illustrated in Figure 3.5. As seen in Figure 3.5a, under relatively dry air, the conversions of heptane, acetaldehyde, and acetone were 46%, 74%, and 93% at a residence time of 78 s, respectively, and 100% conversion of MTBE was achieved at 62.4 s, as previously discussed in Section 3.1. During the photocatalytic degradation of these VOCs, *tert*-butyl formate (TBF) and formic acid were detected as intermediate gas-phase products of MTBE and heptane, respectively.

The conversion efficiency of most VOCs was decreased with an increase in RH from 6% to 40% (Figure 3.5b). The heptane degradation was almost halved with this increase in RH. Higher air humidity had an indistinct influence on the complete conversion of MTBE. Complete MTBE conversion over 600² of TiO₂-coated glass for 78 s was achieved under humid air conditions. TBF was detected as the only by-product of MTBE in both dry and humid conditions [II]. The degradation of acetone was highly influenced by the RH, decreasing from 93% at RH 6% to 30% at RH 40%. Acetaldehyde was the only compound with oxidation uninfluenced by variations in RH. No significant changes in the conversion of acetaldehyde (ca. 75% conversion at 78.0 s) were observed with the increase in RH from 6% to 40%. It is known that transport of reactant molecules through water molecules depends on the solubility of the molecules in water. Acetaldehyde is a water-soluble polar molecule, explaining the “immunity” of its photocatalytic oxidation to differences in air humidity [II].

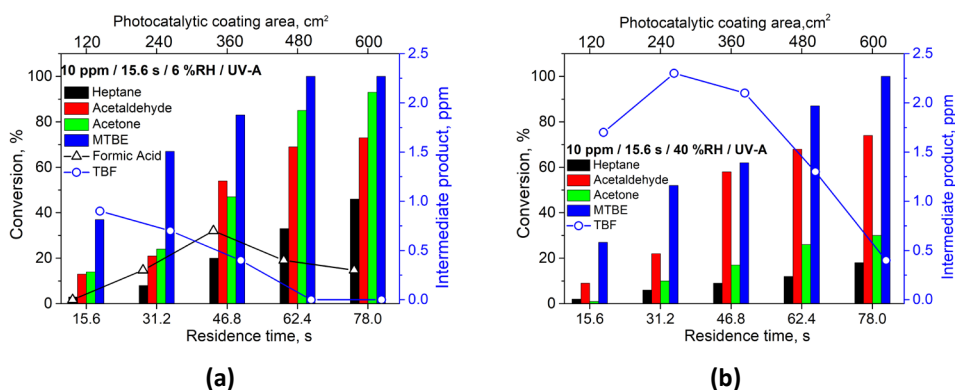


Figure 3.5. Photocatalytic conversion of different VOCs on TiO_2 thin film deposited on borosilicate glass at 350°C under (a) dry (6% RH) air and (b) humid (40% RH) air conditions. VOCs inlet concentration 10 ppm.

3.2.2 Effect of airflow rate

The effect of the airflow rate of VOCs on the surfaces of the TiO_2 thin films was investigated with initial pollutant concentrations of 5 ppm under 6% RH.

It is generally agreed that the airflow rate has two different effects on the photocatalytic reactions. First, with increases in airflow rate, the residence time of VOC molecules in the reactor decreases, causing a decrease in the adsorption of the pollutant and decreased conversion. Second, an increase in the airflow rate (decreased residence time) increases the mass transfer of pollutants between the air and the photocatalyst surface, resulting in an increased photocatalytic reaction rate [74].

In this study, the residence time in the reactor section was shifted from 15.6 s to 7.8 s as the airflow rate was increased from $0.5\text{ L}\cdot\text{min}^{-1}$ to $1.0\text{ L}\cdot\text{min}^{-1}$ (Figure 3.6).

As seen in Figure 3.6a, the complete degradation of 5 ppm MTBE and acetone was achieved within 46.8 s and 62.4 s, respectively, whereas the maximum conversions of heptane and acetaldehyde of 65% and 80%, respectively, were observed at 78.0 s. In Figure 3.6b, a general decrease in the VOCs conversion is observed at the photocatalytic coating area of 600 cm^2 (at residence time of 39.0 s) when compared to the same catalyst area corresponding with two times higher residence time of 78.0 s (Figure 3.6a).

When comparing the equal residence times in the reactor at different airflow regimes, then at a shorter residence time of 15.6 s (one section of the reactor in Figure 3.6a and two sections in Figure 3.6b), the conversion of VOCs was decreased despite the increased photocatalytic area in the two sections of the reactor in Figure 3.6b. However, at a residence time of 31.2 s (two sections of the reactor in Figure 3.6a and four sections in Figure 3.6b), doubling the airflow rate favoured the photocatalytic degradation of VOCs at the higher photocatalytic surface: the conversions of all the compounds were increased from 25, 38, 47, and 86% to 34, 47, 64, and 100% for heptane, acetone, acetaldehyde, and MTBE, respectively. The process of photocatalytic oxidation of acetaldehyde and MTBE was revealed as especially benefitting from the intensification of mass transfer in the reactor at the same residence time (31.2 s). Thus, again, the effect of the different airflow regimes was expected to be different for each VOC [II].

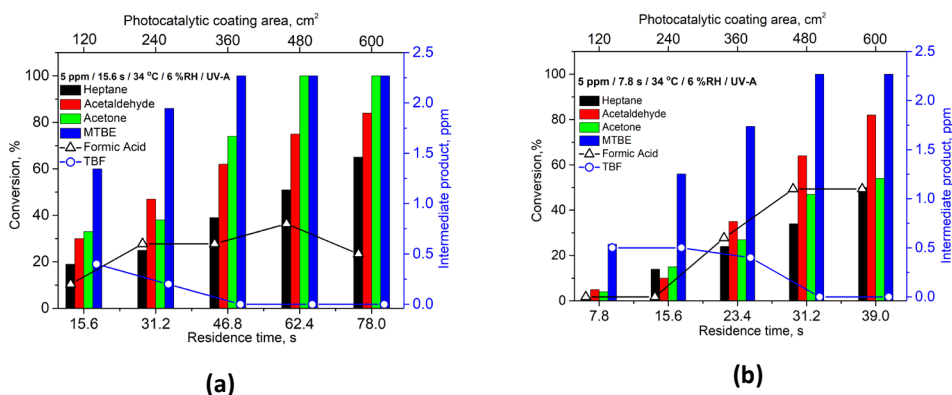


Figure 3.6. Photocatalytic conversion of different VOCs on TiO₂ thin film deposited on borosilicate glass at 350 °C under different airflow rates (a) 0.5 L min⁻¹ (15.6 s per section) and (b) 1.0 L min⁻¹ (7.8 s per section) VOC inlet concentration 5 ppm; RH 6%.

The order of conversion of VOCs at the residence time of 39 s in five sections was MTBE > acetaldehyde > acetone > heptane (Figure 3.6b), while it was MTBE > acetone > acetaldehyde > heptane at the longer residence time of 46.8 s (Figure 3.6a). Acetaldehyde and MTBE conversion were only slightly influenced by the shorter residence times, but the impact of the shorter residence time was much larger for photocatalytic degradation of acetone. This could be attributed to the different reaction rates of each VOC [II].

3.2.3 Effect of visible light

The photocatalytic activity of the TiO₂ thin films was investigated under visible light. The study used 5 ppm MTBE and acetone under visible light and 6% RH (Figure 3.7). The results were compared to those obtained from the samples measured under UV light, 6% RH, and 5 ppm inlet concentration, as presented in Section 3.2.2, Figure 3.6a.

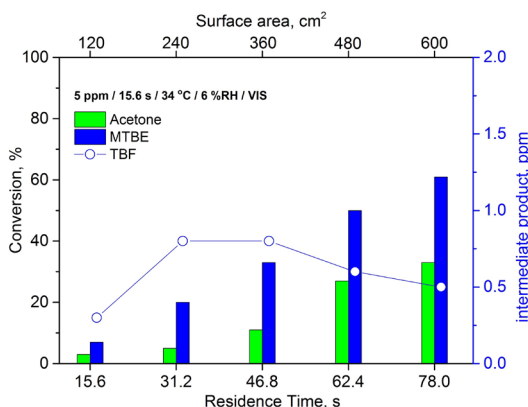


Figure 3.7. Photocatalytic conversion of MTBE and acetone under visible light on TiO₂ thin film deposited on borosilicate glass at 350 °C. MTBE and acetone inlet concentration 5 ppm; RH 6%; residence time 15.6 s per section.

Under visible light, the TiO₂ thin film showed 60% and 33% conversion of MTBE and acetone, respectively, at a residence time of 78.0 s. TBF was detected as an intermediate decomposition product of MTBE. In comparison, while using the same

operating parameters under UV-A light, the TiO₂ film showed 100% MTBE conversion at the residence time of 46.8 s over 360 cm² and 100% conversion of acetone at the residence time of 62.4 s over 480 cm² (Figure 3.6a). The significant decrease in the photocatalytic performance of the TiO₂ film under visible light was attributed to the optical bandgap exceeding 3.2 eV, which determined its photocatalytic activity under near-UV irradiation.

However, the visible-light activity of the TiO₂ film could also be associated with the formation of oxygen vacancies. In several studies [144], it was demonstrated that the presence of oxygen vacancies in TiO₂ could effectively expand the visible-light absorption range of TiO₂ because oxygen vacancies can form shallow donor states (sub-energy levels) below the conduction band [136].

In summarize Section 3.2, the TiO₂ thin film deposited at 350 °C effectively degraded 100% MTBE, 90% acetone, and 75% acetaldehyde vapor with the inlet concentration of 10 ppm under dry-air (6% RH) conditions without the formation of gas-phase intermediate products. Complete degradation of MTBE and 80% conversion of acetaldehyde were also achieved under humid-air (40% RH) conditions. TBF was detected as an intermediate decomposition product of MTBE during the photocatalytic conversion of MTBE under a humid atmosphere. The residence time was based on the mass transfer of VOCs, which is expected to differ for each VOC. Further, TiO₂ thin films deposited at 350 °C were photocatalytically active under visible light, degrading 60% of MTBE and 33% of acetone with inlet concentrations of 5 ppm; the origin of this phenomenon is a subject for further studies.

3.3 Influence of thickness on photocatalytic activity of TiO₂ thin films

This section was intended to determine the optimal thickness range of ultrasonic spray pyrolysis-deposited TiO₂ thin films for photocatalytic applications. Thus, the effect of film thickness on the material characteristics and photocatalytic activity has been studied. The results are presented in paper III.

3.3.1 Surface morphology, structural and optical properties of TiO₂ thin films

Morphological and structural properties

The thickness of the TiO₂ thin films was adjusted by altering the solution concentration and the number of spray cycles.

According to SEM cross-sectional images [III], the thicknesses of the TiO₂ films sprayed from the 0.1M solution were 65, 165, and 455 nm and those from the 0.2 M solution were 50, 205, and 635 nm, respectively, when using 2, 6 and 15 spray cycles.

AFM images (scan area 2 μm × 2 μm) of the TiO₂ films sprayed from the 0.1 M and 0.2 M solutions applying 2, 6, and 15 spray cycles are presented in paper III, Figure 2. The TiO₂ films deposited from the 0.1 M solution (2 and 6 spray cycles) consisted of fine grains with sizes of ca. 20–40 nm. Upon increasing the number of spray cycles to 15, the surfaces of the TiO₂ films showed agglomerated grains with sizes in the range ca. 40–150 nm. TiO₂ films prepared from the 0.2 M solution possessed average grain sizes of ca. 50–70 nm; however, the size of the agglomerates varied in the range ca. 50–100 nm with the increase in spray cycle numbers from 2 to 15. These findings correlate with our earlier research on TiO₂ films deposited from a 0.2 M solution by pneumatic spray pyrolysis, suggesting that TiO₂ films obey a 3-D growth mechanism regardless of the substrate type. In this growth mechanism, separate islands are formed in the first stage and following the growth with larger islands during further deposition [145].

All TiO₂ films exhibited anatase crystalline structures regardless of the precursor concentration and cycle number [III]. The mean crystallite size of TiO₂ thin films prepared from the 0.1 M solution was increased from 30 nm to 50 nm and that of those from the 0.2 M solution from 25 nm to 40 nm as the spray cycle number increased from 2 to 15, respectively. Compared to TiO₂ films sprayed from the 0.2 M solution, the films deposited from 0.1 M solution showed slightly higher mean crystallite values [III]. This could be the result of the lower amount of organic residues on the surfaces of TiO₂ films sprayed from the 0.1 M solution compared to that present on those deposited from the 0.2 M solution, as the deposition time per cycle was kept constant at 87 s.

Optical properties of TiO₂ thin films

The total transmittance and absorbance spectra are presented in paper III. Figure 3.8 shows the thickness of the TiO₂ films as a function of the spray cycle number (described in the paper III). The film thickness values obtained from the SEM cross-sectional images are presented in Figure 3.8.

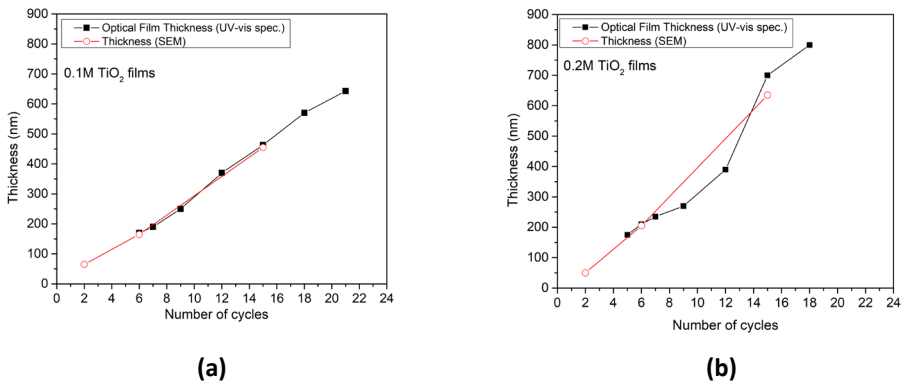


Figure 3.8. TiO₂ thin film thickness dependence on spray cycle numbers and solution concentration (a) 0.1M and (b) 0.2M. Film thickness values obtained from SEM-cross section images and UV-Vis spectroscopy using Fizeau method.

The thickness of TiO₂ films deposited from the 0.1 M solution increased from 170 to 640 nm by increasing the number of spray cycles from 6 to 21. The thickness of the TiO₂ films deposited from the 0.2 M solution increased from 210 to 860 nm by increasing the number of spray cycles from 6 to 18. As expected, the thickness of the films deposited from the 0.2 M solution was slightly higher than that the ones from the 0.1 M solution due to the higher solution concentration. The slight discrepancy in the thickness values obtained from SEM and total transmittance for the 15-cycled TiO₂ film could originate from the local thickness measured by SEM and the average thickness obtained by UV-VIS spectroscopy.

The transmittance spectrum revealed that all films were transparent in the spectral range 250–800 nm and demonstrated the average transmittance of 70–80% [paper III, Figure 4], regardless of the solution concentration and the spray cycle numbers. A Tauc plot was applied to determine the indirect bandgap of TiO₂ films; the obtained values for all films remained at 3.40 ± 0.05 eV.

To summarize, both the solution concentration and number of spray cycles influence the film thickness and affect the surface morphology, as shown above. The TiO₂ film

thickness is increased with increasing the solution concentration from 0.1 M to 0.2 M and with increasing the number of spray cycles from 2 to 15. The surfaces of the TiO₂ thin films from the 0.1 M solution with 2 and 6 spray cycles consisted of fine grains of ca. 20–40 nm, while those of the TiO₂ films deposited from the 0.2 M solution had larger grain sizes of ca. 50–70 nm. However, agglomerated grains were observed on TiO₂ films prepared with 15 spray cycles, regardless of the solution concentration. The mean crystallite size increased from 25 nm to 50 nm by increasing the number of cycles from 2 to 15, similar to the behavior of the film thickness. A slightly larger mean crystallite size was found in the TiO₂ films deposited from the 0.1 M solution than in those deposited the 0.2 M solution. Based on the optical studies, the TiO₂ film thickness increased from 50 to 800 nm with increases in the precursor concentration from 0.1 to 0.2 M and in the number of spray cycles from 1 to 21. All TiO₂ films exhibited a total transmittance of 70%–80% in the visible spectral region.

3.3.2. Photocatalytic activity

The influence of film thickness on the photocatalytic performance was determined by stearic acid degradation test under UV-A light irradiation over TiO₂ thin films prepared using 0.1M and 0.2M solutions.

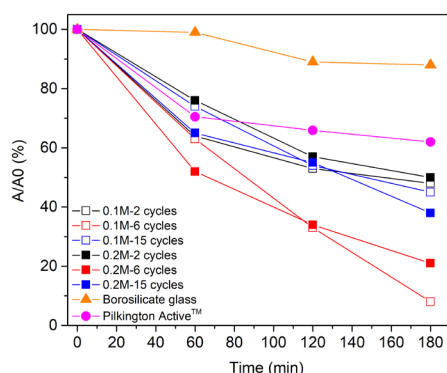


Figure 3.9. The degradation of stearic acid as a function of ultraviolet (UV-A) irradiation time on TiO₂ films deposited from 0.1 and 0.2M solution applying 2, 6, and 15 spray cycles.

TiO₂ films deposited using 2 (thickness ca. 50–65 nm) and 15 spray cycles (thickness 450 nm (0.1M) and 635 nm (0.2M)) showed ca. 50% degradation of stearic acid in 180 min under UV-A irradiation (Figure 3.9). TiO₂ films deposited using 6 spray cycles (thickness ca. 170 nm (0.1 M) and 210 nm (0.2 M)) showed ca. 90% degradation of stearic acid after 180 min of UV-A irradiation. For comparison, the commercial self-cleaning glass Pilkington Activ™ (thickness ca. 65 nm) showed 35% stearic acid degradation, which was approximately 1.4 times lower than that of the sprayed TiO₂ films with similar thicknesses of ca. 50–60 nm (2 spray cycles) under the same measurement conditions (Figure 3.9).

The reaction rate (k) constants of stearic acid degradation on the TiO₂ films from 0.1 M and 0.2 M solutions as a function of spray cycles and Pilkington Activ™ as a reference are presented in Figure 3.10.

The TiO₂ films deposited from both 0.1 M and 0.2 M solutions employing 6 and 7 spray cycles showed reaction rate constants almost 3.5 times higher than those of the films with other thicknesses in both solution series (Figure 3.10). The lower photodegradation

rate of the TiO₂ films prepared using 1, 2, and 3 spray cycles (<100 nm in thickness) compared to the 200 ± 30-nm-thick-TiO₂ films was due to their lower absorption of UV-A light [see Figure 5 in paper III], which provided more photogenerated reaction carriers. However, thicker TiO₂ films (>200 ± 30 nm) deposited with more than 7 spray cycles showed a decrease in their photocatalytic activity irrespective of the solution concentration. This phenomenon is characteristic of thin films [146–147] and has been explained by the increased recombination rate of photoinduced charge carriers [146, 148].

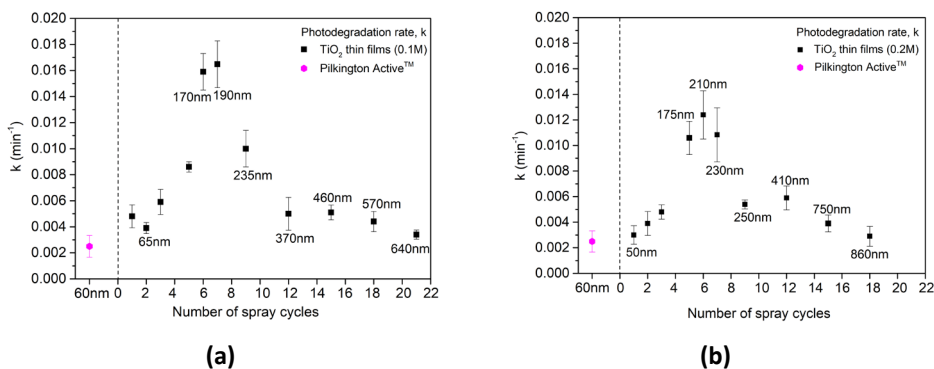


Figure 3.10. Photodegradation rate constant (k) values of stearic acid (standard errors shown by errors bars) for TiO₂ films deposited from solution with a concentration of (a) 0.1M and (b) 0.2M as a function of the number of spray cycles.

TiO₂ films prepared from the 0.1 M solution with 7 spray cycles (Figure 3.10a) showed a slightly higher reaction rate constant of 0.01648 min⁻¹ compared to the film with similar thickness (5 cycles) obtained from the 0.2 M solution of 0.01094 min⁻¹ (Figure 3.10). TiO₂ films deposited from the 0.1 M solution showed favourable combinations of multiple film properties, such as a higher mean crystallite size (45 nm vs. 35 nm), with smaller grain size (20–40 nm vs. 70 nm), thus enhancing the photocatalytic activity.

In summary, the 150–250-nm-thick-TiO₂ thin films could be of particular interest for the development of photocatalytic materials as they entail a low manufacturing cost because they achieve the higher performance with the lower precursor concentration (0.1 M TTIP) without requiring higher film thickness values. Moreover, the current work confirms that in the case of solution-based chemical methods, not only the film thickness but also the solution concentration-derived effects on film properties should be considered in optimizing the deposition protocol for the TiO₂ thin films. However, further studies are required to interpret the decrease in the reaction rate after reaching the maximum photocatalytic activity at a thickness of ca 250 nm.

Conclusion

This thesis discussed the properties of TiO₂ thin films deposited by ultrasonic spray pyrolysis as semiconductor photocatalysts. The novelty of this study lies in the creation of new knowledge on optimal deposition conditions for TiO₂ thin films, confirmed by the systematic study of degradation of several VOCs using multi-section plug-flow reactor or stearic acid degradation test. This work extends the potential of ultrasonic spray pyrolysis deposited TiO₂ thin films in large-area and transparent photocatalytic air- and self-cleaning applications in building elements.

Therefore, the main highlights from the thesis can be summarized as follows:

1. TiO₂ thin films, deposited onto window and borosilicate glass by ultrasonic spray pyrolysis in the temperature range of 250–450 °C and annealed at 500 °C for 1 h in air, showed the thicknesses of 110–330 nm and root mean square roughness of 0.6–1.2 nm. All films comprised of crystalline anatase phase. The mean crystallite size remained in the range of 13–35 nm and 22–26 nm for the films sprayed onto window and borosilicate glass substrates, respectively. The total transmittance of TiO₂ films was ca. 80% in the visible spectral range and the bandgap was 3.4 eV. The wettability test results showed that the surfaces of the TiO₂ thin films exhibited superhydrophilic behaviour after 30 min of UV treatment ($WCA \leq 10^\circ$). The XPS study revealed that the surface of TiO₂ films deposited at 350 °C possessed higher [Vo]/[Ti-O] and [OH⁻]/[Ti-O] ratio than in the case of the films deposited at 450 °C. Moreover, TiO₂ films deposited onto window glass possessed higher Na concentrations (ca. 10.0 at.%) on the film surfaces compared to those deposited on borosilicate glass (3.0 at.%). TiO₂ thin films deposited at 350 °C on window glass showed ca. 80% of MTBE degradation (inlet concentration of 10 ppm) at photocatalytic coating area of 600 cm² (residence time 78.0 s), while those deposited on borosilicate glass showed 100% conversion of MTBE from the surface area of 480 cm² (residence time 62.4 s). These results revealed that the surface chemical composition of TiO₂ films deposited by ultrasonic spray pyrolysis dependent on the deposition temperature and substrate type. The results revealed the crucial role of TiO₂ thin film properties upon the gas-phase photocatalytic activity of TiO₂ thin films deposited by ultrasonic spray pyrolysis.
2. TiO₂ films with a thickness of 190 nm, deposited onto borosilicate glass at 350 °C and annealed at 500 °C for 1 h in air, exhibited degradation of 90% acetone (inlet concentration of 10 ppm) and 75% acetaldehyde (inlet concentration of 10 ppm) at a residence time of 78 s under dry-air (6% RH) conditions without the formation of gas-phase intermediate decomposition products. Complete degradation of MTBE (inlet concentration of 10 ppm) and 80% conversion of acetaldehyde (inlet concentration of 10 ppm) were achieved under humid-air (40% RH) conditions at a residence time of 78 s. The VOC conversion was increased with increasing the airflow rate from 0.5 to 1.0 L·min⁻¹ for heptane (from 25 to 34%), acetone (from 38 to 47%), acetaldehyde (from 47 to 64%), and MTBE (from 86 to 100%) at the residence time of 31.2 s, relative humidity 6% and VOCs initial concentration of 5 ppm. TiO₂ thin films showed photocatalytic performance under visible light, degrading 60% MTBE and 33% acetone (with inlet concentration of 5 ppm). The results showed that TiO₂ thin films can degrade several VOCs under different measurement conditions.

3. TiO₂ thin films deposited on borosilicate glass at 350 °C from a solution with titanium(IV)isopropoxide concentration of 0.1 M and 0.2 M resulted in film thickness from 65 to 640 nm and from 50 to 860 nm, respectively, with increasing the number of spray cycles in the range of 1-21. XRD studies showed that the mean crystallite size of anatase phase remained in the range of 30–50 nm and 25–40 nm for films deposited from 0.1 M and 0.2 M solutions, respectively. All TiO₂ films demonstrated a total transmittance of 70%–80% in the visible spectral range. The photocatalytic and self-cleaning activity of TiO₂ thin films was studied by the stearic acid degradation test under UV-A light. The TiO₂ thin film with a thickness of 190 nm and 210 nm deposited from 0.1M and 0.2M solution, respectively, exhibited highest activity towards stearic acid degradation under UV-A radiation with a corresponding reaction rate constant $k = 0.0016 \text{ min}^{-1}$ and $k = 0.011 \text{ min}^{-1}$. For comparison, commercial Pilkington Activ™ self-cleaning glass showed $k = 0.003 \text{ min}^{-1}$.

This study revealed that the optimal conditions for TiO₂ thin films by ultrasonic spray pyrolysis for photocatalytic air- and self-cleaning applications are: the concentration of titanium (IV)isopropoxide in the spray solution 0.1 M, deposition temperature 350 °C and the film thickness ca. 200 nm.

This thesis introduces the ultrasonic spray pyrolysis method as a viable method for the deposition of TiO₂ thin films. The developed TiO₂ thin films exhibit potential applicability as future coating materials for air-cleaning window and coatings also exhibit self-cleaning abilities.

References

- [1] E. Keidel, Die beeinflussung der lichtechtheit von teerfarblacken durch titanweiss. *Farben-Zeitung*, vol. 34, p. 1242–1243, 1929.
- [2] C.F. Goodeve, J.A. Kitchener, Photosensitisation by titanium dioxide. *Trans. Faraday Soc.*, vol. 34, p. 570–579, 1938.
- [3] A. Fujishima, K. Honda, Electrochemical photolysis of water at a semiconductor electrode. *Nature*, vol. 238, p. 37–38, 1972.
- [4] A. Fujishima, K. Kohayakawa, K. Honda, Hydrogen production under sunlight with an electrochemical photocell. *J. Electrochem. Soc.*, vol. 122, Issue 11, p. 1487, 1975.
- [5] A. Fujishima, K. Honda, A Hydrogen/oxygen drawing method using electrochemical photoelectric cells. Japan Patent Office (JPO) JPS51123779A, 1975.
- [6] M. Kaneko and I. Okura, *Photocatalysis: Science and Technology*, Berlin, Springer Heidelberg, 2002.
- [7] A.O. Ibhaddon, P. Fitzpatrick „Heterogeneous photocatalysis: Recent advances and applications.” *Catalysts*, vol. 3, p. 189–218, 2013.
- [8] W. S. Verbruggen, TiO₂ photocatalysis for the degradation of pollutants in gas phase: From morphological design to plasmonic enhancement. *J. Photochem. Photobiol C: Photochemistry Reviews*, vol. 24, p. 64–82, 2015.
- [9] K.Nakata, A. Fujishima, TiO₂ photocatalysis: Design and applications. *J. Photochem. Photobiol C: Photochemistry Reviews*, vol. 13, p. 169–189, 2012.
- [10] Y.A. Shan, M.I.T. Ghazi, A. S. Rashid Immobilisation of titanium dioxide onto supporting materials in heterogeneous photocatalysis: A review. *Appl. Catal. A: General*, vol. 389, p. 1–8, 2010.
- [11] K. Schnelle, R. Dunn, M. Ternes, *Air Pollution Control Technology Handbook*, Boca Raton, Taylor & Francis Group, 2016.
- [12] P.V. Laxma Reddy, K. Ki-Hyun, K.Yong-Hyun, A Review of photocatalytic treatment for various Air Pollutants. *Asian J. Atmos. Environ.*, vol. 5–3, p. 181–188, 2011.
- [13] D.M. Hernandez-Alonso, F. Fresno, S. Suarez, M.J. Coronado, Development of alternative photocatalysts to TiO₂: Challenges and opportunities. *Energy Environ. Sci.*, vol. 2, p. 1231–1257, 2009.
- [14] M.K. Lee, L. Chin Wei, K. Sing Ngai, J. Ching Juan, Recent developments of zinc oxide based photocatalyst in water treatment technology: A review. *Water Res.*, vol. 88, p. 428–448, 2016.
- [15] M.B. Tahir, G. Nabi, M. Rafique, N.R. Khalid, Nanostructured-based WO₃ photocatalysts: Recent development, activity enhancement, perspectives and applications for wastewater treatment. *Int. J. Environ. Sci. Technol.*, vol. 14, p. 2519–2542, 2017.
- [16] M.A. Al-Hamdi, U. Rinner, M. Sillanpää, Tin dioxide as a photocatalyst for water treatment: A review. *Process Saf. Environ. Prot.*, vol. 107 p. 190–205, 2017.
- [17] M. Mishra, D. Chun, α -Fe₂O₃ as a photocatalytic material: A review. *Appl. Catal. A: General*, vol. 498, p.126–141, 2015.
- [18] C.N.C. Hitam, A.A. Jalil, Review on exploration of Fe₂O₃ photocatalyst towards degradation of dyes and organic contaminants. *Journal of Environmental Management*, vol. 258, issues 15, p. 110050, 2020.
- [19] M. Miyauchi, A. Nakajima, T. Watanabe, K. Hashimoto, Photocatalysis and photoinduced hydrophilicity of various metal oxide thin films. *Chem. Mater.*, vol. 14, p. 2812–2816, 2002.

- [20] D.M.Hernández-Alonso, B.A. Hungria, A. Martinez-Arias, M.J. Coronado, J. Soria, EPR study of the photoassisted formation of radicals on CeO₂ nanoparticles employed for toluene photooxidation." *Appl. Catal. B: Environ.*, 50, p. 167–175, 2004.
- [21] F. Zhang, X. Wang, H. Liu, C. Liu, Y. Wan, Z. Cai Recent advances and applications of semiconductor photocatalytic technology. *Appl. Sci.*, vol. 9, p. 2489, 2019.
- [22] A.R. Khataee, M.B. Kasiri, Photocatalytic degradation of organic dyes in the presence of nanostructured titanium dioxide: Influence of the chemical structure of dyes. *J. Mol. Catal. A. Chem.*, vol. 328, p. 8–26, 2010.
- [23] D. Wood, S. Stephanie, S. Taylr, C. Elli, S. Bill, V. Heyst, An overview of photocatalyst immobilization methods for air pollution remediation. *Chem. Eng. J.*, vol. 391, p. 123490, 2020.
- [24] H. Ren, P. Koshy, W. Chen, S. Qi, C.C. Sorrell, Photocatalytic materials and technologies for air purification. *J. Hazard. Mater.*, vol. 325 p. 340–366, 2017.
- [25] R. Qian, H. Zong, J. Schneider, G. Zhou, T. Zhao, Y. Li, J. Yang, W.D. Bahnemann, H.J. Pan, Charge carrier trapping, recombination and transfer during TiO₂ photocatalysis: An overview. *Catalysis Today*, vol. 335 p. 78–90, 2019.
- [26] W. Chen, P. Koshy, Y. Huang, E. Adabifiroozjarei, Y. Yao, C.C. Sorrell, Effects of precipitation, liquid formation, and intervalence charge transfer on the properties and photocatalytic performance of cobalt- or vanadium-doped TiO₂ thin films. *Int. J. Hydrog. Energy*, vol. 41 p. 19025–19056, 2016.
- [27] S. Zhu, D. Wang, Photocatalysis: Basic principles, diverse forms of implementations and emerging scientific opportunities. *Adv. Energy Mater.*, vol. 7, 1700841, 2017.
- [28] Retrieved from www.ube.es/index.html
- [29] Retrieved from www.borgenmagazine.com/panasonics-photocatalytic-water-purification
- [30] A. Erkan, U. Bakir, G. Karakas, Photocatalytic microbial inactivation over Pd doped SnO₂ and TiO₂ thin films. *J. Photochem. Photobiol. A.: Chemistry*, vol. 184, issue 3, p. 313–321, 2006.
- [31] M. Sökmen, S. Değerli, A. Aslan, Photocatalytic disinfection of *Giardia intestinalis* and *Acanthamoeba castellanii* cysts in water. *Exp. Parasitol.*, vol. 119, issue 1, p. 44–48, 2008.
- [32] A.C. Linkous, J.G. Carter, B.D. Locuson, J.A. Ouellette, K.D. Slattery, A.L. Smith, Photocatalytic inhibition of algae growth using TiO₂, WO₃, and cocatalyst modifications. *Environ. Sci. Technol.*, vol. 34, p. 4754–4758, 2000.
- [33] Zan L., Fa W., Peng T., Gong Z. Photocatalysis effect of nanometer TiO₂ and TiO₂-coated ceramic plate on Hepatitis B virus. *J. Photochem. Photobio. B: Biology*, vol. 86, p. 165–169, 2007.
- [34] A.H. Foster, B.I. Ditta, S. Varghese, A. Steele, Photocatalytic disinfection using titanium dioxide: spectrum and mechanism of antimicrobial activity. *Appl. Microbiol. Biotechnol.*, vol. 90, p. 1847–1868, 2011.
- [35] S. Banerjee, D.D. Dionysiou, C.S. Pillai, Self-cleaning applications of TiO₂ by photo-induced hydrophilicity and photocatalysis. *Appl. Catal. B: Environ.*, vol. 176–177, p. 396–428, 2015.
- [36] P. Nostell, A. Roos, B. Karlsson, Optical and mechanical properties of sol-gel antireflective films for solar energy applications. *Thin Solid Films*, vol. 351, issue 1–2, p. 170–175, 1999.
- [37] K. Ichimura, S. Oh, M. Nakagawa, Light-Driven motion of liquids on a photoresponsive. *Surf. Sci.*, vol. 288, p. 1624–1626, 2000.

- [38] J. Cai, J. Ye, S. Chen, X. Zhao, D. Zhang, S. Chen, Y. Ma, S. Jin, L. Qi Self-cleaning, broadband and quasi-omnidirectional antireflective structures based on mesocrystalline rutile TiO₂ nanorod arrays. *Energy Environ. Sci.*, 5, 7575, 2012.
- [39] J. Zhao, X. Yang, Photocatalytic oxidation for indoor air purification: a literature review. *Build Environ.*, vol. 38, issue 5, p. 645–654, 2003.
- [40] A. Fujishima, X. Zhang, Titanium dioxide photocatalysis: present situation and future approaches. *C. R. Chimie*, vol. 9, p. 750–760, 2006.
- [41] J. Chen, C. Poon, Photocatalytic construction and building materials: From fundamentals to applications. *Build Environ.*, vol. 44 p. 1899–1906, 2009.
- [42] S.O. Hay, T. Obee, Z. Luo, T. Jiang, Y. Meng, J. He, S.C. Murphy, S. Suib, The viability of photocatalysis for air Purification. *Molecules*, vol. 20, p. 1319–1356, 2015.
- [43] H. Agbe, E. Nyankson, N. Raza, D. Dodoo-Arhin, A. Chauhan, G. Osei, V. Kumar, K. Kim, Recent advances in photoinduced catalysis for water splitting and environmental applications. *J. Ind. Eng. Chem. Res.*, vol. 72, p. 31–49, 2019.
- [44] Retrieved from www.prnewswire.com/news-releases/photocatalyst-market-size-is
- [45] Retrieved from www.futuremarketsinc.com/the-global-market-for-photocatalytic-nanocoatings
- [46] S. Wang, H.M. Ang, O.M. Tade, Volatile organic compounds in indoor environment and photocatalyticoxidation: State of the art. *Environ. Int.*, vol. 33, p. 694–705, 2007.
- [47] N.L. Nagda, H.E. Rector, A critical review of reported air concentrations of organic compounds in aircraft cabins. *Indoor Air*, vol. 13, p. 292–301, 2003.
- [48] A. Cincinelli, T. Martellini, Indoor air quality and health. *Int. J. Environ. Res. Public Health*, vol. 14, p. 1286, 2017.
- [49] Bilthoven Division Strategic approaches to indoor air policy-making. World Health Organization, 1999. Retrieved from apps.who.int/iris/handle/10665/108169
- [50] J. Namiesnik, T. Gorecki, B. Kozdron-Zabiegala, J. Lukasiak, Indoor air quality, pollutants, their sources and concentration levels. *Build. Environ.*, vol. 27, issue 3, p. 339–356, 1992.
- [51] M. Jafari, A.A. Khajevandi, S.A. Mousavi Najarkola, M.S. Yekaninejad, M.A. Pourhoseingholi, L. Omid, S. Kalantary, Association of sick building syndrome with indoor air parameters. *Tanaffos*, vol. 14, issue 1, p. 55–62, 2015.
- [52] A. Berenjian, N. Chan, J.H. Malmiri, Volatile organic compounds removal methods: A review. *Am. J. Biochem. Biotechnol.*, vol. 8, issue 4, p. 220–229, 2012.
- [53] Retrieved from www.epa.gov/report-environment/indoor-air-quality
- [54] P.A. Jones, Indoor air quality and health. *Atmos. Environ.*, vol. 33, p. 4535–4564, 1999.
- [55] I.F. Khan, Kr.A. Ghoshal, Removal of volatile organic compounds from polluted air. *J. Loss Prev Process Ind.*, vol. 13, p. 527–545, 2000.
- [56] W. Jo, K. Kim, K. Park, Y. Kim, H. Lee, J. Park, Comparison of outdoor and indoor mobile source-related volatile organic compounds between low-and high-floor apartments. *J. Environ. Res.*, vol. 92, p. 166–171, 2003.
- [57] S. Yang, V. Perret, C.H. Jörin, H. Niculita-Hirzel, G.J. Pernot, D. Licina, Volatile organic compounds in energy efficient dwellings in Switzerland. *Indoor Air*, vol. 30, p. 481–491, 2020.
- [58] M.C. Degallaix, Air cleaning devices: A growing market polluted by confusing communication-certified performances for air cleaners. *J. Rehva*, vol. 1, p. 49–51, 2017.

- [59] M.C. Schmidt, A.M Buchbinder, E. Weitz, M.F. Geiger, Photochemistry of the indoor air pollutant acetone on Degussa P25 TiO₂ studied by chemical ionization mass spectrometry. *J. Phys. Chem. A*, vol. 111, p. 13023–13031, 2007.
- [60] C.P. Chang, J.N. Chen, M.C. Lu, Heterogeneous photocatalytic oxidation of acetone for air purification by near UV-irradiated titanium dioxide. *J. Environ. Sci. Health A*, vol. 38, p. 1131–1143, 2003.
- [61] W.H. FarLend, Health and environmental effects document for N-Heptane: Final draft. United States Environmental Protection Agency, Washington DC, 1989.
- [62] S. Preis, L.J. Falconer, Asensio P.R., Santiago C.N., Kachina A., Kallas J. Photocatalytic oxidation of gas-phase methyl tert-butyl ether and tert-butyl alcohol. *Appl. Catal. B: Environ.*, vol. 64, p. 1–2, 79–87, 2006.
- [63] Indoor Environments Division Residential air cleaners: A technical summary portable air cleaners and furnace and HVAC filters. 3rd edition, US EPA, Washington DC, 1989.
- [64] Indoor Environments Division Guide to Air Cleaners in the Home.” US EPA, Washington DC, 2014 Retrieved from www.epa.gov/sites/production/files/2014-07/documents/aircleaners.pdf
- [65] Retrieved from <https://molekule.science/pros-cons-hepa-filter>
- [66] B. Pant, M. Park, S.J. Park, Recent advances in TiO₂ films prepared by sol-gel methods for photocatalytic degradation of organic pollutants and antibacterial activities. *Coatings*, vol. 9, p. 613, 2019.
- [67] T. Son Le, T. Hien Dao, D. Cuong Nguyen, H. Chau Nguyen, I.L. Balikhin, Air purification equipment combining a filter coated by silver nanoparticles with a nano-TiO₂ photocatalyst for use in hospitals. *Adv. Nat. Sci. Nanosci. Nanotechnol.*, vol. 6, p. 8, 2015.
- [68] Air science Technology Co., Ltd., Air Steril. Retrieved from www.airpurifier.com.hk/product-en.htm
- [69] V. Augugliaro, V. Loddo, M. Pagliaro, P. Giovanni, L. Palmisano, Clean by light irradiation: practical applications of supported TiO₂. Royal Society of Chemistry publishing, Cambridge, 2010.
- [70] M. Musa, J.M. Juoi, M.Z. Rosli, D.N. Johari, Effect of Degussa P25 on the morphology, thickness and crystallinity of sol-gel TiO₂ coating. *Solid State Phenom.*, vol. 268, p. 224–228, 2017.
- [71] N.S. Ali Shah, Z. Shah, M. Hussain, M. Khan, Hazardous effects of titanium dioxide nanoparticles in ecosystem. *Bioinorg. Chem. Appl.*, Article ID 4101735, p. 12, 2017.
- [72] W.K. Shah, W. Wenxin Li, A review on catalytic nanomaterials for volatile organic compounds VOC removal and their applications for healthy buildings. *Nanomaterials*, vol. 9, p. 910, 2019.
- [73] C.G. Granqvist, A. Azens, P. Heszler, L. B. Kish, L. Osterlund, Nanomaterials for benign indoor environments: Electrochromics for “smart windows”, sensors for air quality, and photo-catalysts for air cleaning. *Sol. Energy Mater. Sol. Cells*, vol. 91, p. 355–365, 2007.
- [74] H.A. Mamaghani, F. Haghghat, C. Lee, Photocatalytic oxidation technology for indoor environment air purification: The state-of-the-art. *Appl. Catal. B: Environ.*, vol. 203, p. 247–269, 2017.
- [75] A. Sclafani, L. Palmisano, M. Schiavello, Influence of the preparation methods of titanium dioxide on the photocatalytic degradation of phenol in aqueous dispersion. *J. Phys. Chem.*, vol. 94, p. 829–832, 1990.
- [76] B. Ohtani, O.O. Prieto-Mahaney, D. Li, R. Abe, What is Degussa (Evonik) P25? Crystalline composition analysis, reconstruction from isolated pure particles and photocatalytic activity test. *J. Photochem. Photobiol. A: Chem.*, vol. 216 p. 179–182, 2010.

- [77] N. Xu, H. Huang, H. Ouyang, H. Wang, Preparation of the heterojunction catalyst N-doping carbon quantum dots/P25 and its visible light photocatalytic activity. *Scientific Reports*, vol. 9, p. 9971, 2019.
- [78] Y. Lu, D. Wang, C. Ma, H. Yang, The effect of activated carbon adsorption on the photocatalytic removal of formaldehyde. *Build. Environ.*, vol. 45 p. 615–621, 2010.
- [79] M. Jafarikoju, M.M. Sohrabi, S.J. Royaei, A. Hassanvand, Evaluation and optimization of a novel immobilized photoreactor for the degradation of gaseous toluene. *Clean Soil Air Water*, vol. 43, p. 662–670, 2015.
- [80] T. Guo, Z. Bai, C. Wu, T. Zhu, Influence of relative humidity on the photocatalytic oxidation (PCO) of toluene by TiO₂ loaded on activated carbon fibers: PCO rate and intermediates accumulation. *Appl. Catal. B: Environ.*, 79, 171–178, 2008.
- [81] H. Einaga, S. Futamura, T. Ibusuki, Photocatalytic decomposition of benzene over TiO₂ in a humidified airstream. *Phys. Chem. Chem. Phys.*, vol. 1 p. 4903–4908, 1999.
- [82] J. Kirchnerova, M.L. Herrera Cohen, C. Guy, D. Klvana, Photocatalytic oxidation of n-butanol under fluorescent visible light lamp over commercial TiO₂ (Hombicat UV100 and Degussa P25). *Appl. Catal. A: Gen.*, 282, 321–332, 2005.
- [83] M. Hajaghazadeh, V. Vaiano, D. Sannino, H. Kakooei, R. Sotudeh-Gharebagh, P. Ciambelli, Heterogeneous photocatalytic oxidation of methyl ethyl ketone under UV-A light in an LED-fluidized bed reactor. *Catal. Today*, vol. 230 p. 79–84, 2014.
- [84] C.L. Bianchi, S. Gatto, C. Pirola, A. Naldoni, A. Di Michele, G. Cerrato, V. Crocellà, V. Capucci, Photocatalytic degradation of acetone, acetaldehyde and toluene in gas-phase: comparison between nano and micro-sized TiO₂. *Appl. Catal. B: Environ.*, vol. 146, p. 123–130, 2014.
- [85] J. Taranto, D. Frochot, P. Pichat, Photocatalytic treatment of air: comparison of various TiO₂, coating methods, and supports using methanol or n-octane as test pollutant. *Ind. Eng. Chem. Res.*, vol. 48, p. 6229–6236, 2009.
- [86] G. Vincent, P.M. Marquaire, O. Zahraa, Abatement of volatile organic compounds using an annular photocatalytic reactor: study of gaseous acetone. *J. Photochem. Photobiol. A: Chem.*, vol. 197 p. 177–189, 2008.
- [87] S.W. Verbruggen, K. Masschaele, E. Moortgat, T.E. Korany, B. Hauchecorne, J.A. Martens, S. Lenaerts, Factors driving the activity of commercial titanium dioxide powders towards gas phase photocatalytic oxidation of acetaldehyde. *Catal. Sci. Technol.*, vol. 2, p. 2311–2318, 2012.
- [88] J. Jeong, K. Sekiguchi, K. Sakamoto, Photochemical and photocatalytic degradation of gaseous toluene using short-wavelength UV irradiation with TiO₂ catalyst: comparison of three UV sources. *Chemosphere*, vol. 57, p. 663–671, 2004.
- [89] S. Preis, A. Kachina, N.C. Santiago, J. Kallas, The dependence on temperature of gas-phase photocatalytic oxidation of methyl tert-butyl ether and tert-butyl alcohol. *Catal. Today*, 101, 353–358, 2005.
- [90] E. Galanos, S. Pouloupoulo, C. Philippopoulos, Photocatalytic destruction of methyl-tert-butyl ether in the gas phase using titanium dioxide. *J. Environ. Sci. Health Part A* 37, 1665–1675, 2002.
- [91] S. Joks, D. Klauon, M. Krichevskaya, S. Preis, F. Qi, A. Weber, A. Moiseev, J. Deubener, Gas-phase photocatalytic activity of nanostructured titanium dioxide from flame aerosol synthesis. *Appl. Catal. B Environ.*, vol. 111–112, p. 1–9, 2012.
- [92] H. Dong, G. Zeng, L. Tang, C. Fan, C. Zhang, X. He, Y. He, An overview on limitations of TiO₂-based particles for photocatalytic degradation of organic pollutants and the corresponding countermeasures. *Water Research*, vol. 79 p. 128–146, 2015.

- [93] S. Biran Ay, N. Kosku Perkgoz, Nanotechnological Advances in catalytic thin films for green large-area surfaces. *J. Nanomater.*, Article ID 257547, p.20, 2015.
- [94] A. Antonello, G. Soliveri, D. Meroni, G. Cappelletti, S. Ardizzone, Photocatalytic remediation of indoor pollution by transparent TiO₂ films. *Catalysis Today*, vol. 230, p. 35–40, 2014.
- [95] O. Lyandres, D. Finkelstein-Shapiro, P. Chakthranont, M. Graham, A.K. Gray, Preferred orientation in sputtered TiO₂ thin films and its effect on the photo-oxidation of acetaldehyde. *Chem. Mater.*, vol. 24, p. 3355–3362, 2012.
- [96] B.I. Stefanov, G.A. Niklasson, C.G. Granqvist, L. Österlund, Gas-phase photocatalytic activity of sputter-deposited anatase TiO₂ films: Effect of (001) preferential orientation, surface temperature and humidity. *J. Catal.*, vol. 335, p. 187–196, 2016.
- [97] H. Tomaszewski, K. Eufinger, H. Poelman, D. Poelman, R. De Gryse, P. Smet, B.G. Marin, Effect of substrate sodium content on crystallization and photocatalytic activity of TiO₂ films prepared by DC magnetron sputtering. *Int. J. Photoenergy*, Article ID 95213, p. 5, 2007.
- [98] T. Takahashi, K. Prabakar, T. Nezuka, T. Yamazaki, Sputtering pressure dependent photocatalytic properties of TiO₂ thin films. *J. Vac. Sci. Technol. A*, vol. 24, p. 1161, 2006.
- [99] G.M. Nielsen, S. In, C.K.P. Vesborg, T. Pedersen, P.K. Almqvist, H.I. Andersen, O. Hansen, I.B. Chorkendorff, A generic model for photocatalytic activity as a function of catalyst thickness. *J. Catal.*, vol. 289, p. 62–72, 2012.
- [100] K. Sang-Jun, K. Ki-Joong, C. Min-Chul, J. Sang-Chul, B. Su-Il, C. Soon Kye, J. Woon-Jo, A. Ho-Geun, Photocatalytic activity of nanosized TiO₂ thin film prepared by magnetron sputtering method. *J. Nanosci. Nanotechnol.*, vol. 11, p. 2, 2011.
- [101] K. Kim, K.N. Dey, O.H. Seo, D.Y. Kim, C.D. Lim, M. Lee, Photocatalytic decomposition of toluene by nanodiamond-supported TiO₂ prepared using atomic layer deposition. *Appl. Catal. A: General*, vol. 408, p. 148–155, 2011.
- [102] W.S. Verbruggen, S. Deng, M. Kurttepel, J.D. Cott, M.P. Vereecken, S. Bals, J.A. Martens, C. Detavernier, Photocatalytic acetaldehyde oxidation in air using spacious TiO₂ films prepared by atomic layer deposition on supported carbonaceous sacrificial templates. *Appl. Catal. B: Environ.*, vol. 160–161, p.204–210, 2014.
- [103] P.O. Oviroh, R. Akbarzadeh, D. Pan, R.A. Coetzee Maarten, T. Jen, New development of atomic layer deposition: processes, methods and applications. *Sci. Technol. Adv. Mater.*, vol. 20, p. 469, 2019.
- [104] C.M. Blount, D. H. Kim, J. L. Falconer, Transparent thin-film TiO₂ photocatalysts with high activity. *Environ. Sci. Technol.*, vol. 35, p. 2988–2994, 2001.
- [105] C. Raillard, V. Hequet, P. Le Cloirec, J. Legrand, Photocatalytic oxidation of methyl ethyl ketone over sol-gel and commercial TiO₂ for the improvement of indoor air. *Water Sci. Tech.*, vol. 53, p. 107–115, 2006.
- [106] N. Negishi, S. Matsuzawa, K. Takeuchi, P. Pichat, Transparent micrometer-thick TiO₂ films on SiO₂-coated glass prepared by repeated dip-coating/calcination: characteristics and photocatalytic activities for removing acetaldehyde or toluene in air. *Chem. Mater.*, vol. 19, p. 3808–3814, 2007.
- [107] T. Watanabe, S. Fukayama, M. Masahiro, A. Fujishima, K. Hashimoto, Photocatalytic activity and photo-induced wettability conversion of TiO₂ thin film prepared by sol-gel process on a soda-lime glass." *J. Sol gel. Sci. Technol.*, vol. 19, p. 71–76, 2000.
- [108] E. Morten, M.E. Simonsen, M.B. Sørensen, E.G. Sjøgaard, Comparison of methods for evaluation of activity of photocatalytic films. *Environ. Sci. Pollut. Res.*, vol. 19 p. 3772–3781, 2012.

- [109] P. Kluson, H. Luskova, T. Cajthaml, O. Solcova, Non thermal preparation of photoactive titanium (IV) oxide thin layers." *Thin Solid Films*, vol. 495, p. 18–23, 2006.
- [110] J.M. Coronado, M.E. Zorn, I. Tejedor Tejedor, M.A. Anderson, Photocatalytic oxidation of ketones in the gas phase over TiO₂ thin films: a kinetic study on the influence of water vapor. *Appl. Catal. B-Environ.*, vol. 43, p. 329–344, 2003.
- [111] W. Ho, J. C. Yu, S. Lee, Photocatalytic activity and photo-induced hydrophilicity of mesoporous TiO₂ thin films coated on aluminum substrate. *Appl. Catal. B: Environ.*, vol. 73, p. 135–143, 2007.
- [112] N. Quici, M.L. Vera, H. Choi, G.L. Puma, D.D. Dionysiou, M.I. Litter, H. Destailat, Effect of key parameters on the photocatalytic oxidation of toluene at low concentrations in air under 254+185 nm UV irradiation. *Appl. Catal. B: Environ.*, vol. 95, p. 312–319, 2010.
- [113] Y. Pin-Chuan, H. Shih-Tse, L. Chi-Wen, H. Dao-Hong, Photocatalytic destruction of gaseous toluene by porphyrin-sensitized TiO₂ thin films. *J. Taiwan. Inst. Chem. Eng.*, vol. 42, p. 470–479, 2011
- [114] M. Addamo, V. Augugliaro, A. Di Paola, E. García-López, V. Loddo, G. Marci, L. Palmisano, Photocatalytic thin films of TiO₂ formed by a sol–gel process using titanium tetraisopropoxide as the precursor. *Thin Solid Films*, 516, 3802–3807, 2008.
- [115] E. Galanos, S. Pouloupoulos, C. Philippopoulos, Photocatalytic destruction of methyl tert butyl ether in the gas phase using titanium dioxide. *J. Environ. Sci. Heal. A.*, A37, 9, 1665–1675, 2002.
- [116] S. Biswas, A. Majumder, M. F. Hossain, T. Takahashi, A. Fujishima, Effect of annealing temperature on the photocatalytic activity of sol-gel derived TiO₂ thin films. *J. Vac. Sci. Technol. A*, vol. 26, p. 678, 2008.
- [117] W.H. Ching, M. Leung, D.Y.C. Leung, Solar photocatalytic degradation of gaseous formaldehyde by sol–gel TiO₂ thin film for enhancement of indoor air quality. *Solar Energy*, vol. 77, p. 129–135, 2004.
- [118] X. Zhao, M. Liu, Y. Zhu, Fabrication of porous TiO₂ film via hydrothermal method and its photocatalytic performances. *Thin Solid Films*, vol. 515, p. 7127–7134, 2007.
- [119] M. Miki-Yoshida, V. Collins-Martinez, P. Amezaga-Madrid, A. Aguilar-Elguezabal, Thin films of photocatalytic TiO₂ and ZnO deposited inside a tubing by spray pyrolysis. *Thin Solid Films*, vol. 419, p. 60–64, 2002.
- [120] O. Sugiyama, M. Okuya, S. Kaneko, Photocatalytic ability of TiO₂ porous film prepared by modified spray pyrolysis deposition technique. *J. Ceram. Soc. Jpn.*, vol. 117, issue 2, p. 203–207, 2009.
- [121] A. Nakajima, A. Nakamura, N. Arimitsu, Y. Kameshima, K. Okada, Processing and properties of transparent sulfated TiO₂ thin films using sol–gel method. *Thin Solid Films*, vol. 516, p. 6392–6397, 2008.
- [122] W. Xianyu, M.K. Park, W. Lee, Thickness effect in the photocatalytic activity of TiO₂ thin films derived from sol-gel process. *Korean J. Chern. Eng.*, vol. 18, p. 903–907, 2001.
- [123] G. Varshney, S. Kanel, D.M. Kempisty, V. Varshney, A. Agrawal, E. Sahle-Demessie, R.S. Varma, M.N. Nadagouda, Nanoscale TiO₂ films and their application in remediation of organic pollutants. *Coord. Chem. Rev.*, vol. 306, p. 43–64, 2016.
- [124] D. Perednis, L. Gauckler, Thin film deposition using spray pyrolysis. *J. Electroceramics*, vol. 14, p. 103–111, 2005.
- [125] S.M. Sabnis, P.A. Bhadane, P.G. Kulkarni, Process flow of spray pyrolysis technique. *IOSR J. Appl. Phy.*, vol. 4, Issue 5, p. 7–11, 2013.

- [126] C. Guild, S. Biswas, Y. Meng, T. Jafari, M.A. Gaffney, L. S. Suib, Perspectives of spray pyrolysis for facile synthesis of catalysts and thin films: An introduction and summary of recent directions. *Catal. Today*, vol. 238, p. 87–94, 2014.
- [127] S. Ifang, M. Gallus, S. Liedtke, R. Kurtenbach, P. Wiesen, J. Kleffmann, Standardization methods for testing photo-catalytic air remediation materials: Problems and solution. *Atmos. Environ.*, vol. 91, p. 154–161, 2014.
- [128] A. Nakaruk, D. Ragazon, C.C. Sorrell, Anatase thin films by ultrasonic spray pyrolysis. *J. Analytical and Appl. Pyrol.*, vol. 88, p. 98–101, 2010.
- [129] M. Kask, J. Bolobajev, M. Krichevskaya, Gas-phase photocatalytic degradation of acetone and toluene, and their mixture in the presence of ozone in continuous multi-section reactor as possible air post-treatment for exhaust from pulsed corona discharge. *Chem. Eng. J.*, vol. 399, 125815, 2020.
- [130] J. Montero, L. Österlund, Photodegradation of stearic acid adsorbed on copper oxide heterojunction thin films prepared by magnetron sputtering. *Chem. Eng.*, vol. 2, p. 40, 2018.
- [131] A.T. Oluwabi, I.O. Acik, A. Katerski, A. Mere, M. Krunks, Structural and electrical characterisation of high-k ZrO₂ thin films deposited by chemical spray pyrolysis method. *Thin Solid Films*, vol. 662, p. 129–136, 2018.
- [132] I. Oja, Mere, M. Krunks, R. Nisumaa, C-H. Solterbeck, M. Es-Sounic, Structural and electrical characterization of TiO₂ films grown by spray pyrolysis. *Thin Solid Films*, vol. 515, p. 664–677, 2006.
- [133] I. Gromyko, M. Krunks, T. Dedova, A. Katerski, D. Klauson, I. Oja Acik, Surface properties of sprayed and electrodeposited ZnO rod layers. *Appl. Surf. Sci.*, vol. 405, p. 521–528, 2017.
- [134] W.-F. Chen, P. Koshy, C.C. Sorrel, Effects of film topology and contamination as a function of thickness on the photo-induced hydrophilicity of transparent TiO₂ thin films deposited on glass substrates by spin coating. *J. Mater. Sci.*, vol. 51, p. 2465–2480, 2016.
- [135] H. Chen, C.E. Nanayakkara, V.H. Grassian, Titanium dioxide photocatalysis in atmospheric chemistry. *Chem. Rev.*, vol. 112, p. 5919–5948, 2012.
- [136] X. Pan, M. Yang, X. Fu, N. Zhang, Y. Xu, Defective TiO₂ with oxygen vacancies: synthesis, properties and photocatalytic applications. *Nanoscale*, vol. 5, p. 3601, 2013.
- [137] C. Guillard, B. Beaugiraud, C. Dutriez, J. Herrmann, H. Jaffrezic, N. Jaffrezic Renault, M. Lacroix, Physicochemical properties and photocatalytic activities of TiO₂-films prepared by sol-gel methods. *Appl. Catal. B: Environ.*, vol. 39, p. 331–342, 2002.
- [138] H. Tada, M. Tanaka, Dependence of TiO₂ photocatalytic activity upon its film thickness. *Langmuir*, vol. 13, p. 360–364, 1997.
- [139] H. Chen, C.E. Nanayakkara, V.H. Grassian, Titanium dioxide photocatalysis in atmospheric chemistry. *Chem. Rev.*, vol. 112, p. 5919–5948, 2012.
- [140] N. Sakai, A. Fujishima, T. Watanabe, K. Hashimoto, Quantitative evaluation of the photoinduced hydrophilic conversion properties of TiO₂ thin film surfaces by the reciprocal of contact angle. *J. Phys. Chem. B*, vol. 107, p. 1028–1035, 2003.
- [141] Y. Paz, A. Heller, Photo-oxidatively self-cleaning transparent titanium dioxide films on soda lime glass: The deleterious effect of sodium contamination and its prevention. *J. Mater. Res.*, vol. 12, p. 2759–2766, 1997.
- [142] H.J. Nam, T. Amemiya, M. Murabayashi, K. Itoh, Photocatalytic activity of sol-gel TiO₂ thin films on various kinds of glass substrates: The effects of Na⁺ and primary particle size. *J. Phys. Chem. B*, vol. 108, issue 24, p. 8254–8259, 2004.

- [143] J. Krýsaa, P. Novotná, Š. Kmenta, A. Mills, Effect of glass substrate and deposition technique on the properties of sol gel TiO₂ thin films. *J. Photoch. Photobio A*, vol. 222, p. 81–86, 2011.
- [144] B.B. Adormaa, W.K. Darkwah, Y. Ao, Oxygen vacancies of the TiO₂ nano-based composite photocatalysts in visible light responsive photocatalysis. *RSC Adv.*, vol. 8, p. 33551, 2018.
- [145] I. Oja Acik, A. Junolainen, V. Mikli, M. Danilson, M. Krunks, Growth of ultra-thin TiO₂ films by spray pyrolysis on different substrates. *Appl. Surf. Sci.*, vol. 256, p. 1391–1394, 2009.
- [146] C. Wu, C.Y. Lee, Y. Lo, C. Lin, C. Wu, Thickness-dependent photocatalytic performance of nanocrystalline TiO₂ thin films prepared by sol–gel spin coating. *Appl. Surf. Sci.*, vol. 280, p. 737–744, 2013.
- [147] J.K. Kumar, R.C.N. Raju, A. Subrahmanyam, Thickness dependent physical and photocatalytic properties of ITO thin films prepared by reactive DC magnetron sputtering. *Appl. Surf. Sci.*, vol. 257, p. 3075–3080, 2011.
- [148] A. Mills, A. Lepre, N. Elliott, S. Bhopal, P.I. Parkin, S.A. O’Neill, Characterisation of the photocatalyst Pilkington Activ™ a reference film photocatalyst? *J. Photoch. Photobiol. A. Chem.*, vol. 160, p. 213–224, 2003.

Acknowledgment

Firstly, I would like to express my sincere gratitude to my supervisors Prof. Ilona Oja Acik, Prof. Malle Krunk, and Dr. Atanas Katerski, for their guidance, patience, and generous supports throughout my doctoral research.

I would like to thank the co-authors and colleagues at the Department of Materials and Environmental Technology. I would like to say a special thank you to Dr. Marina Krichevskaya for her guidance, supports, and assistance with photocatalytic measurements performed in the Laboratory of Environmental Technology, Tallinn University of Technology.

I would like to acknowledge the following projects for the financial support during my doctoral research: Estonian Ministry of Education and Research project IUT194, Estonian research council grant PRG627, Tallinn University of Technology based financing project B24, and the European Union through the European Regional Development Fund project TK141 “Advanced materials and high-technology devices for energy recuperation systems,” and ASTRA “TUT Institutional Development Programme for 2016–2022” Graduate School of Functional Materials and Technologies (2014-2020.4.01.16-0032).

From the bottom of my heart, I would like to say a big thank you to my family, Camilo, Can, Kaan, and Erkin for being with me on this journey with their moral support and encouragement.

Abstract

TiO₂ thin films by ultrasonic spray pyrolysis for photocatalytic air-cleaning applications

Semiconductor photocatalysis is a developing technology for improving indoor air quality with the ability to remove volatile organic compounds (VOCs), bacteria, and fungi from indoor air. Some portable air cleaning devices comprising photocatalytic plates, coated with TiO₂ powder are commercially available. The main limitation of these devices is their use of commercial TiO₂ powders, which suffer from low adhesion properties.

TiO₂ thin films on large-area surfaces in building elements have been proposed due to the durable and functional features such as high mechanical resistivity, high transparency for window coatings, easy-to-clean surface, and cost-effectiveness. The photocatalytic performance of TiO₂ thin films depends on several factors, mostly related to the film properties, which are primarily determined by the film deposition method. Different techniques such as sputtering and sol-gel methods have been studied to achieve TiO₂ thin films suitable for air cleaning. Despite the favourable properties of ultrasonic spray pyrolysis, no publications on the gas-phase photocatalytic decomposition of common VOCs such as acetone and acetaldehyde on TiO₂ thin films fabricated by the ultrasonic spray pyrolysis method were found available.

Therefore, this thesis aims to fabricate photocatalytic TiO₂ thin films by ultrasonic spray pyrolysis, which will be suitable for air and self-cleaning applications. The scope of this work is to focus on the effects of the deposition temperature on decomposition of various VOCs under different operating parameters of the multi-section plug-flow reactor and of film thickness on the decomposition of stearic acid.

TiO₂ thin films were deposited by ultrasonic spray pyrolysis onto a window and borosilicate glass in the temperature range 250–450 °C. The sprayed TiO₂ thin films were smooth and compacted with thicknesses in the range 100–330 nm. All TiO₂ thin films consisted of anatase phase with mean crystallite sizes in the ranges 13–35 nm and 22–26 nm for the samples prepared on window and borosilicate glass substrates, respectively. The TiO₂ thin films deposited at 350 °C showed the highest amount of oxygen vacancies and hydroxyl groups on the film surfaces, as well as superhydrophilic behaviour.

In this work, for the first time, ultrasonically sprayed TiO₂ thin films prepared on borosilicate glass at 350 °C were evaluated for the photodegradation of methyl *tert*-butyl ether (MTBE), heptane, acetone, and acetaldehyde using a multi-section plug-flow reactor. The results showed that the TiO₂ films were effective in degrading MTBE (100%) and acetaldehyde (80%) in humid-air conditions (40% relative humidity) and high airflow rates (1.0 L·min⁻¹) under UV-A light. TiO₂ thin films deposited at 350 °C with a surface area of 600 cm² showed 60% MTBE and 33% acetone degradation under visible light.

The impact of film thickness on the photocatalytic activity of TiO₂ films was examined by the photodegradation of stearic acid under UV-A radiation. The optimum thicknesses of the TiO₂ films were in the range 170–230 nm, suggesting a photocatalytic efficiency ca 2.6 times higher than that of the reference sample of commercial Pilkington Activ™. Photocatalytic test results revealed that the 190 nm-thick-TiO₂ film deposited from an 0.1 M solution demonstrated the finest grain structure and the highest photocatalytic activity, contributing to ca. 95% degradation of stearic acid degradation in 180 min under UV-A light with a reaction rate constant $k = 0.01648 \text{ min}^{-1}$.

In conclusion, ultrasonic spray pyrolysis for the deposition of TiO₂ thin films in photocatalytic air-cleaning applications was reported for the first time in this thesis. The presented results are of practical importance in the development of TiO₂ films for low-cost and large-area fabrication for photocatalytic air-cleaning applications.

Lühikokkuvõte

TiO₂ õhukesed kiled ultraheli pihustuspürolüüsi meetodil õhu fotokatalüütiliseks puhastamiseks

Pooljuhtmaterjalidest valmistatud fotokatalüütilised pinnakatted on üks võimalikest tuleviku tehnoloogiatest siseruumide õhu kvaliteedi parandamisel. Antud tehnoloogia võimaldab lagundada siseruumide õhus leiduvaid lenduvaid orgaanilisi ühendeid, baktereid ja seeni. Täna turul olevates fotokatalüütilistes õhupuhastuse seadmetes kasutatakse TiO₂ nanopulbrist kokkupressitud kihte. Sellise tehnoloogia peamine kitsaskoht on TiO₂ nanopulbrist valmistatud kihtide nõrk adhesioon aluspinnaga. Alternatiivse lahendusena on välja pakutud suurepinnaliste ehituselementide nagu näiteks aknaklaaside katmine TiO₂ õhukese kilega. TiO₂ õhukese kile peamised eelised nanopulbrist koosneva pinnakatte ees on mehaaniline vastupidavus, läbipaistvus nähtava valguse piirkonnas, isepuhastusvõime ja kulutõhusus. TiO₂ õhukese kile saasteainete fotokatalüütilise lagundamise võimekus sõltub mitmest kile omadusest nagu struktuur, morfoloogia ja kile pinna keemiline koostis, mis omakorda on tingitud kilede sadestamise meetodite iseärasustest. Õhu puhastuse rakendust silmas pidades on kõige levinumad meetodid TiO₂ õhukese kilede sadestamiseks: magnetron pihustamine ja sool-geel meetodid. Hoolimata ultraheli pihustuspürolüüsi (USP) meetodi eelistest (võimalus efektiivselt katta suuri pindalasiid, protsessi kiirus ja lähtematerjali säästlik kasutus) ei ole uuritud sellel meetodil sadestatud TiO₂ kilede võimekust lagundada lenduvaid orgaanilisi ühendeid. Doktoritöö eesmärk oli töötada välja sadestustehnoloogia ultraheli pihustuspürolüüsi meetodil TiO₂ õhukese kilede valmistamiseks, mis on võimelised fotokatalüütiliselt lagundama lenduvaid orgaanilisi ühendeid ning on sobilikud kasutamiseks isepuhastuvate pinnakatetena. Töös uuriti kilede sadestustemperatuuri ja lahuse kontsentratsiooni mõju ultraheli pihustuspürolüüsi meetodil sadestatud TiO₂ õhukese kilede struktuursetele, optilistele ja morfoloogilistele omadustele ning erinevate mudelsaasteainete fotokatalüütilise lagundamise võimekusele.

TiO₂ õhukesed kiled sadestati ultraheli pihustuspürolüüsi meetodil akna- ja boorsilikaatklaasist alustele sadestustemperatuuride vahemikus 250–450 °C koos järelkuumutamisega 500 °C juures 1 tund. Saadud TiO₂ õhukesed kiled on järgmiste omadustega: optiline läbilaskvus nähtava valguse piirkonnas 80%, keelutsoon 3,4 eV ja kilede paksus vahemikus 100–330 nm. Kõik saadud kiled koosnesid TiO₂ anataasi faasist, mille keskmine kristalliidi suurus oli aknaklaasil vahemikus 13–35 nm ja boorsilikaatklaasil vahemikus 22–26 nm. TiO₂ kile pinna keemiline koostis määrati röntgen fotoelektronspektroskoopia meetodil. Mõõtmistulemuste analüüsist selgus, et 350 °C juures sadestatud kilede pind sisaldas suuremat hapniku vakantside ([Vo]/[Ti-O]) ja hüdroksüülrühmade ([OH⁻]/[Ti-O]) osakaalu võrreldes 450 °C juures sadestatud kilega. Lisaks sellele omasid 350 °C juures sadestatud kiled ka superhüdrofiilseid pinnaomadusi.

Dokoritöös testiti esmakordselt USP meetodil sadestatud TiO₂ kilede võimekust lagundada lenduvaid orgaanilisi ühendeid. Õhukese kilede fotokatalüütilist aktiivsust uuriti õhu mudelsaasteainete nagu metüül-tert-butüüleetri (MTBE), atsetooni, heptaani ja atseetaldehüüdi fotokatalüütilisel lagundamisel gaasifaasis. Kilede fotokatalüütilist aktiivsust uuriti mitme sektsiooniga fotokatalüütilises pidevvoolureaktoris, mille reaktori ühe sektsiooni fotokatalüütilise katte pindala on 120 cm², ja kogu reaktoris 600 cm².

Tulemustest selgus, et TiO₂ kiled, mis olid sadestatud 350 °C juures boorsilikaatklaasile, omasid kõige suuremat fotokatalüütilist aktiivsust mudelsaasteainete lagundamisel.

Temperatuuril 350 °C boorsilikaatklaasile sadestatud TiO₂ kile korral leiti, et fotokatalüsaatori 600 cm² suurune pind on efektiivne lagundama 100% MTBE, 93% atsetooni, 78% atsetaldehyüdi, 46% heptaani UV-A kiirguse all järgmiste mõõtmisparameetrite korral: saasteaine algkontsentratsioon 5 ppm, õhuvoolu kiirus 0,5 Lmin⁻¹ ja suhteline õhuniiskuse 6%. Mõlemad, nii suhtelise õhuniiskuse (40%) kui ka õhuvoolukiiruse suurendamine (1 Lmin⁻¹) avaldasid mõju saasteainete fotokatalüütilise lagundamise efektiivsusele. Nähtava valguse all lagundasid TiO₂ kiled 60% MTBE ja 33% atsetooni saasteaine algkontsentratsiooni 5 ppm, õhuvoolu kiiruse 0,5 Lmin⁻¹ ja suhtelise õhuniiskuse 6% juures. TiO₂ kile paksuse mõju fotokatalüütilisele isepuhastusvõimele uuriti steariinhappe fotodegradatsiooni teel UV-A kiirguse all. Leiti, et ultraheli pihustuspürolüüsi meetodil sadestatud TiO₂ kilede optimaalne paksus on vahemikus 170–230 nm, omades ca. 2,6 korda suuremat fotokatalüütilist efektiivsust kui tööstuslik Pilkington Activ™ klaas. Steariinhappe fotokatalüütilise lagundamise testide tulemused näitasid, et lähtelahusest, milles titaan(IV)isopropoksiidi kontsentratsioon on 0,1 M, sadestatud 190 nm paksune TiO₂ kile omab võrreldes 0,2 M lahusest sadestatud kilega suuremaid algomeerunud terade kogumike kile pinnal (20–40 nm vs 70 nm), suuremat ruutkeskmist pinnakaredust (1.6 nm vs 1.1 nm), suuremat keskmist kristalliidi suurust (45 nm vs 35 nm), mis päädivad kõrgema steariinhappe lagundamise kiiruskonstandiga ($k = 0,01648 \text{ min}^{-1}$ vs $0,01094 \text{ min}^{-1}$) UV-A valguse all 180 min jooksul.

Kokkuvõtteks: doktoritöös töötati välja tehnoloogilised parameetrid fotokatalüütiliselt aktiivse TiO₂ kile sadestamiseks USP meetodil. Esmakordselt näidati USP meetodil sadestatud TiO₂ kilede võimast lagundada lenduvaid orgaanilisi ühendeid kasutades testimiseks mitme sektsiooniga fotokatalüütilist pidevoolureaktorit. Eksperimentaalselt tehti kindlaks optimaalsed tehnoloogilised tingimused fotokatalüütiliselt aktiivsete TiO₂ kilede sadestamiseks USP meetodil: lähtelahuses titaan(IV)isopropoksiidi ja atsetüülatssetooni molaarsuhe on 1:4 ja titaan(IV)isopropoksiidi kontsentratsioon 0,1 M; sadestustemperatuur 350 °C ja kile paksus 200 nm. Esitatud tulemused on suure praktilise tähtsusega TiO₂ kilede väljatöötamisel suurte pindade katmiseks fotokatalüütiliste õhupuhastuse ja pindade isepuhastuse rakenduste jaoks.

Appendix 1

Publication I

I. Dunder, M. Krichevskaya, A. Katerski, I. Oja Acik. TiO₂ thin films by ultrasonic spray pyrolysis as photocatalytic material for air purification. Royal Society Open Science, 2019, 6, 181578.

Research



Cite this article: Dundar I, Krichevskaya M, Katerski A, Acik IO. 2019 TiO₂ thin films by ultrasonic spray pyrolysis as photocatalytic material for air purification. *R. Soc. open sci.* **6**: 181578. <http://dx.doi.org/10.1098/rsos.181578>

Received: 23 October 2018

Accepted: 21 January 2019

Subject Category:

Chemistry

Subject Areas:

materials science/inorganic chemistry/
environmental chemistry

Keywords:

TiO₂ thin film, spray pyrolysis, photocatalysis, air purification, superhydrophilicity, wettability

Authors for correspondence:

Ibrahim Dundar

e-mail: ibrahim.dundar@ttu.ee

Ilona Oja Acik

e-mail: ilona.oja@ttu.ee

One contribution to ISIEM2018 special collection.

This article has been edited by the Royal Society of Chemistry, including the commissioning, peer review process and editorial aspects up to the point of acceptance.



TiO₂ thin films by ultrasonic spray pyrolysis as photocatalytic material for air purification

Ibrahim Dundar¹, Marina Krichevskaya²,

Atanas Katerski¹ and Ilona Oja Acik¹

¹Department of Materials and Environmental Technology, Laboratory of Thin Film Chemical Technologies, and ²Department of Materials and Environmental Technology, Laboratory of Environmental Technology, Tallinn University of Technology, Ehitajate tee 5, 19086 Tallinn, Estonia

ID, 0000-0002-4519-7009

In this study, we showed that the TiO₂ thin films deposited onto window glass are practicable for air purification and self-cleaning applications. TiO₂ films were deposited onto window glass by ultrasonic spray pyrolysis method. Different deposition temperatures were used in the range of 250–450°C. The structural, morphological, optical properties and surface chemical composition were investigated to understand probable factors affecting photocatalytic performance and wettability of the TiO₂ thin films. The TiO₂ thin films were smooth, compacted and adhered adequately on the substrate with a thickness in the range of 100–240 nm. X-ray diffraction patterns revealed that all the TiO₂ thin films consisted of anatase phase structure with the mean crystallite size in the range of 13–35 nm. The optical measurements showed that the deposited films were highly transparent (approx. 85%). The wettability test results showed that the TiO₂ thin films sprayed at 350°C and 450°C and annealed at 500°C for 1 h were superhydrophilic. The photocatalytic activity of the films was tested for the degradation of methyl tert-butyl ether (MTBE) in multi-section plug-flow reactor. The TiO₂ film deposited at 350°C exhibited the highest amount of conversion of MTBE, approximately 80%.

1. Introduction

Volatile organic compounds (VOCs) are widespread air contaminants in both outdoors and indoors. VOCs cause serious diseases including damage to kidney, liver and central nervous system; eye, nose and throat irritation; loss of coordination and nausea. Some compounds cause cancer in animals; some are considered to cause cancer in humans [1].

Methyl tert-butyl ether (MTBE) is a VOC widely used as an octane number booster in fuels for gasoline engines and thus

contributing to the outdoor and indoor air pollution. Several studies have been done about photocatalytic decomposition of gas-phase MTBE on immobilized commercial TiO₂ (P25) (TiO₂, TiO₂/Pt-, S- and N-doped TiO₂) particles coated onto the support materials or walls of photocatalytic reactors, which are mostly annular tubular batch or continuous reactors [2–6]. In these studies, the effect of various reaction parameters such as temperature, initial MTBE concentration, oxygen concentration, residence time, relative humidity (RH) and the photocatalytic degradation of MTBE under visible light region were investigated.

TiO₂ exhibits a remarkable promise in the photocatalytic treatment of VOCs due to high photocatalytic activity under UV light and photostability. In addition, TiO₂ is chemically inert, corrosion resistant and inexpensive [7]. Generally, the immobilized form of TiO₂ photocatalyst has been prepared with either commercial TiO₂ nanopowders or thin films composed by nanosized TiO₂ crystals. Coatings prepared from nanopowders are less mechanically stable, i.e. have weaker adhesion to the substrate than thin films [8,9]. Moreover, the latest toxicity studies on TiO₂ powders indicated that TiO₂ nanoparticles, smaller than 20–30 nm, may cause a severe health risk [10,11]. Thus, the immobilization of TiO₂ with good adhesion, for example, in the form of thin films became a necessity to avoid the release of nanoparticles into the atmosphere. Nanopowder coating has low transmittance in the visible spectral range [12], which limits the field of applications as indoor or outdoor photocatalyst. TiO₂ thin films, however, are less studied in the gas-phase photo-oxidation due to the lower photocatalytic efficiency compared with the coatings made of commercial TiO₂ nanopowders [8].

To extend TiO₂ thin film applicability, a photocatalytic thin film must meet the following requirements: high photocatalytic activity, superhydrophilicity, high transparency, mechanical features regarding adhesion to substrate and stability against abrasion. A desirable coating technique that provides durable and stable coating, effective contact between the catalyst and the contaminant, cost-efficiency and suitability for large-scale applications [13] is needed to obtain the required material characteristics. Further, the deposition of TiO₂ photocatalyst onto window glass has a promising prospect for the degradation of air pollutants and self-cleaning application because window glass has significant market potential and is a cheap support material.

Different methods have been used to fabricate photoactive TiO₂ coatings with different characteristics for air purification such as sol–gel dip coating, spin coating [9,14], chemical vapour deposition [15], sputtering [16] and electrochemically assisted deposition [17]. Sol–gel dip coating is considered as the most common deposition method of photocatalytic TiO₂ coatings for the degradation of gaseous organic pollutants. However, despite the factors making it favourable such as simplicity and low-cost, it is not easy to fabricate the photocatalytic layer with desired mechanical properties [7].

Addamo *et al.* [9] have used sol–gel dip coating technique to deposit TiO₂ thin films of different thickness (100–300 nm; transparency 70%) on glass substrates and test their photocatalytic activity for degradation of gaseous 2-propanol. It was reported that the highest degradation rate was obtained on the film with the thickness value of 250 nm [9]. Ardizzone *et al.* [17] deposited single- and double-layer TiO₂ thin films on glass substrates by electrochemically assisted method. The average thickness of the films and transparency was 450 nm and 75%, respectively. TiO₂ thin films with double layer showed 100% ethanol (275 ppm) degradation in 120 min under UV irradiation [17].

Ultrasonic spray pyrolysis is a simple, fast, inexpensive and freely applicable method of deposition for large area coatings. Despite the easy scale-up in industry and the possibility to promptly cover large areas, to the best of our knowledge, there is a very limited number of studies about TiO₂ thin films deposited by ultrasonic spray pyrolysis in the literature. Da *et al.* [18] prepared TiO₂ and N-doped TiO₂ thin films, and Rasoulnezhad *et al.* [19] deposited TiO₂ and Fe-doped TiO₂ thin films on glass substrates by ultrasonic spray pyrolysis. The photocatalytic activity of coatings was studied by the degradation of methylene blue in aqueous phase under UV or visible light.

In a recent review paper on photocatalytic materials for air treatment, it has been noted that there are still a few investigations and explanations on the correlation between material properties and the photocatalytic activity towards specific VOC [20].

The present paper is a comprehensive study of unmodified TiO₂ thin film synthesized by ultrasonic spray pyrolysis and applied for the abatement of air pollutants. No publications on the decomposition of VOC MTBE on transparent TiO₂ thin films fabricated at different temperatures reporting their photocatalytic activity regarding the materials characteristics were found available, thus this study would supply more insights into this topic.

Therefore, the aim of the study was to deposit transparent TiO₂ thin films by ultrasonic spray pyrolysis and to investigate their structural, morphological, optical properties, surface chemical composition, wettability and photocatalytic activity toward MTBE conversion as a function of the deposition temperature. Multi-section plug-flow reactor was used for the study of photocatalytic activity of TiO₂ films.

2. Material and methods

2.1. Synthesis and materials characterization

TiO₂ thin films were deposited onto commercial window glass with a thickness of 2 mm by using the ultrasonic spray pyrolysis technique. The spray solution was composed of titanium (IV) isopropoxide (0.2 mol l⁻¹) and acetylacetone in a molar ratio of 1:4 in ethanol. The spraying rate was set up to 2.5 ml min⁻¹ and compressed air was applied as the carrier gas with a flow rate of 8 l min⁻¹. The distance of the ultrasonic nozzle to the hot plate, where the substrates were placed, was fixed at 7 cm. The number of spray cycles was set to six. The hot plate temperature was adjusted to 250°C, 350°C and 450°C, named as deposition temperature throughout the article. All as-deposited samples were annealed at 500°C for 1 h in air in a furnace Nabertherm L5/11/06D, and are named as as-prepared samples throughout the article.

X-ray diffraction (XRD) and Raman spectroscopy methods were used to investigate the structure of the samples. XRD patterns were recorded on a Rigaku Ultima IV diffractometer with Cu K α radiation ($\lambda = 1.5406 \text{ \AA}$, 40 kV at 40 mA). The measurements were carried out in 2 theta configurations with the scan range of 20–60°, with a scanning speed of 2° min⁻¹ and with a step of 0.02°. The mean crystallite size was calculated by the Scherrer method from the FWHM (full width at half maximum) of the (101) reflection of TiO₂ anatase phase. Raman spectra were obtained on a micro-Raman spectrometer HORIBA Jobin Yvon Model HR800 in the spectral range of 100–800 cm⁻¹. A 532 nm laser line was used for excitation, which gives 5 mW of power at 10 μ m laser spot size during the measurement.

The surface morphology of the samples was investigated by scanning electron microscopy (SEM) and atomic force microscopy (AFM) measurements. The surface morphology and the film thickness of the films were obtained with the help of Zeiss HR FESEM Ultra 55 scanning electron microscopy with an acceleration voltage of 4.0 kV. The surface morphology of the films was studied using NT-MDT Solver 47 PRO atomic force microscopy system, measurement was carried out in the non-contact mode with a resolution in the range of 3 nm, and the investigated area was 1000 \times 1000 nm per scan. The surface roughness analysis was carried out through the three-dimensional AFM scan, which was in accordance with the ISO 4287/1 standard. Water contact angle (CA) measurements were applied to investigate the wettability of the films. DSA 25 (KRÜSS Instrument) was used at room temperature, applying a sessile drop fitting method. Four spots were averaged for per substrate. UV-A irradiation in the surface wettability test was performed using Actinic BL 15 W fluorescent lamp (Philips), with max emission at 365 nm. X-ray photoelectron spectroscopy (XPS) study was performed with use of a Kratos Analytical AXIS ULTRA DLD spectrometer in conjunction with a 165 mm hemispherical electron energy analyser and delay-line detector. The analysis was carried out with monochromatic Al K α X-rays (1486.6 eV) operating at 15 kV and 225 W. All XPS spectra were recorded using an aperture slot of 300 \times 700 μ m and pass energy of 20 eV. Binding energy (BE) values for TiO₂ were calculated based on the C1s peak at 285.0 eV. The total transmittance spectra of the TiO₂ films on glass substrate and glass substrate as reference were measured in the 250–800 nm range using a Jasco V-670 UV-VIS-NIR spectrophotometer equipped with a 40 nm integrating sphere.

2.2. Evaluation of photocatalytic activity

The photocatalytic activity of thin films was studied following the photocatalytic degradation of model air pollutant MTBE (C₅H₁₂O) in gas phase. The inlet concentration of the gaseous pollutant was 10 ppm. The study of the photocatalytic activity of thin films was carried out in a multi-section plug-flow photocatalytic reactor. The multi-section reactor consists of five sections, where the section volume is 130 ml and the surface area of photocatalytic coating in one section of the reactor is 120 cm² with the overall surface area of 600 cm² in the whole reactor. Fourier transform infrared analyser (FT-IR, Interspec 200-X) with the Specac Tornado 8-m 1.33 l gas cell and in-line humidifier were assembled to

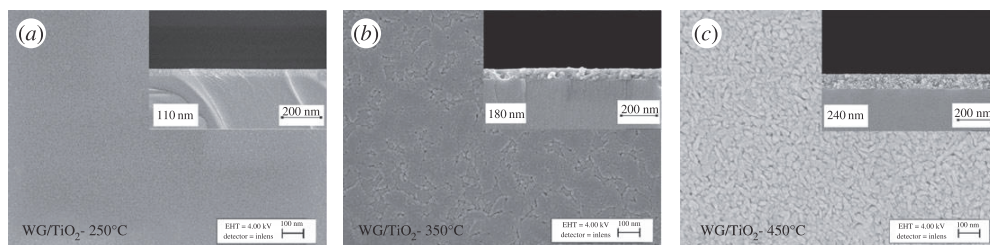


Figure 1. SEM surface images of TiO_2 thin films deposited on window glass at (a) 250°C, (b) 350°C, (c) 450°C, and annealed at 500°C for 1 h. Inset of figures (a), (b) and (c) shows the cross-sectional SEM images of the corresponding TiO_2 thin film.

Table 1. Summary of the morphological and structural properties of TiO_2 thin films deposited at different temperatures.

deposition temperature (°C)	thickness (nm)	RMS (nm)	phase	mean crystallinity size (nm)	degree of crystallinity (%)
250	110	n.a.	anatase	13	33
350	180	0.8	anatase	35	85
450	240	1.2	anatase	32	98

the reactor. A 15 W fluorescent lamp (Actinic BL, Philips) with UV-A emission intensity of 3.3 mW cm^{-2} (integrated into the range of 180–400 nm, with max emission at 365 nm, UV-B/UV-A ratio less than 0.2%) was placed over each section of the reactor. The RH in the gas stream was 6% determined at 20°C and temperature in the reactor was 30°C, maintained by the heat of the lamp and controlled with the temperature controller (Omega CN9000A).

The VOC feed tank was charged with polluted air by tank evacuation and injection of a respective amount of MTBE through the injection port. After 20 min of evaporation, the tank was filled with compressed air to pressure three bars and left for the balancing of concentration fluctuations for 90 min. The gas flow controller provided a gas flow rate of 0.5 l min^{-1} thus keeping the residence time of 15.6 s in the reactor section.

The MTBE peaks were measured at the IR bands from 1063 to 1124 cm^{-1} . The gas-phase intermediate product of photocatalytic oxidation of MTBE, tert-butyl formate (TBF), was also monitored quantitatively (at the IR bands from 1138 to 1190 cm^{-1}), by FT-IR outlet gas analysis using FDM VPFTIR HiRes quantitative spectra library. No other gas-phase products were observed, except carbon dioxide and water.

The reference experiments to examine the MTBE adsorption and photochemical degradation were carried out. No adsorption of MTBE on TiO_2 thin film catalyst in dark conditions was obtained. No photochemical decomposition of MTBE was observed under UV light in the absence of the catalyst. In both reference experiments, the initial concentration of pollutant remained unchanged (no difference between the reactor inlet and outlet) during 30 min of polluted air passing through the five sections of the reactor.

3. Results and discussion

3.1. Surface morphology

The SEM images of the TiO_2 films deposited onto window glass substrate at temperatures from 250°C to 450°C and annealed at 500°C for 1 h are presented in figure 1. The TiO_2 films are smooth, dense and free from cracks. According to the results, the surface morphology of the films deposited onto window glass changes with the increase of deposition temperature from 250°C to 450°C (figure 1a–c). The TiO_2 film deposited at 250°C has a plane surface structure and shows grains with a size of approximately 20 nm. The films deposited at 450°C have larger well-distinguished grains with a size of approximately 50 nm. TiO_2 film sprayed at 350°C has mixed surface morphology consisting of the morphology of the films deposited at 250°C and 450°C.

The thickness of all as-prepared thin films was determined from their SEM cross-sectional images. We observed that the TiO_2 thin films deposited on window glass have a thickness value of 110, 180 and 240 nm when grown at temperatures of 250, 350 and 450°C, respectively (table 1). The increase in the

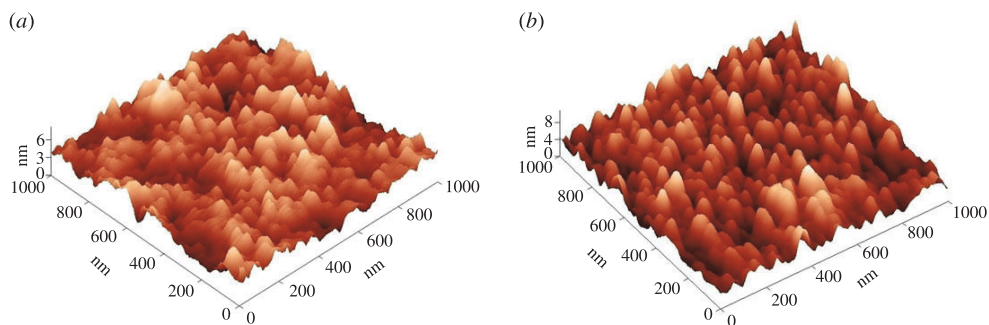


Figure 2. AFM images of TiO₂ thin films deposited on window glass at (a) 350°C and (b) 450°C and annealed at 500°C for 1 h.

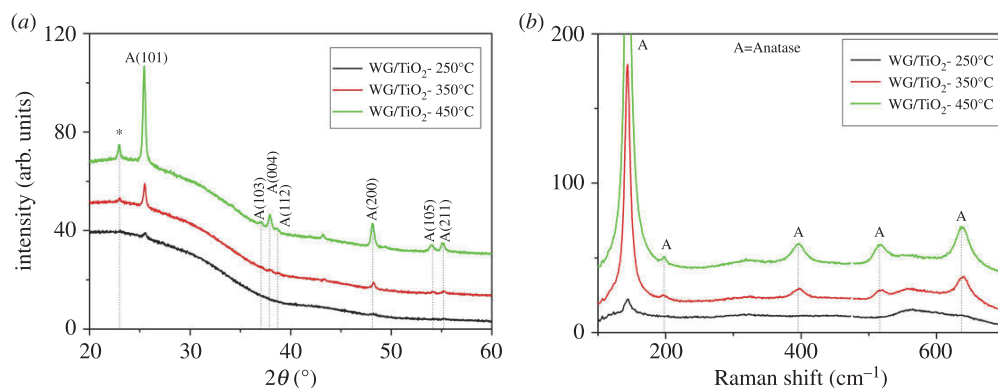


Figure 3. (a) XRD patterns and (b) Raman spectra of TiO₂ films deposited at 250°C, 350°C and 450°C onto window glass. All films were annealed at 500°C for 1 h in air.

film thickness with deposition temperature has been found also in other studies, e.g. in the case of ZrO₂ and TiO₂ deposition by spray pyrolysis [21,22].

Figure 2 shows the three-dimensional AFM deflection images of TiO₂ films deposited at 350°C and 450°C onto window glass and annealed at 500°C for 1 h (figure 2*a,b*). The surface morphology of TiO₂ film deposited at 350°C showed plane surface (figure 2*a*). The surface transforms to individually distinctive grains when increasing the deposition temperature to 450°C (figure 2*b*).

The root mean square (RMS) roughness was calculated from the AFM height profile of the scanned area of 1 × 1 μm. The TiO₂ thin film deposited at 350°C and 450°C showed RMS roughness values of 0.8 and 1.2 nm, respectively (table 1). The slightly higher RMS roughness of the TiO₂ film deposited at 450°C could be due to the different topography of the film and the cavities formed between the well-distinguished grains, also confirmed by SEM photos (figure 1*c*).

3.2. Structural properties

The XRD patterns of the TiO₂ films were analysed to obtain information on phase composition, the mean crystallite size and the degree of crystallinity. Figure 3*a* shows the XRD patterns of TiO₂ films deposited at 250°C, 350°C and 450°C onto window glass substrates and annealed at 500°C for 1 h in air. As shown in figure 3*a*, the XRD patterns of TiO₂ films exhibited diffraction peaks at 2 theta of 25.5°, 37.8°, 48.2°, 53.9° and 55°, which belong to the TiO₂ anatase structure [23]. Additional diffraction peak appeared at 2 theta of 22.9° belongs to SiO₂ from the substrate. No diffraction peaks corresponding to rutile or brookite phase of TiO₂ were observed. The mean crystallite size of TiO₂ was calculated from the (101) peak of anatase phase by the Scherrer formula. The mean crystallite size of films on window glass increased in the range of 13–35 nm with the increase of deposition temperature from 250°C to 450°C (table 1).

The degree of crystallinity of the TiO₂ thin films was determined by calculating crystalline/amorphous ratios based on scattered intensity (I) of anatase at 2 theta of 25.5° and 48.2° and intensity

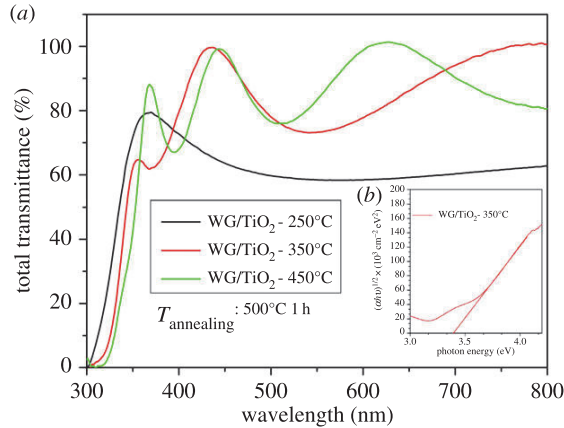


Figure 4. (a) Total transmittance spectra for TiO₂ thin films deposited at 250°C, 350°C and 450°C onto window glass and annealed at 500°C for 1 h. (b) The inset shows the band gap value of as-prepared TiO₂ sample deposited at 350°C.

from amorphous phase. The peak intensity of the amorphous phase was detected after applying profile fitting used for the separation of amorphous phase from crystalline phase (equation (3.1)) [24]

$$\text{Crystallinity, \%} = \frac{I_{\text{crystalline phase}}}{I_{\text{crystalline phase}} + I_{\text{amorphous phase}}} \quad (3.1)$$

The degree of crystallinity of the TiO₂ film grew from 33% to 98% with the deposition temperature increased from 250°C to 450°C (table 1). This confirms that the crystallization evolution of TiO₂ films is determined by the deposition temperature despite all samples being annealed at the same temperature. Similar behaviour, where the crystallinity of the film was controlled by both the deposition and annealing temperature, has been observed also for TiO₂ thin films deposited by pulsed pneumatic spray pyrolysis method [22].

Figure 3b shows the Raman spectra of the TiO₂ films deposited at different temperatures at 250°C, 350°C and 450°C onto window glass and annealed at 500°C for 1 h. The Raman spectra showed bands at 143 (*E_g*), 197 (*E_g*), 396 (*B_{1g}*) and 637 (*E_g*) cm⁻¹, which are characteristic of TiO₂ anatase phase with no peaks belonging to the rutile or brookite TiO₂ phase, thereby confirming the XRD results.

3.3. Optical properties

The optical transmittance spectra of TiO₂ thin films deposited at different temperatures and annealed at 500°C were measured in the wavelength range between 250 and 800 nm. The total transmittance of the TiO₂ film deposited at 350°C and 450°C is approximately 85% in the spectral region of 400–800 nm (figure 4a). The TiO₂ film deposited at 250°C showed lower optical transmittance compared with the films deposited at higher temperatures, which could be attributed to the differences in the nature of microstructure, thicknesses and surface morphology of the TiO₂ films.

Equation (3.2) was applied to determine absorption coefficient (α) to calculate the optical band gap value, where T and d represent the total transmittance of the film and the thickness of the film, respectively.

$$\alpha = \frac{\ln(1/T)}{d} \quad (3.2)$$

The band gap E_g was calculated using T_{auc} equation; k is constant, E_g is band gap ($n = 1/2$ for indirect or $n = 2$ for direct transitions) and $h\nu$ is the photon energy

$$\alpha = \frac{k(h\nu - E_g)^n}{h\nu} \quad (3.3)$$

Figure 4b presents the band gap values determined by extrapolating the linear region of the plot of $(ah\nu)^{1/2}$ against the photon energy to detect the indirect band gap values. TiO₂ thin films deposited at 250°C, 350°C and 450°C showed E_g values of 3.53, 3.38 and 3.41 eV, respectively. The optical band

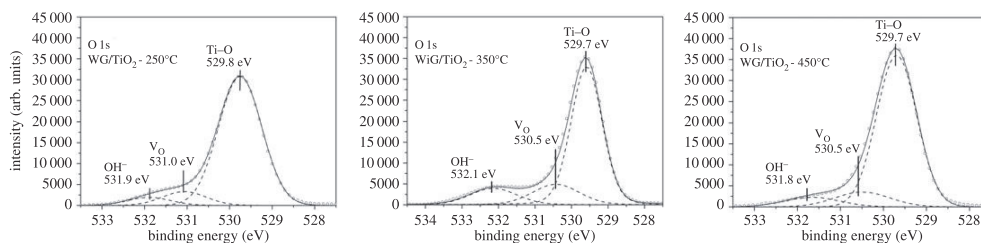


Figure 5. XPS spectra of as-prepared TiO_2 thin films deposited onto window glass substrates in the BE region of O1s.

gap value of bulk TiO_2 is 3.20 eV. The higher band gap value than that of the bulk TiO_2 has been observed in the different studies of the TiO_2 thin films deposited by spray pyrolysis methods [25,26].

3.4. Chemical composition and wettability

XPS studies were performed to investigate the chemical composition and bonding structure of the as-prepared TiO_2 thin films. Figure 5 shows the oxygen (O1s) core level spectra of the surface of TiO_2 films deposited at different temperatures and annealed at 500°C.

Lorentzian–Gaussian (function pseudo-Voigt) fitting analysis were used to deconvolute the asymmetric O1s core level peaks. Shirley type fitting was used as the background subtraction. In the O1s core level spectra of the as-prepared TiO_2 films (figure 5), the peak observed at BE value of 529.7 ± 0.3 eV is attributed to Me–O bond, thereby, it is ascribed to the presence of Ti–O bond. The peak observed at BE value of 530.5 ± 0.5 eV could be attributed to the presence of oxygen vacancies (V_O) [27,28]. The shoulder peak located at BE value of 532.1 ± 0.3 eV reveals that the surface of the TiO_2 film involves surface hydroxyl groups (OH^-) [28,29].

Atomic concentrations of the components such as Ti–O, V_O and OH^- found in the O1s core level spectrum were calculated from the integrated areas of O1s core level spectra by using Snowfields' cross-sections. Atomic ratios of the components $[\text{OH}^-]/[\text{Ti–O}]$ and $[\text{V}_\text{O}]/[\text{Ti–O}]$ are presented in table 2.

According to the $[\text{OH}^-]/[\text{Ti–O}]$ ratios (table 2), the amount of OH^- groups on the as-prepared TiO_2 films on window glass increased from 0.06 up to 0.18 at% with the increase in the deposition temperature from 250°C to 350°C. However, a slight drop in the $[\text{OH}^-]/[\text{Ti–O}]$ ratio was observed for the as-prepared TiO_2 film deposited at 450°C. A decrease in the amount of OH^- groups was observed in TiO_2 thin films deposited by sol–gel methods: Simonsen *et al.* [30] reported a decrease in OH^- groups on the microwave assisted sol–gel TiO_2 thin films with the increase in calcination temperature. Chen *et al.* [28] studied TiO_2 thin film grown by sol–gel spin coating and reported an increase in the number of hydroxyl groups with an increase of film thickness; but with a further growth of thickness a decrease in the amount of OH^- groups on the film surface was observed. Ennaceri *et al.* [31] reported gradual increase in the amount of surface OH^- groups with the increase in the thickness of the TiO_2 thin films deposited by ultrasonic spray pyrolysis. The results of the present study disagree with the observation study of Ennaceri *et al.* [31], because the TiO_2 thin film deposited at 450°C is thicker than the sample deposited at 350°C, showing the high influence of deposition temperature on the surface chemical features. Furthermore, following the $[\text{V}_\text{O}]/[\text{Ti–O}]$ ratios, the amount of oxygen vacancies on the surface of TiO_2 films increased with the increase in the deposition temperature from 250°C to 350°C (table 2). It was found that the highest amount of oxygen vacancies on the TiO_2 film surface belongs to the film fabricated at 350°C (table 2). The lower number of oxygen vacancies defects on TiO_2 thin film deposited at 450°C could be attributed to the higher deposition temperature: the intensive heat treatment could repair the oxygen vacancy defects. Liu *et al.* [32] studied TiO_2 thin films deposited by ultrasonic spray pyrolysis and annealed at different temperatures; a decrease in oxygen surface defects on TiO_2 thin film with an increase in annealing temperature was reported.

Thus, XPS results showed that the film deposited at 350°C has the highest amount of OH^- groups and oxygen vacancy defects and less carbon content on the surface of the film (table 2). The OH^- on TiO_2 surface are considered very effective for photocatalytic degradation of organic pollutants as they are generally the precursors of hydroxyl radicals. In addition, the surface oxygen vacancy defects are crucial because water can dissociate on oxygen vacancies with the formation of two bridging OH^- groups creating more OH^- groups on the film surface, which is beneficial for adsorbing VOCs by forming hydrogen bonds with functional groups [28,33]. The carbon impurities were found giving an

Table 2. Results of the XPS and the water CA studies of as-prepared TiO₂ thin films deposited onto window glass at different temperatures.

XPS study of as-prepared samples					CA value		
deposition temperature (°C)	Na (at%)	C (at%)	[Vo]/[Ti–O] (at%)	[OH]/[Ti–O] (at%)	as-prepared	UV treatment (30 min)	aged (three months)
250	13.0	18.3	0.10	0.06	~33° 	~7° 	~17° 
350	10.0	6.3	0.23	0.18	~7° 	~0° 	~10° 
450	11.0	9.8	0.13	0.13	~6° 	~0° 	~18° 

inhibiting effect to the active sites on the surface of TiO₂ thin films, and thus decreasing the photocatalytic activity [14].

Na⁺ content was analysed by XPS to estimate Na⁺ diffusion from the substrate to the film surface (table 2). According to XPS data (table 2), the amount of Na⁺ on the surface of TiO₂ films is 10–13 at%. Na⁺ content decreases with the increase in deposition temperature, which can be attributed to the higher film thickness, inhibiting diffusion of Na⁺ ions to the surface. The detrimental effect of Na⁺ diffusion from window glass to the film surface during the heat treatment was investigated in several studies. In this respect, different negative influences of Na⁺ diffusion on TiO₂ film properties have been proposed: disorder of crystallinity of TiO₂ [34,35], prevention of the formation of the anatase phase [36], the production of recombination centres for photogenerated electron–hole pairs [34,35].

Surface wettability of the TiO₂ films deposited at various temperatures was tested by measuring the water CA. Table 2 shows the average water CA values of the as-prepared, UV-treated and aged TiO₂ thin films. All as-prepared samples were stored in the plastic boxes for three months.

The surface wettability of as-prepared TiO₂ thin films depends on the deposition temperature. The film deposited at 250°C shows water CA value of around 33°, whereas the water CA value of the samples deposited at 350°C and 450°C is below 10°, confirming the superhydrophilic nature of the samples [37]. The superhydrophilic nature of the films deposited at 350°C and 450°C could be attributed to the higher content of OH[−] and Vo on the film surface compared with the film deposited at 250°C (table 2). It is commonly reported in the literature that as the OH[−] content on the film surface increases, van der Waals and hydrogen bonding between the OH[−] groups and water occurs, which is expected to augment the hydrophilicity, i.e. to enhance of the wetting [28,37]. Additionally, the presence of the surface oxygen defects enhance the wetting properties, leading to the trapping of OH[−] groups [28]. Simonsen *et al.* [30] studied the effect of OH[−] groups on superhydrophilic properties of TiO₂ thin films with different characteristics: a linear correlation between the OH[−] amount on the surface of the film and the water CA was observed. On the other hand, Chen *et al.* reported that the TiO₂ thin film which has the lowest level of OH[−] and Vo, also demonstrated the superhydrophilic property under UV light [28].

After UV treatment for 30 min, the water CA of all as-prepared samples drops below 10°, indicating superhydrophilic behaviour. Moreover, the UV-treated samples deposited at 350°C and 450°C showed the water CA value of 0° irrespective of the deposition temperature. Most often, the enhancement of wetting properties of TiO₂ surface under UV irradiation was attributed to the creation of photo-induced oxygen vacancies [28,37], reconstruction of the surface hydroxyl groups [37,38] and photo-induced removal of carbon residues on TiO₂ surface [37,39].

The UV-treated samples were aged by storing them in the plastic box for three months. The increase in water CA irrespective of the deposition temperature was observed (table 2), whereas the adsorption of carbon residues on the surface of TiO₂ films in air could be the reason of this tendency [40]. TiO₂ films deposited at 350°C exhibited less changes in water CA over time, compared to the other TiO₂ films. The

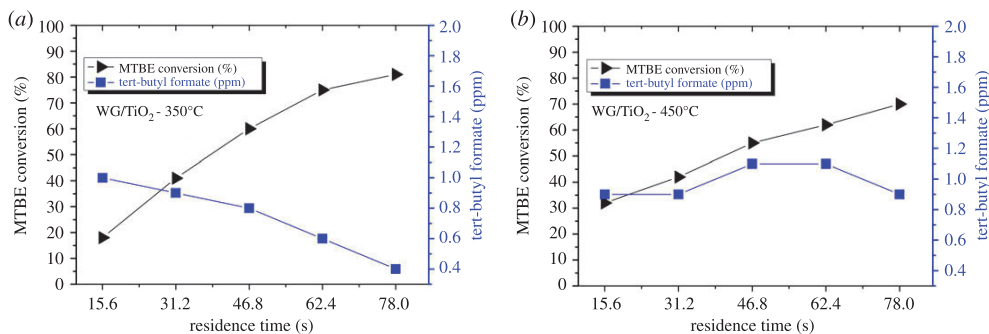


Figure 6. Photocatalytic conversion of MTBE on TiO_2 thin films deposited onto window glass at (a) 350°C and (b) 450°C . All samples were annealed at 500°C ; MTBE inlet concentration 10 ppm; RH 6%; reactor temperature 30°C .

TiO_2 films deposited on window glass at 350°C maintained their superhydrophilicity, i.e. a water CA of 10° even after a storage in a plastic box for three months.

3.5. Photocatalytic activity

Photocatalytic activity of TiO_2 thin films was studied following the photocatalytic gas-phase degradation of MTBE in the multi-section continuous plug-flow reactor at operating conditions kept constant for all the experimental runs: residence time 15.6 s per section, RH 6% and reactor temperature 30°C .

In different studies, acetone, TBF ($\text{C}_5\text{H}_{10}\text{O}_2$), isobutene and tert-butyl alcohol have been detected as the intermediate products of gas-phase photocatalytic degradation of MTBE apart from final oxidation products CO_2 and H_2O [4,41]. In this study, the only gas-phase intermediate product observed during the degradation of MTBE was TBF. Other intermediates presumably formed during further degradation of MTBE or TBF were not detected in gas phase; either they were adsorbed and degraded on the catalytic surface or desorbed in amounts lower than the detection limit of the analytical apparatus (less than 500 ppb).

The photocatalytic oxidation of MTBE characterized by its conversion defined as $(C_{\text{in}} - C_{\text{out}})/C_{\text{in}}$ (%) and the formation of TBF, are illustrated in figure 6 as a function of residence time which was increased by subsequent inclusion of reactor sections. Except for TiO_2 film deposited at 250°C , the degradation of MTBE was examined at five residence times, 15.6, 31.2, 46.8, 62.4 and 78.0 s, using one, two, three, four or all five sections of the reactor, respectively. The photocatalytic activity of TiO_2 thin films was first studied using one section of the reactor, i.e. 120 cm^2 of photocatalytic coating, where the film deposited at 250°C showed the lowest MTBE conversion of (approx. 4%). Thereafter, this was not synthesized in an amount needed for more extensive study. The lower activity of the TiO_2 film deposited at 250°C compared with the films deposited at higher deposition temperature could be attributed to the low crystallinity (table 1) and low OH^- content on the film surface (table 2).

A coating area of 600 cm^2 was applied in the study of photocatalytic activity of the films deposited at 350°C and 450°C . Figure 6 shows MTBE conversions, which, as expected, are higher at longer residence time.

TiO_2 thin film deposited at 350°C exhibited the highest MTBE conversion of approximately 80%. It should be emphasized that the TiO_2 film deposited at 450°C (approx. 70%) is less active than the TiO_2 film grown at 350°C despite the higher crystallization and smaller crystallite size (table 1). This could be explained by the mixed surface morphology of the sample deposited at 350°C if compared to the films deposited at 250°C and 450°C (figure 1) as well as by the higher amount of hydroxyl groups and oxygen defects (see §3.4).

Different stages of typical intermediate formation profile could be observed during the degradation of MTBE on TiO_2 photocatalytic thin films. The amount of TBF formed on the TiO_2 film deposited at 350°C is consistently decreasing (at 78 s only 5% of degraded MTBE appeared as gaseous TBF). Thus the rate of by-product degradation is higher than its formation rate (figure 6a). With the film deposited at 450°C on window glass, the trend towards TBF degradation is observed if residence time is longer than 62 s (about 13% of degraded MTBE formed TBF at 78 s of residence time). There have been several studies revealing that many factors can affect the formation of intermediates in the photodegradation reactions such as type of the catalyst and its amount, the technique used, etc. [41,42].

In the present study, the thickness of TiO₂ thin films increased with an increase to the deposition temperature (table 1). It has been reported [43] that higher photocatalytic activity is attributed to a rougher surface of the film with higher thickness. However, in several studies, it has been reported that with the further increase in the thickness of films, the length of the migration path of the carriers to the surface of the catalyst increases while their generation rate remains constant; the charge carriers experience higher recombination rates, resulting in an overall decrease in the photocatalytic activity [43]. This could be another reason of lower photocatalytic activity of the TiO₂ thin film deposited at 450°C if compared to the TiO₂ film deposited at 350°C.

Usually, it is quite difficult to compare the photocatalytic performance of thin films with that of coatings obtained from nanoparticles. The specific quantity of TiO₂ expressed as mg of titania per cm² of surface area of the coating could serve for a proper comparison of different studies regarding the photocatalytic oxidation of MTBE. In the present study, the specific quantity of TiO₂ in the film deposited at 350°C was around 0.2 mg cm⁻², achieving 80% conversion of MTBE on a coated window glass with the surface area of 600 cm². Preis *et al.* [6] reported the specific quantity of TiO₂ (P25) in the coated reactor (640 cm²) as 1.4 mg cm⁻². The 30% conversion of MTBE (inlet concentration of 100 ppm) with acetone detected as the only gas-phase by-product was observed in this reactor (the reactor temperature was 59.8°C). Galanos *et al.* [5] indicated the specific quantity of TiO₂ in the coated reactor as 3.5 mg cm⁻². This TiO₂ coating showed 90% of MTBE (500 ppm) conversion in up to 36.6 s of residence time. Acetone and TBF were the only intermediate by-products detected during the photocatalytic reaction. Park *et al.* [4] presented the calculated reaction rate values during the photocatalytic degradation of MTBE as a function of different specific quantities of TiO₂. It has been found that the highest reaction rate (0.85 μmol min⁻¹) was obtained with the TiO₂ (P25) coating of 0.6 mg cm⁻² and that the reaction rate stayed constant even after the increase in the specific catalyst quantity.

4. Conclusion

Highly transparent, smooth and crack-free TiO₂ thin films were deposited onto commercially available window glass by ultrasonic spray pyrolysis method in the temperature range of 250–450°C, followed by annealing at 500°C for 1 h in air. The effect of the deposition temperature on the morphological, structural, optical and surface chemical composition was examined to comprehend the factors affecting wettability and photocatalytic activity of the deposited TiO₂ films. According to SEM cross-sectional images, the thickness of the TiO₂ films increased from 110 to 240 nm with the increase of the deposition temperature from 250°C to 450°C. According to XRD, all as-prepared TiO₂ films possess anatase crystalline structure, and the degree of crystallinity increased from 33% to 98% with the increase of the deposition temperature from 250°C to 450°C. The mean crystallite size of the films was found to depend on the deposition temperature and remained in the range of 13–35 nm. Surface wettability test showed that as-prepared TiO₂ thin films sprayed at 350°C and 450°C are superhydrophilic [CA ≤ 10°], showing CA values of 7° and 6°, respectively, and CA value of 0° after 30 min UV treatment. The surface of the film deposited at 350°C remained superhydrophilic even after ageing for three months. According to the XPS study, the amount of oxygen defects and OH⁻ groups on the TiO₂ film surface depends on the deposition temperature. The TiO₂ thin film deposited at 350°C exhibited the highest amount of oxygen defects and OH⁻ groups on the film surface, and high amount of Na⁺ (10 at%).

This study showed, that transparent and superhydrophilic TiO₂ thin films with the specific quantity of 0.2 mg cm⁻² and surface area of 600 cm² is effective to degrade approximately 80% of MTBE and its intermediate product TBF; and is thereby prospective coating for self-cleaning and air purification applications.

Data accessibility. Data available from the Dryad Digital Repository: <https://datadryad.org/resource/doi:10.5061/dryad.b24p647> [44].

Authors' contributions. I.D. carried out the material synthesis and material characterizations (XRD, Raman spectroscopy, optical properties and wettability test), participated in data collection for photocatalytic activity test, participated in the design of the all figures and tables, and participated in writing of manuscript and drafted the manuscript. M.K. carried out photocatalytic activity test, interpretation of data and participated in writing of manuscript. I.O.A. carried out the design of the study, participated in data analysis and writing of the manuscript. A.K. participated in synthesis and made XPS data analysis. All authors gave final approval for publication.

Competing interests. We declare we have no competing interests.

Funding. I.D. is supported by the Estonian Ministry of Education and Research, Estonian Research Council project IUT19-4, Estonian Centre of Excellence project TK141 and EU regional Fund project 2014-2020.4.01.16-0032. I.O.A. and A.K. are supported by the Estonian Ministry of Education and Research, Estonian Research Council projects IUT19-4 and Estonian Centre of Excellence project TK141. M.K. is supported by the Estonian Ministry of Education and Research, Estonian Research Council projects IUT1-7. This work has been partially supported by ASTRA 'TUT Institutional Development Programme for 2016–2022' Graduate School of Functional Materials and Technologies (2014-2020.4.01.16-0032).

Acknowledgments. The authors acknowledge Dr V. Mikli for SEM, Dr M. Danilson for XPS measurements and Mr A. O. Titilope for AFM measurements.

References

- https://www.epa.gov/indoor-air-quality-iaq/volatile-organic-compounds-impact-indoor-air-quality (accessed August 2018).
- Preis S, Falconer JL, Asensio RP, Santiago NC, Kachina A, Kallas J. 2006 Photocatalytic oxidation of gas-phase methyl tert-butyl ether and tert-butyl alcohol. *Appl. Catal. B* **64**, 79–87. (doi:10.1016/j.apcatb.2005.11.002)
- Jo WK, Yang CH. 2010 Visible-light-induced photocatalysis of low-level methyl-tertiary butyl ether (MTBE) and trichloroethylene (TCE) using element-doped titanium dioxide. *Build. Environ.* **45**, 819–824. (doi:10.1016/j.buildenv.2009.08.021)
- Park SE, Joo H, Kang JW. 2003 Photodegradation of methyl tertiary butyl ether (MTBE) vapor with immobilized titanium dioxide. *Solar Energy Mater. Solar Cells* **80**, 73–84. (doi:10.1016/S0927-0248(03)00133-8)
- Galanos E, Pouloupou S, Philippopoulos C. 2002 Photocatalytic destruction of methyl-tert-butyl ether in the gas phase using titanium dioxide. *J. Environ. Sci. Health Part A* **37**, 1665–1675. (doi:10.1081/ESE-120015428)
- Preis S, Kachina A, Santiago NC, Kallas J. 2005 The dependence on temperature of gas-phase photocatalytic oxidation of methyl tert-butyl ether and tert-butyl alcohol. *Catal. Today* **101**, 353–358. (doi:10.1016/j.cattod.2005.03.015)
- Varshney G, Kanel SR, Kempisty DM, Varshney V, Agrawal A, Sahle-Demessie E, Varma RS, Nadagouda MN. 2016 Nanoscale TiO₂ films and their application in remediation of organic pollutants. *Coord. Chem. Rev.* **306**, 43–64. (doi:10.1016/j.ccr.2015.06.011)
- Paz Y. 2010 Application of TiO₂ photocatalysis for air treatment: patents' overview. *Appl. Catal. B* **99**, 448–460. (doi:10.1016/j.apcatb.2010.05.011)
- Addamo M, Augugliaro V, Di Paola A, Garcia-Lopez E, Loddo V, Marci G, Palmisano L. 2008 Photocatalytic thin films of TiO₂ formed by a sol-gel process using titanium tetraisopropoxide as precursor. *Thin Solid Films* **516**, 3802–3807. (doi:10.1016/j.tsf.2007.06.139)
- Wu J, Liu W, Xue C, Zhou S, Lan F, Bi L, Xu H, Yang X, Zeng FD. 2009 Toxicity and penetration of TiO₂ nanoparticles in hairless mice and porcine skin after subchronic dermal exposure. *Toxicol. Lett.* **191**, 1–8. (doi:10.1016/j.toxlet.2009.05.020)
- Skocaj M, Filipic M, Petkovic J, Novak S. 2011 Titanium dioxide in our everyday life; is it safe? *Radiol. Oncol.* **45**, 227–247. (doi:10.2478/v10019-011-0037-0)
- Arabatzi IM, Antonarakis S, Stergiopoulos T, Hiskia A, Papaconstantinou E, Bernard MC, Falaras P. 2002 Preparation, characterization and photocatalytic activity of nanocrystalline thin film TiO₂ catalysts towards 3,5-dichlorophenol degradation. *J. Photochem. Photobiol., A* **149**, 237–245. (doi:10.1016/S1010-6030(01)00645-1)
- Shayegan Z, Lee CS, Haghghat F. 2018 TiO₂ photocatalyst for removal of volatile organic compounds in gas phase—a review. *Chem. Eng. J.* **334**, 2408–2439. (doi:10.1016/j.cej.2017.09.153)
- Seo HO, Woo TG, Park EJ, Cha BJ, Kim IH, Han SW, Kim YD. 2017 Enhanced photocatalytic activity of TiO₂ films by removal of surface carbon impurities; the role of water vapor. *Appl. Surf. Sci.* **420**, 808–816. (doi:10.1016/j.apsusc.2017.05.223)
- Byun D, Jin Y, Kim B, Lee JK, Park D. 2000 Photocatalytic TiO₂ deposition by chemical vapour deposition. *J. Haz. Mater. B* **73**, 199–206. (doi:10.1016/S0304-3894(99)00179-X)
- Stefanov BI, Niklasson GA, Granqvist CG, Österlund L. 2016 Gas-phase photocatalytic activity of sputter-deposited anatase TiO₂ films: effect <001> preferential orientation, surface temperature and humidity. *J. Catal.* **335**, 187–196. (doi:10.1016/j.jcat.2015.12.002)
- Antonello A, Soliveri G, Meroni D, Cappelletti G, Ardizzone S. 2014 Photocatalytic remediation of indoor pollution by transparent TiO₂ thin films. *Catal. Today* **230**, 35–40. (doi:10.1016/j.cattod.2013.12.033)
- Da L, Zhang J, Shao L, Chaoyana C, Guiang L, Yuanzheng Y. 2011 Preparation and photocatalytic properties of nanometer TiO₂ thin films by improved ultrasonic spray pyrolysis. *Rare Met.* **30**, 233. (doi:10.1007/s12598-011-0276-7)
- Rasoulzadeh H, Hosseinzadeh G, Ghasemian N, Hosseinzadeh R, Keihan AH. 2018 Transparent nanostructured Fe-doped TiO₂ thin films prepared by ultrasonic assisted spray pyrolysis technique. *Mater. Res. Express* **5**, 056401. (doi:10.1088/2053-1591/aabe5e)
- Ren H, Koshy P, Chen W, Qi S, Sorrell CC. 2017 Photocatalytic material and technologies for air purification. *J. Hazard. Mater.* **325**, 340–366. (doi:10.1016/j.jhazmat.2016.08.072)
- Oluwabi AT, Aikio IO, Katerski A, Mere A, Krunk M. 2018 Structural and electrical characterisation of high-k ZnO₂ thin films deposited by chemical spray pyrolysis method. *Thin Solid Films* **662**, 129–136. (doi:10.1016/j.tsf.2018.07.035)
- Oja I, Mere A, Krunk M, Nisumaab R, Solterbeck C-H, Es-Souic M. 2006 Structural and electrical characterization of TiO₂ films grown by spray pyrolysis. *Thin Solid Films* **515**, 664–677.
- Powder Diffraction File (PDF), (PDF-2/Release 2013 RDB) (01-070-7348).
- https://www.rigaku.com/en/service/software (accessed August 2018).
- Rauta NC, Mathews T, Chandramohan P, Srinivasanb MP, Dasha S, Tyagi AK. 2011 Effect of temperature on the growth of TiO₂ thin films synthesized by spray pyrolysis: structural, compositional and optical properties. *Mater. Res. Bull.* **46**, 2057–2063. (doi:10.1016/j.materresbull.2011.06.043)
- Deshmukh HP, Shinde PS, Patil PS. 2006 Structural, optical and electrical characterization of spray-deposited TiO₂ thin films. *Mater. Sci. Eng. B* **130**, 220–227. (doi:10.1016/j.mseb.2006.03.016)
- Gromyko I, Krunk M, Dedova T, Katerski A, Klauson D, Oja Aikio I. 2017 Surface properties of sprayed and electrodeposited ZnO rod layers. *Appl. Surf. Sci.* **405**, 521–528. (doi:10.1016/j.apsusc.2017.02.065)
- Chen W, Koshy P, Christopher Sorrel C. 2016 Effects of film topology and contamination as a function of thickness on the photo-induced hydrophilicity of transparent TiO₂ thin films deposited on glass substrates by spin coating. *J. Mater. Sci.* **51**, 2465–2480. (doi:10.1007/s10853-015-9559-y)
- Jimmy C, Yu J, Yuk Tang H, Zhang L. 2002 Effect of surface microstructure on the photoinduced hydrophilicity of porous TiO₂ thin films. *J. Mater. Chem.* **12**, 81–85. (doi:10.1039/b102909f)
- Simonsen ME, Li Z, Søgaard EA. 2009 Influence of the OH groups on the photocatalytic activity and photoinduced hydrophilicity of microwave assisted sol-gel TiO₂ film. *Appl. Surf. Sci.* **255**, 8054–8062. (doi:10.1016/j.apsusc.2009.05.013)
- Ennaceri H, Boujnah M, Taleb A, Khalidoun A, Saez-Araoz R, Ennaoui A, El Kenz A, Benyoussef

- A. 2017 Thickness effect on the optical properties of TiO₂-anatase thin films prepared by ultrasonic spray pyrolysis: experimental and ab initio study. *Int. J. Hydrogen Energy* **42**, 19 467–19 480. (doi:10.1016/j.ijhydene.2017.06.015)
32. Liu H, Hong S, Sun W, Wei S, Yu S. 2015 TiO₂-based metal–semiconductor–metal ultraviolet photodetectors deposited by ultrasonic spray pyrolysis technique. *IEE Trans. Electron Dev.* **63**, 79–85. (doi:10.1109/TED.2015.2436701)
33. Zhong L, Haghghat F. 2015 Photocatalytic air cleaners and materials technologies, abilities and limitations. *Build. Environ.* **91**, 191–203. (doi:10.1016/j.buildenv.2015.01.033)
34. Novotna P, Krysa J, Maixner J, Kluson P, Novak P. 2010 Photocatalytic activity of sol–gel TiO₂ thin films deposited on soda lime glass and soda lime glass precoated with a SiO₂ layer. *Surf. Coatings Technol.* **204**, 2570–2575. (doi:10.1016/j.surfcoat.2010.01.043)
35. Zita J, Maixner J, Krysa J. 2010 Multilayer TiO₂/SiO₂ thin sol–gel films: effect of calcination temperature and Na⁺ diffusion. *J. Photochem. Photobiol., A* **216**, 194–200. (doi:10.1016/j.jphotochem.2010.07.030)
36. Krysa J, Novotna P, Kment S, Mills A. 2011 Effect of glass substrate and deposition technique on the properties of sol-gel TiO₂ thin films. *J. Photochem. Photobiol., A* **222**, 81–86. (doi:10.1016/j.jphotochem.2011.05.005)
37. Banerjee S, Dionysiou DD, Pillai SC. 2015 Self-cleaning applications of TiO₂ by photo-induced hydrophilicity and photocatalysis. *Appl. Catal., B* **176–177**, 396–428. (doi:10.1016/j.apcatb.2015.03.058)
38. Sakai N, Fujishima A, Watanabe T, Hashimoto K. 2001 Enhancement of the photoinduced hydrophilic conversion rate of TiO₂ film electrode surfaces by anodic polarization. *J. Phys. Chem. B* **105**, 3023–3026. (doi:10.1021/jp003212r)
39. Zubkov T, Stahl D, Thompson TL, Panayotov D, Diwald O, Yates JT. 2005 Ultraviolet light-induced hydrophilicity effect on TiO₂(110)(1 x 1). Dominant role of the photooxidation of adsorbed hydrocarbons causing wetting by water droplets. *J. Phys. Chem. B* **109**, 15 454–15 462. (doi:10.1021/jp058101c)
40. Holtzinger C, Rapenne L, Chaudouet P, Berthome G, Langlet M. 2012 Thickness effects in naturally superhydrophilic TiO₂–SiO₂ nanocomposite films deposited via a multilayer sol–gel route. *J. Sol-Gel Sci. Technol.* **64**, 465–479. (doi:10.1007/s10971-012-2878-4)
41. Boulamanti AK, Philippopoulos CJ. 2008 Photocatalytic degradation of methyl tert-butyl ether in the gas-phase: a kinetic study. *J. Hazard. Mater.* **160**, 83–87. (doi:10.1016/j.jhazmat.2008.02.087)
42. Seddigi ZS, Ahmed SA, Ansari SP, Yarkandi NH, Danish E, Oteef MDY, Cohelan M, Ahmed S, Abulkibash AM. 2014 Photocatalytic degradation of methyl tert-butyl ether (MTBE): a review. *Adv. Environ. Res.* **3**, 11–28. (doi:10.12989/aer.2014.3.1.011)
43. Wu C, Lee Y, Lo Y, Lin C, Wu C. 2013 Thickness-dependent photocatalytic performance of nanocrystalline TiO₂ thin films prepared by sol–gel spin coating. *Appl. Surf. Sci.* **280**, 737–744. (doi:10.1016/j.apsusc.2013.05.053)
44. Dundar I, Kritsevskaia M, Katerski A, Acik IO. 2019 Data from: TiO₂ thin films by ultrasonic spray pyrolysis as photocatalytic material for air purification. Dryad Digital Repository. (doi:10.5061/dryad.b24p647)

Publication II

I. Dundar, M. Krichevskaya, A. Katerski, M. Krunks, I. Oja Acik. Photocatalytic degradation of different VOCs in the gas-phase over TiO₂ thin films prepared by ultrasonic spray pyrolysis. *Catalysts*, 2019, 9, 915.

Article

Photocatalytic Degradation of Different VOCs in the Gas-Phase over TiO₂ Thin Films Prepared by Ultrasonic Spray Pyrolysis

Ibrahim Dundar ^{1,*}, Marina Krichevskaya ^{2,*}, Atanas Katerski ¹, Malle Krunks ¹ and Ilona Oja Acik ^{1,*}

¹ Department of Materials and Environmental Technology, Laboratory of Thin Film Chemical Technologies Tallinn University of Technology, Ehitajate tee 5, 19086 Tallinn, Estonia; atanas.katerski@taltech.ee (A.K.); malle.krunks@taltech.ee (M.K.)

² Department of Materials and Environmental Technology, Laboratory of Environmental Technology, Tallinn University of Technology, Ehitajate tee 5, 19086 Tallinn, Estonia

* Correspondence: ibrahim.dundar@taltech.ee (I.D.); marina.kritsevskaja@taltech.ee (M.K.); ilona.oja@taltech.ee (I.O.A.)

Received: 20 September 2019; Accepted: 31 October 2019; Published: 2 November 2019



Abstract: In this study, we deposited TiO₂ thin films onto borosilicate glass by ultrasonic spray pyrolysis at 350 and 450 °C. The aim of study is to determine the effect of deposition temperature on photocatalytic activity of TiO₂ thin films and to investigate the performance of TiO₂ thin films on photocatalytic degradation of methyl tert-butyl ether (MTBE), acetone, acetaldehyde, and heptane as functions of different operating parameters. TiO₂ thin films deposited at 350 and 450 °C have a thickness value of 190 and 330 nm, respectively. All as-prepared TiO₂ films possess an anatase crystalline structure. According to the X-ray photon spectroscopy (XPS) study, the TiO₂ thin film deposited at 350 °C showed a higher amount of oxygen vacancies and hydroxyl groups on the film surface after UV treatment. The aged-TiO₂ thin film deposited at 350 °C showed a water contact angle (WCA) value of 0° after 10 min UV irradiation, showing superhydrophilic surface behavior. The TiO₂ film deposited at 350 °C exhibited the highest amount of conversion of MTBE (100%). The results also showed that TiO₂ films are capable of photocatalytic degradation of MTBE (100%) and acetaldehyde (approx. 80%) in humid air conditions and high airflow rate. The visible-light-activity of TiO₂ thin films was tested with 5 ppm MTBE and acetone. TiO₂ thin films deposited at 350 °C with a surface area of 600 cm² showed 60% of MTBE and 33% of acetone degradation under VIS light.

Keywords: TiO₂; thin film; spray pyrolysis; photocatalytic; VOCs; indoor air; superhydrophilic

1. Introduction

Volatile organic compounds (VOCs) are the most common air pollutants, which are present in both indoor and outdoor air. It was reported that the VOC concentration indoors is often 2 to 5 times higher than that of the outdoors [1]. Among VOCs, acetone and acetaldehyde are common chemicals used extensively in a variety of industrial and domestic applications and are found in appreciable concentrations in indoor air [2,3]. Methyl tert-butyl ether (MTBE) and heptane are fuel components released to the atmosphere from gasoline and motor vehicle exhaust [4,5]. They are considered as outdoor generated VOCs, which also affect indoor air quality, especially in buildings close to parking lots or streets. Therefore, it is essential to obtain healthy living environments in modern buildings, integrated with air cleaning solutions [6]. According to the international standard, acetone and acetaldehyde together with heptane, toluene, and formaldehyde are the model air pollutants for the potential international standard testing of air cleaners [7].

The most widely studied semiconductor materials as photocatalysts in air treatment systems are commercial TiO₂ nanopowders such as P25, UV100, PC105, and PC500 and coatings prepared by those powders [8–11]. These are expected to have a high photocatalytic activity for gas-phase pollutant degradation due to their large available surface area. However, nanopowder coatings have high potential to agglomerate and detach from the substrate, causing a reduction in their photocatalytic activity [12,13] and low transmittance in the visible spectral range [14], which limits the field of applications such as indoor or outdoor photocatalysts.

Nanocrystalline TiO₂ thin films, however, are vital for safeguarding human health due to their strong adhesion to the substrate. Thus, the synthesis of thin films has advantages in the development of sustainable photocatalysts for applications containing flowing gas streams compared to nanopowder coatings [12,13]. The photocatalytic performance of TiO₂ thin films depends on several factors mostly related to thin film properties, primarily conditioned by the preparation method. Photocatalytic thin films can be fabricated by vacuum and non-vacuum deposition methods. The most common vacuum techniques that have been used to fabricate TiO₂ thin films for photocatalytic applications are atomic layer deposition [15] and sputtering methods [16]. Non-vacuum solution based methods, however, have several advantages compared to vacuum based techniques, such as cost-effectiveness, resource savings, and rapid deposition.

The most common non-vacuum technique that was used to fabricate TiO₂ thin films for photocatalytic applications is the sol-gel method (Supplementary Materials Table S1). Among them, many studies have been done on the gas-phase photocatalytic degradation of acetaldehyde [17–22] and acetone [22–27] on TiO₂ thin films, while a few studies were done on photocatalytic oxidation of MTBE and heptane. Supplementary Materials Table S1 shows that the photocatalytic decomposition of MTBE and heptane was mostly studied on TiO₂ powder coatings [27–31]. In our previous study, TiO₂ thin films were examined for photocatalytic conversion of gaseous MTBE on the TiO₂ surface. The TiO₂ film deposited on window glass exhibited conversion of MTBE of approximately 80% [5]. To the best of our knowledge, no prior studies have examined photodecomposition of heptane on transparent TiO₂ thin films. As seen in Supplementary Materials Table S1, the results of these studies are hardly comparable due to the different evaluation techniques and reactor types besides operating conditions during photocatalytic tests, such as pollutant type, flow rate, temperature, irradiation intensity, and photocatalytic coating area.

Among the non-vacuum solution based techniques, spray pyrolysis is a robust, cost-effective, and easily up-scalable chemical method [32,33]. In the spray pyrolysis method, aerosols are generated by a nebulizer (e.g., pneumatic, ultrasonic, or electrostatic) or an ultrasonic generator and carried in a gas flow through a furnace [34,35] or onto a hot plate [5]. Among the various nebulization techniques available, the use of ultrasonic spray pyrolysis (USP) was favoured because of the generation of small-sized initial droplets, and the inherent low velocity of the initially formed aerosol [35].

Despite the several advantages of USP-synthesized thin films, no publications on the decomposition of VOCs such as acetone, acetaldehyde, and heptane on transparent TiO₂ thin films fabricated by USP reporting their photocatalytic activity regarding the materials characteristics were found available; thus, this study supplies more insights into this topic. The present paper is a comprehensive study of TiO₂ thin films synthesized by USP and applied for the abatement of different VOCs.

Hereby, two purposes were considered for this study: firstly, to evaluate the photocatalytic performance of TiO₂ thin films deposited at different temperatures; and secondly, to investigate the effect of humidity, airflow regime, and light source (i.e., UV and VIS) on the abatement of air pollutants on TiO₂ thin films. MTBE, acetone, acetaldehyde, and heptane were individually used to evaluate the photocatalytic activity for gas-phase reactions in the multi-section plug-flow reactor.

2. Results

2.1. Material Characterization

2.1.1. Surface Morphology

Figure 1 shows the surface morphology of as-prepared TiO₂ thin films on borosilicate glass. TiO₂ film deposited at 350 °C (Figure 1a) showed a plane surface structure, whereas the film deposited at 450 °C (Figure 1c) showed a grain-like structure. The thickness of TiO₂ films sprayed at 350 and 450 °C were 190 and 330 nm (Table 1), respectively, as estimated from the cross-sectional scanning electronic microscope (SEM) images (inset in Figure 1a,c).

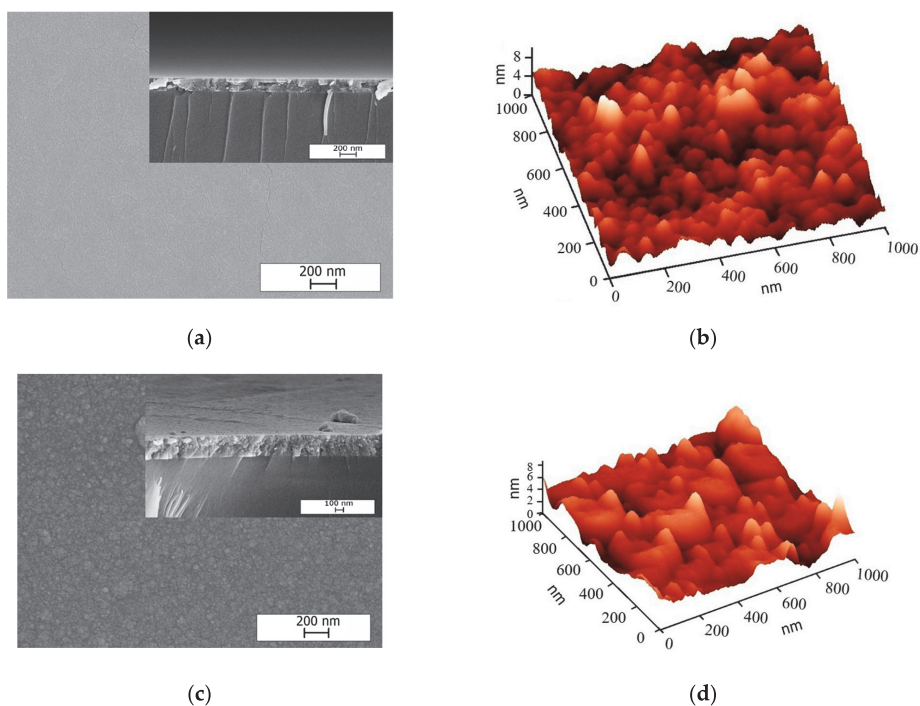


Figure 1. SEM surface image (a,c) and AFM image (b,d) of as-prepared TiO₂ thin films deposited on borosilicate glass at 350 and 450 °C. Insets of (a) and (c) show the cross-sectional SEM images of the corresponding TiO₂ thin films.

Table 1. XPS results. Summary of different ratios obtained by XPS data for the aged-TiO₂ thin films before and after UV-treatment.

Deposition Temperature (°C)	Aged-TiO ₂ Samples (before UV-Treatment)		After UV-Treatment	
	(Vo)/(Ti–O) (at%/at%)	(OH ⁻)/(Ti–O) (at%/at%)	(Vo)/(Ti–O) (at%/at%)	(OH ⁻)/(Ti–O) (at%/at%)
350	0.17	0.08	0.12	0.11
450	0.09	0.30	0.09	0.05

Figure 1b,d depicts three-dimensional (3-D) atomic force microscope (AFM) images of TiO₂ films on borosilicate substrate. TiO₂ thin films deposited at 350 °C showed grains with a size of ca 50 nm. TiO₂ films deposited at 450 °C showed grains with a size of ca 50 nm and agglomerated grains with a

size of ca 200 nm. Different surface topography of the films deposited at 350 to 450 °C resulted also in a slight increase of the root mean square (RMS) roughness from 0.6 to 1.0 nm, respectively. The SEM and AFM images revealed the formation of agglomeration as elliptical clusters for the TiO₂ thin film deposited at 450 °C. The formation of agglomerated grains was observed in TiO₂ thin films deposited by spray pyrolysis at high temperatures [36].

2.1.2. Structural Properties

Figure 2 shows the XRD patterns of TiO₂ films deposited at 350 and 450 °C onto borosilicate glass. The XRD patterns exhibited reflection peaks at 2 theta of 25.3°, 37.9°, 48.1°, 54.1°, and 55.2° corresponding to reflections from (101), (004), (200), (105), and (211) crystal planes of the anatase structure (JCPDS 01-070-6826) [37]. No other crystalline phases of TiO₂ were detected. The Scherrer formula was applied to calculate the mean crystallite size of TiO₂ films using the (101) peak of the anatase phase. Similar mean crystallite sizes of 26 and 22 nm were found for the TiO₂ films deposited at 350 and 450 °C, respectively. This confirms that deposition temperature did not have any remarkable effect on the structural properties of sprayed TiO₂ thin films.

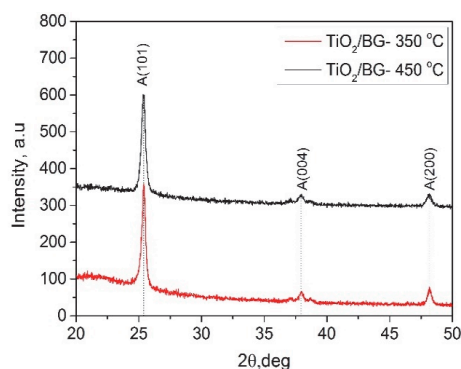


Figure 2. XRD patterns of TiO₂ films deposited at 350 and 450 °C onto borosilicate glass. All films were annealed at 500 °C for 1 h in air.

2.1.3. Optical Properties

Figure 3 shows the total transmittance spectra of TiO₂ thin films deposited at 350 and 450 °C and annealed at 500 °C for 1 h. Both TiO₂ films showed total transmittance of ca. 80% in the visible spectral region. The indirect band gap of the TiO₂ film was determined according to the Tauc plot [5]. The optical band gap of both samples was found to be 3.38 eV (inset of Figure 3).

2.1.4. XPS Study

XPS is a useful and sophisticated measurement technique for investigating the chemical constituents of a material, the ionic states of the constituent elements, and the ratio of the amounts of the different ionic states of a single constituent element. Estimation of oxygen vacancies and carbon species was confirmed from the XPS data in many studies [38–42] with the deconvoluted O1s and C1s XPS spectrum of the TiO₂.

The surface chemical composition and bonding structure of the aged and UV-treated TiO₂ thin films were investigated with the analysis of XPS data. Figures 4 and 5 show the O1s and C1s core level spectra of aged-TiO₂ thin films deposited at 350 and 450 °C before and after UV-treatment, respectively. The asymmetric O1s and C1s core level peaks were deconvoluted by using Lorentzian–Gaussian (function pseudo-Voigt) fitting analysis. The background subtraction was applied by using Shirley type fitting [5].

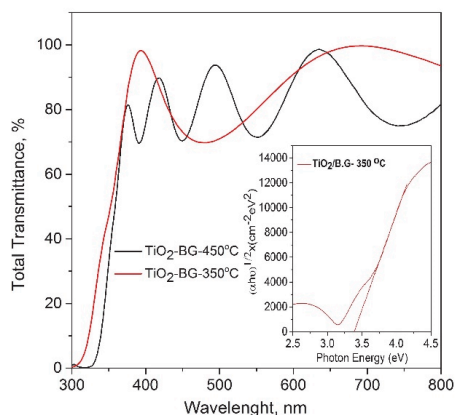


Figure 3. Total transmittance spectra of as-prepared TiO₂ thin films. The inset shows the optical band gap value of the TiO₂ thin film deposited at 350 °C.

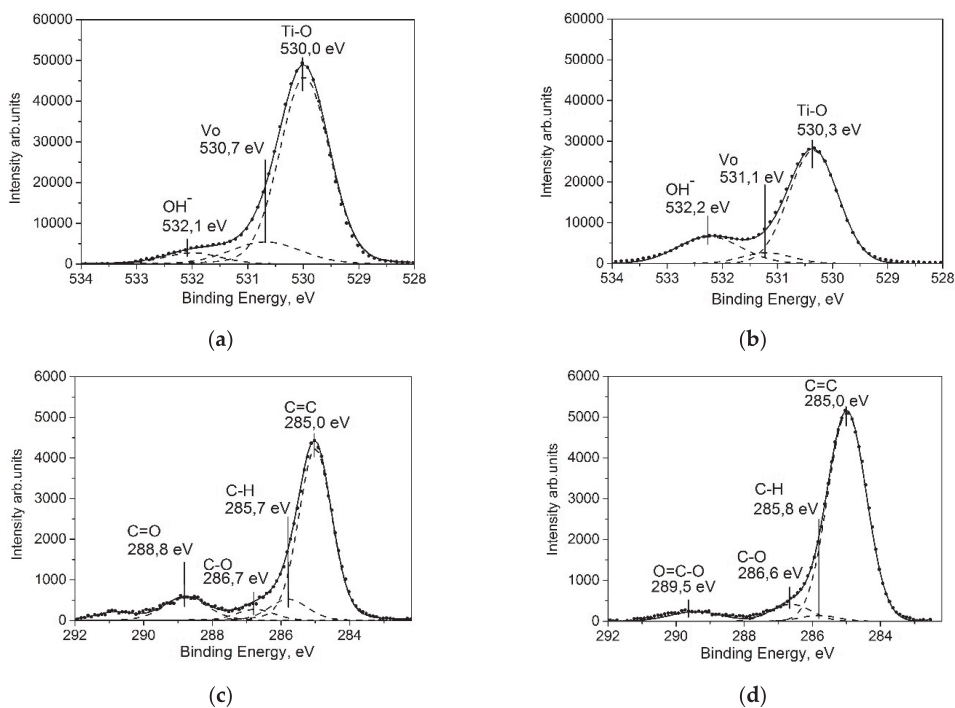


Figure 4. XPS spectra of aged-TiO₂ thin films deposited at (a) 350 and (b) 450 °C in the binding energy (BE) region of O1s. XPS spectra of aged-TiO₂ thin films deposited at (c) 350 and (d) 450 °C in the BE region of C1s.

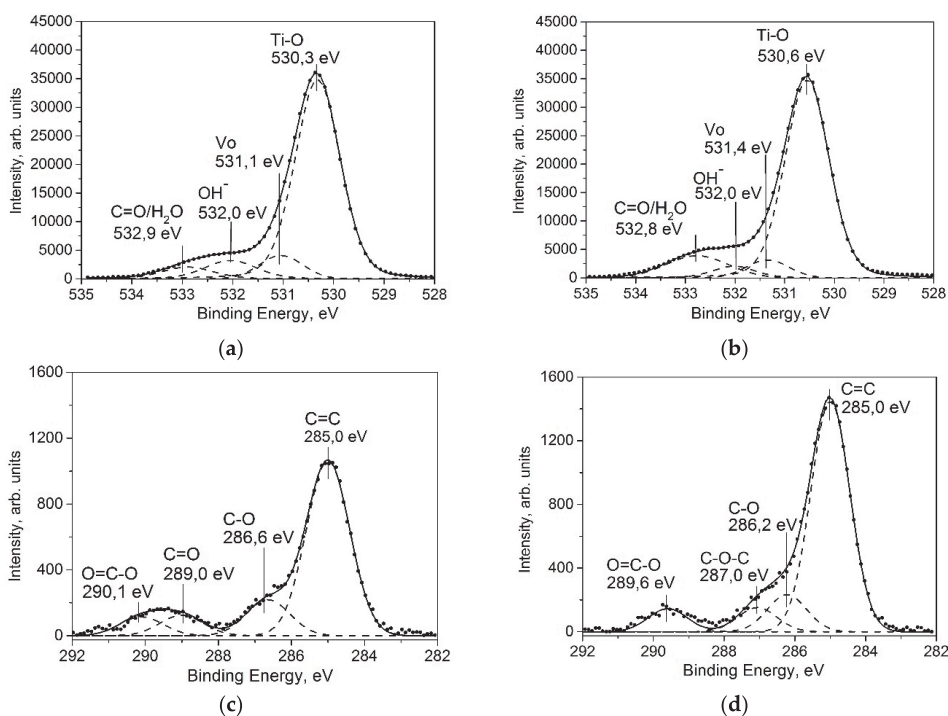


Figure 5. XPS spectra of aged-TiO₂ thin films after UV surface cleaning. TiO₂ thin films deposited at (a) 350 and (b) 450 °C in the BE region of O1s. XPS spectra of TiO₂ thin films deposited at (c) 350 and (d) 450 °C in the BE region of C1s.

XPS Data Analysis of Aged-TiO₂ Thin Films

The O1s core level peak of the aged-TiO₂ thin films was deconvoluted into three peaks (Figure 4a,b). The peak observed in binding energy (BE) value at 530.0 ± 0.3 eV was assigned to the Ti–O bond and the peak at BE value at 530.7 ± 0.4 eV was ascribed to the presence of oxygen vacancy defects (Vo). In addition, the peak at 532.1 ± 0.1 eV was attributed to surface hydroxyl groups (OH[−]), revealing that the film surface contained adsorbed surface OH[−] groups [43–45].

Figure 4c,d show the C1s core level spectra of aged-TiO₂ thin films deposited at 350 and 450 °C, respectively. The spectra could be resolved into four peaks at BE of 285.0, 285.7, and 286.7, ± 0.1 , and 288.8 ± 0.3 eV. In both TiO₂ samples, the C1s peaks located at 285.0 and 285.7 ± 0.1 eV corresponded to C=C and C–C/C–H, respectively [43]. It is highly probable that hydrocarbons and other carbon-like species could be formed on the surface of TiO₂ layers as a result of preparation procedure or due to carbon contamination arising from aging of samples in ambient atmosphere [43,46]. Further, there were other peaks observed at 286.7 ± 0.1 , 288.8 (Figure 4c), and 289.6 eV (Figure 4d) that belonged to oxygen species containing carbonyl moieties, such as C–O, C=O, and O=C–O, respectively [41–43,47,48]. Moreover, the peak positioned at 290.07 ± 0.4 eV could have resulted from the π – π shake-up process (Figure 4c) [42].

The Scofield' cross-sections were applied to investigate the integrated areas of O1s core level spectra for the calculation of atomic concentrations of the components, such as Ti–O, Vo, and OH[−] presented in the O1s and C1s core level spectrums. The ratios of the components (OH[−])/(Ti–O) and (Vo)/(Ti–O) are shown in Table 1. As seen in Table 1, the amount of oxygen vacancies ((Vo)/(Ti–O) ratios) on the surface of TiO₂ films decreased from 0.17 up to 0.09 with the increase in the deposition temperature from 350 to 450 °C. This result agrees with our previous study, showing that the amount

of oxygen vacancies decreases with increasing deposition temperature [5]. The lower number of oxygen vacancy defects on TiO₂ thin films deposited at 450 °C can be attributed to the effect of the high heat deposition temperature that repairs the surface oxygen defects [5]. It should be noted that the deposition temperature has a large effect on the properties of TiO₂ films deposited by spray pyrolysis. Even though the TiO₂ thin films were exposed to annealing treatment at high temperatures, it was shown in our previous studies that the structural, morphological, and chemical properties of TiO₂ thin films were found to depend on the film deposition temperature [5,32,49]. As seen in Table 1, the aged-TiO₂ films showed an increase in the amount of OH⁻ groups on the film surface with increasing deposition temperature. In the literature, it was observed that there is an inconsistency trend on the amount of OH⁻ groups on the film surface concerning the increase in the film thickness [42] and heat treatment [48]. Simonsen et al. [48] reported that the surface of the TiO₂ films grown by microwave assisted sol-gel at 550 °C had the lowest amount of surface OH⁻ groups, while the hydroxyl groups on the film surface increased gradually with an increase in calcination temperature from 25 to 450 °C. A similar fluctuation in the amount of OH⁻ groups was observed also in our previous study [5].

XPS Data Analysis of Aged-TiO₂ Thin Films after UV-Treatment

Figure 5 represents the O1s and C1s core level spectra of UV-treated aged-TiO₂ thin films fabricated at 350 and 450 °C.

The O1s core level spectra of the surface of the UV-treated aged-TiO₂ thin films could be deconvoluted into four peaks (Figure 5a,b). The peaks at 530.3 ± 0.3, 531.1 ± 0.3, and 532.0 eV were assigned as Ti–O, Vo, and OH⁻, respectively. In the literature, the peak observed in the BE value at 532.9 ± 0.1 was associated with different species, such as C–O, C=O, or chemisorbed-H₂O molecules [41,50]. As seen in Table 1, after UV-treatment, the TiO₂ thin film deposited at 350 °C possessed a higher level of oxygen vacancies on the top of the film surface compared to the 450 °C deposited sample. The amount of hydroxyl groups ((OH)/(Ti–O), Table 1), however, decreased considerably after UV treatment in the case of the TiO₂ thin film sprayed at 450 °C.

A smaller amount of carbon species was observed on the surface of TiO₂ thin films after UV-treatment (Figure 5c,d) compared to XPS results of aged-TiO₂ films (Figure 4c,d), showing the modification of the surface composition of aged-TiO₂ films after UV-treatment. Similar to the aged-TiO₂ samples, the peaks at the BE values of 285.0 and 286.6 ± 0.4 and 289.6 ± 0.5 eV were attributed to C=C, C–O, and O=C–O, respectively [45–48]. The peak at 287.0 eV in the carbon spectra of the TiO₂ sample grown at 450 °C (Figure 5d) could be assigned as C–O–C [45]. In the case of the TiO₂ film grown at 350 °C, the peak at BE value at 289.0 eV (Figure 5) could be assigned to C=O [41,45]. In addition, it should be noted that the peak located in BE energy at 285.7 attributed to C–H (Figure 4c,d) was not observed in C1s spectra of the UV-treated TiO₂ thin films (Figure 5c,d) due to the decomposition of hydrocarbons on the top of the TiO₂ film surface by the UV treatment [41,51].

2.2. Wettability

The water contact angles (WCA) for as-prepared TiO₂ films deposited at 350 and 450 °C were 12 and 17°, respectively. The films were aged in air over a month, and the increase was observed up to 46 and 55° (Figure 6). The increase in the WCA during aging could be due to the formation of a hydrocarbon layer on the film surface in air (Table 1) [52].

As seen in Figure 6, short UV irradiation of 5 min decreased the WCA of TiO₂ film deposited at 350 °C from 46.8° to 10°. Further UV irradiation (in total 10 min) decreased the WCA even up to 0°. Thus, this revealed that a relatively short UV irradiation time of 5 min was necessary to modify the surface behavior of TiO₂ film deposited at 350 °C from hydrophilic to superhydrophilic. Opposite to that, the WCA of TiO₂ films deposited at 450 °C decreased gradually from 55° to 0° within 35 min (Figure 6).

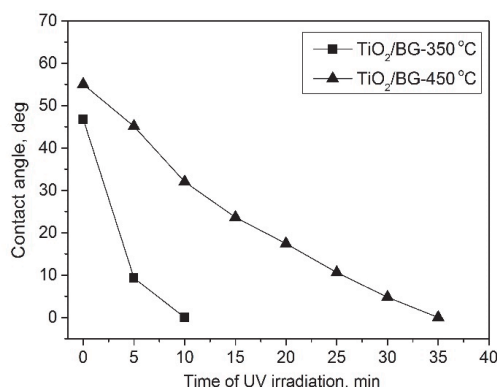


Figure 6. Plot of the WCA of the aged TiO₂ films deposited at 350 and 450 °C vs time of UV irradiation.

Different behaviors of WCA under UV-irradiation of TiO₂ films deposited at 350 and 450 °C can be explained by different surface chemical compositions of TiO₂ thin films. The changes in the degree of hydroxyl groups, oxygen defects, and hydrocarbons present on the TiO₂ surface could be related to the rapid wettability conversion (in total 10 min) of the TiO₂ thin film deposited at 350 °C, correlated with the results obtained by XPS.

In comparison to TiO₂ films, the amount of hydroxyl groups was found to be considerably higher in the TiO₂ thin film deposited at 350 °C after UV irradiation (Table 1), compared to films deposited at 450 °C. This can be explained by the high amount of inherent oxygen vacancy defects on the surface of aged-TiO₂ films (Table 1), leading to the trapping of hydroxyl groups that enhanced the hydrophilic surface [41,42,53]. Moreover, the rapid wetting ability of the TiO₂ sample deposited at 350 °C could be due to the difference in the ability of photodecomposition of the hydrocarbon layer on the TiO₂ surface [51,54].

2.3. Photocatalytic Activity

2.3.1. The Effect of Deposition Temperature on Photocatalytic Activity of TiO₂ Thin Films

Figure 7 shows the photocatalytic conversion of MTBE (10 ppm) on TiO₂ thin films deposited at 350 and 450 °C. Operating conditions for the experimental runs were: residence time 15.6 s per section, relative humidity (RH) 6%, and reactor temperature 34 °C.

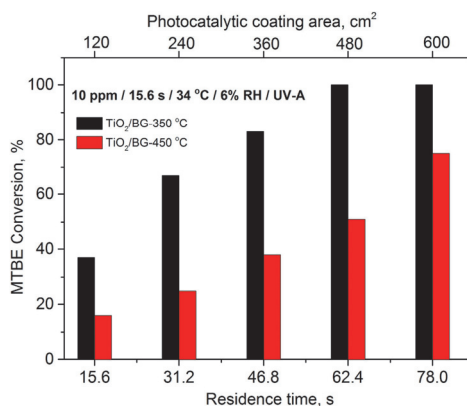


Figure 7. Photocatalytic conversion of MTBE on as-prepared TiO₂ thin films deposited onto glass substrates at 350 and 450 °C; MTBE inlet concentration 10 ppm; RH 6%.

As seen in Figure 7, the TiO₂ thin films deposited at 350 °C showed higher photocatalytic activity than TiO₂ thin films deposited at 450 °C. The MTBE at the initial concentration of ca. 10 ppm was completely converted to CO₂ and H₂O at a residence time of 62.4 s on the TiO₂ thin films deposited at 350 °C, while TiO₂ thin films deposited at 450 °C exhibited MTBE conversion of ca. 75% after 78 s. The higher photocatalytic activity of TiO₂ thin film deposited at 350 °C can be ascribed to several factors including the surface morphology, higher level of oxygen vacancy defects, and OH⁻ groups on the film surface compared to the samples deposited at 450 °C (Table 1). It is a well-known phenomenon that the presence of the surface-active OH⁻ groups benefit photocatalytic reactions. It was reported that OH⁻ groups can participate directly in the interface reactions by trapping photo-generated holes that diffuse to TiO₂ surfaces and producing reactive surface hydroxyl radicals. They can also act as active sites for adsorption/reaction of reactant molecules on TiO₂ [55]. Further, there is a mutual effect between the photo-induced electrons bound by oxygen vacancies and the adsorbed O₂, and thus oxygen vacancies can support O₂ adsorbing [56]. This indicates that oxygen vacancies can favor the adsorbed O₂ to capture photo-induced electrons, simultaneously producing reactive oxygen species (ROS) and, thus, promoting the oxidation of organic substances. Therefore, it can be suggested that oxygen vacancies and other surface defects are in favor of photocatalytic reactions [57].

In the present study, the formation of large grains was observed on the TiO₂ thin film deposited at 450 °C compared to that of the films deposited at 350 °C (Figure 1a,c) due to the agglomeration of grains during the deposition process at higher temperature. This could be one additional reason for the reduction of the photocatalytic activity of TiO₂ films deposited at 450 °C. It was reported that the surface area decreases with the increase in the grain size, which is unfavorable for the enhancement of photocatalytic efficiency [58,59]. Furthermore, the agglomeration decreases the interface between the grains, and thus leads to the reduction of surface active sites available for photocatalytic reactions [59,60].

Further study of the characterization of gas-phase photocatalytic activity of synthesized thin films was carried out with the TiO₂ films deposited at 350 °C due to their higher photocatalytic activity ascertained with MTBE.

2.3.2. The Effect of Air Humidity on Photocatalytic Activity of TiO₂ Thin Films

VOCs, such as MTBE, acetone, acetaldehyde, and heptane were chosen as single model air pollutants for this study. The effect of different operating conditions, i.e., humidity, inlet concentration of pollutant, residence time, and source of irradiation, on the photocatalytic process performance was studied. The effect of increase in air humidity from ca. 6 to 40% RH on photocatalytic oxidation of heptane, acetaldehyde, acetone, and MTBE is presented in Figure 8 (residence time in reactor section was 15.6 s).

The results showed that under lower humidity the conversions of heptane, acetaldehyde, and acetone were 46, 74, and 93% at residence time of 78 s, respectively, and 100% conversion of MTBE was achieved at 62.4 s, as previously discussed (Figure 8a). During the photocatalytic oxidation of those VOCs, tert-butyl formate (TBF) and formic acid were detected as intermediate gas-phase products of MTBE and heptane, respectively. Under a relatively dry atmosphere, the formation of intermediate products followed by their degradation was observed. There was an increase in the concentration of formic acid achieving its maximum at residence time of 46.8 s and subsequently it decreased with the further increase in residence time (at 78.0 s, 1% of degraded heptane emerged as gaseous formic acid), whereas no TBF was observed at residence time of 78 s as this intermediate product was completely degraded.

Air humidity usually dually affects the photodegradation processes. It can contribute to surface re-hydration of photocatalysts, which could lead to the increase in concentration of •OH radicals and hence to an increase in reaction rate. Competitive adsorption between water vapor and the organic compounds, which inhibits the binding of reactant molecules, is also common at higher water vapor content in reactors [61]. Therefore, the effect of air humidity on the performance of photocatalytic

oxidation of MTBE, acetone acetaldehyde, and heptane were investigated on TiO₂ thin films deposited at 350 °C. As could be observed from Figure 8a,b, the conversion efficiency of most VOCs diminished with the increase in the relative humidity from 6 to 40%.

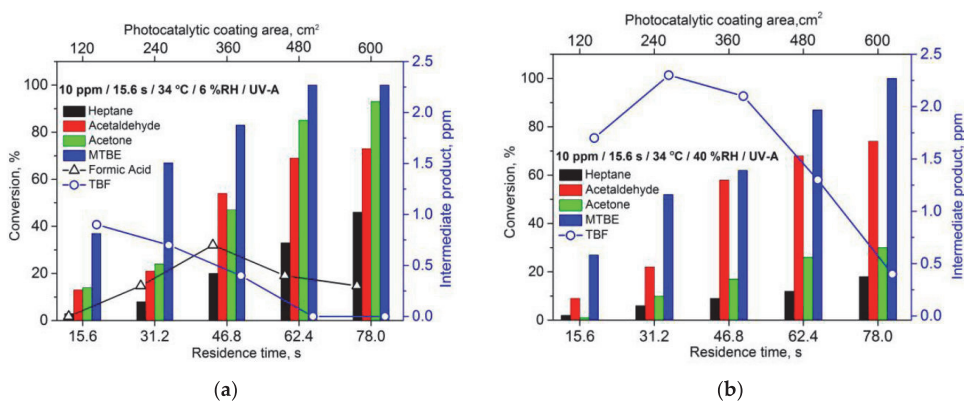


Figure 8. Photocatalytic conversion of different VOCs on TiO₂ thin film deposited at 350 °C under (a) dry (6% RH) air and (b) humid (40% RH) air conditions. VOCs inlet concentration 10 ppm.

The conversion of heptane decreased almost twice with the increase in the relative humidity. In contrast to dry air, in humid air no gaseous organic intermediate products of heptane were monitored, as formic acid was expected to stay adsorbed on the surface of hydrated photocatalyst film.

Humid atmosphere influenced also the formation of the MTBE intermediate product TBF and retarded slightly the overall degradation of MTBE. Complete conversion of MTBE on a coated glass with the surface area of TiO₂ thin film deposited at 350 °C of 600 cm² (78 s) was achieved also under humid air conditions. Only TBF was found as an intermediate product from the degradation of MTBE in dry and humid conditions. In dry air, TBF was converted to CO₂ and H₂O at a residence time of 62.4 s, while the detected amount of TBF was higher at a higher humidity (at 78.0 s, 5% of degraded MTBE appeared as gaseous TBF). Thus, the increase in air humidity was slightly hindering the photocatalytic mineralization of MTBE on thin films.

Acetone degradation was affected by relative humidity, showing a sharp drop in the conversion of acetone from 93 to 30%. No gas-phase intermediate products were detected in either dry or humid air during photodegradation of acetone over TiO₂ films. It is interesting to note that acetone is a polar molecule, which is supposed to penetrate through water to the surface of TiO₂. However, in the present study, it was seen that higher humidity (40% RH) showed a detrimental effect on the adsorption and photocatalytic decomposition of acetone. Similar results were observed during the photodecomposition of acetone [28] and chlorobenzene [62], which are soluble in water, on the TiO₂ surface under high humidity conditions.

The only compound of which oxidation was uninfluenced by variations in air humidity was acetaldehyde. There were no significant changes in the conversion of acetaldehyde (approx. 75% conversion at 78 s) with the increase in relative humidity from 6 to 40%. No gas-phase products other than CO₂ and H₂O were observed during the photocatalytic degradation of acetaldehyde in both dry and humid air conditions (Figure 8a,b). It is known that transport of the reactant molecules through water molecules depends on the solubility of the molecules of interest in water. Acetaldehyde is a polar molecule, which is water-soluble. This explains the “immunity” of photocatalytic oxidation of acetaldehyde molecules to the difference in air humidity. Generalizing, it could be assumed that the potential influence of air humidity on the performance of thin films depends not only on the character of the initial compounds to be oxidized, but also on the character (adsorption affinity, ease of degradation) of the intermediate products. The difference in the trend of acetone and acetaldehyde degradation

under humid conditions is assumed to be attributed to the formation of intermediate products, which in case of acetone presumably deteriorate the overall performance of the photocatalytic process.

2.3.3. The Effect of Residence Time and Inlet Concentration of VOCs on Photocatalytic Activity of TiO₂ Thin Films

The effect of shorter residence time and lower inlet concentration of VOCs was examined on the surface of TiO₂ thin film with initial pollutant concentration of 5 ppm and relative decrease in residence time in the reactor section from 15.6 to 7.8 s (Figure 9).

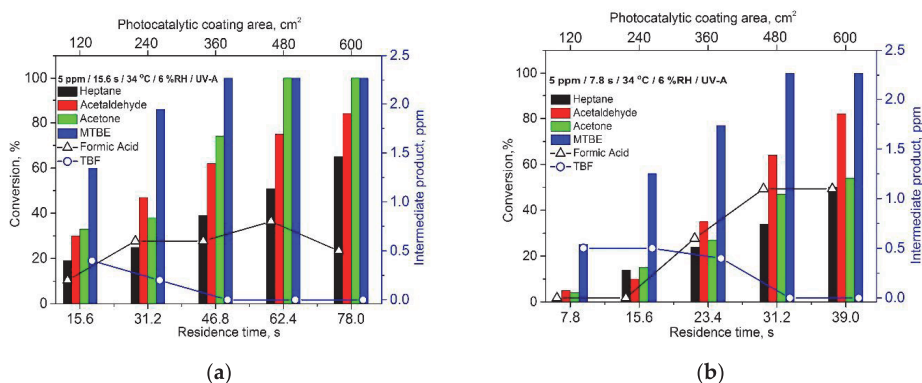


Figure 9. Photocatalytic conversion of different VOCs on TiO₂ thin film deposited at 350 °C under different airflow rates (a) 0.5 L min⁻¹ (15.6 s per section) and (b) 1.0 L min⁻¹ (7.8 s per section) VOC inlet concentration 5 ppm; RH 6%.

The decrease in inlet concentration of VOCs from 10 to 5 ppm (Figures 8a and 9a) resulted in higher conversions of all model compounds. With the decrease in concentration from 10 to 5 ppm in 78 s the conversion of heptane increased from 46 to 65% (4.6 and 3.3 ppm of heptane degraded, respectively) and conversion of acetaldehyde increased from 74 to 85% (7.4 and 4.2 ppm of acetaldehyde degraded, respectively), whereas complete degradation of 5 ppm of acetone and MTBE was obtained within ca. 62 and 47 s, respectively, while 93% of acetone with initial concentration of 10 ppm was degraded (9.3 ppm) in 78 s. Thus, despite the lower conversions of VOCs at higher initial concentrations, the increase in inlet concentration leads to the larger absolute amounts of the degraded compounds.

The residence time in the reactor section shifted from 15.6 to 7.8 s with the increase in the airflow rate from 0.5 L min⁻¹ to 1.0 L min⁻¹. Generally, when the airflow rate is increased, two opposing processes can be envisaged: the decrement in residence time and the enhancement in mass transfer rate, which are, respectively, inhibiting and promoting factors in photocatalytic oxidation processes [63]. By reducing the residence time, the pollutants have shorter time for adsorption on the surface and participating in oxidation reactions. As seen in Figure 9b, a general decrease in the conversion of VOCs was observed within five sections of the reactor, i.e., on the same photocatalytic surface area (600 cm²), but with a twice shorter residence time if compared to the results in Figure 9a. If comparing the same residence time in the reactor at different airflow regimes, then at shorter residence time of 15.6 s (one section of reactor in Figure 9a and two sections in Figure 9b) there is a decrease in the conversions of VOCs despite the higher photocatalytic area in two sections of the reactor in Figure 9b. However, at residence time of 31.2 s (two sections of the reactor in Figure 9a and four sections in Figure 9b), the two times higher airflow rate is favoring the photocatalytic oxidation of VOCs at higher photocatalytic surface: the conversions of all the compounds increased from 25, 38, 47, and 86% to 34, 47, 64, and 100% for heptane, acetone, acetaldehyde, and MTBE, respectively. The process of photocatalytic oxidation of acetaldehyde and MTBE was revealed as especially benefitting from the intensification of mass transfer

in the reactor at the same residence time. Thus, again, the effect of the different airflow regimes was expected to be different for each VOC.

The order in conversion of VOCs at residence time of 39 s in five sections was MTBE > acetaldehyde > acetone > heptane (Figure 9b), while it was MTBE > acetone > acetaldehyde > heptane at longer residence time (Figure 9a). For instance, the conversion of acetaldehyde and MTBE was affected slightly by shorter residence time, while the impact of shorter residence time was remarkable for photocatalytic decomposition of acetone. A sharp decrease in the conversion of acetone from 100% at residence time of 62.4 s (Figure 9a) to 47% at residence time of 31.2 s (Figure 9b) was observed on the same photocatalytic surface area of 480 cm² (four sections), whereas high conversions of acetaldehyde (82% conversion at 39.0 s) and MTBE (100% conversion at 31.2 s) were easily achievable at shorter residence time (Figure 9b). This could be attributed to the different reaction rates of each VOCs. Ibrahim et al. [64] studied the kinetics model of degradation of acetone and acetaldehyde on Degussa P25. It was reported that initial reaction rate of acetaldehyde exceeded that of acetone by more than six times (833 and 125 $\mu\text{mol m}^{-3} \text{min}^{-1}$, respectively).

2.3.4. The Effect of Irradiation Source on Photocatalytic Activity of TiO₂ Thin Films

The photocatalytic activity of TiO₂ thin films sprayed at 350 °C was evaluated with 5 ppm MTBE and acetone in gas-phase under visible light in dry air (Figure 10). TiO₂ thin film showed MTBE conversion of 60% and acetone conversion of 33% at residence time of 78 s. Under the same operating conditions except light source (UV-A light), the sample showed 100% conversion of MTBE at residence 46.8 (360 cm²) and 100% conversion of acetone at residence time 62.4 s (480 cm²) (Figure 9a). The remarkable reduction in photocatalytic activity of TiO₂ film was due to the optical gap width of stoichiometric TiO₂ (>3.1 eV) determining its photocatalytic activity under the action of near UV radiation, which constitutes only a small percent of the visible light spectrum [65,66].

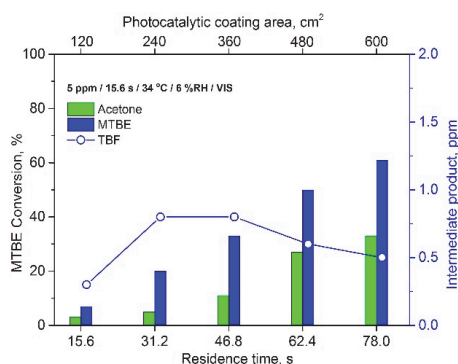


Figure 10. Photocatalytic conversion of MTBE and acetone on TiO₂ thin film deposited at 350 °C under visible light. MTBE and acetone inlet concentration 5 ppm; RH 6%; residence time 15.6 s per section.

TBF was detected as gaseous intermediate of MTBE, while no gaseous intermediate products were monitored during the decomposition of acetone. The highest amount of TBF was observed at residence time of 46.8 s, which was 0.8 ppm of TBF from 1.65 ppm of degraded MTBE (48% of MTBE transformed to TBF). At higher residence times, the amount of TBF on TiO₂ thin film was steadily decreasing, achieving 16% of degraded MTBE oxidized to TBF at 78 sec. In comparison, the TiO₂ thin film was capable of overcoming by-product accumulation at a surface area residence time of 46.8 s (360 cm²) under UV-A light (Figure 9a); moreover, under UV-A light with the same other parameters, no other gaseous products than water and carbon dioxide were observed.

The visible-light-activity of TiO₂ could be related to the defect disorder and the consequent electronic structure. Firstly, it could be ascribed to the formation of oxygen defects on the film surface

(Table 1). It was proposed that the oxygen vacancy defects act as shallow trapping sites, which is related to the formation of some sub-bands in the electronic band structure of TiO₂, considered as the main dominating factor of the visible emission [32]. Additionally, it was observed that TiO₂ thin films still have oxidized carbon species after UV irradiation (C–O, C=O, O=C–O, etc.) on the surface of TiO₂ film, (Figure 5a), known as defect-containing sp²-hybridized carbons. It was reported that these defect-associated functional groups (carbon species) provide surface active sites, which influence the effective charge transfer [47–67].

3. Materials and Methods

3.1. Thin Film Synthesis and Materials Characterization

TiO₂ thin films were fabricated by USP onto borosilicate glass at 350 and 450 °C. The TiO₂ thin films were annealed at 500 °C for 1 h in air in a furnace and are labelled as as-prepared samples throughout the article. The details of the solution preparation and the operating parameters of ultrasonic spray pyrolysis were reported in our previous study [5]. Borosilicate glass was selected as a substrate for TiO₂ thin films since it contains few Na⁺ ions, unlike soda-lime glass substrates [68]; it is known that Na⁺ ions have a detrimental effect on photocatalytic activity [68].

Zeiss HR FESEM Ultra 55 SEM (Jena, Germany) with an acceleration voltage of 4.0 kV was performed to obtain surface morphology and the film thickness. NT-MDT Solver 47 PRO AFM system was used to study the surface morphology of the films. The AFM measurement was carried out in the non-contact mode (resolution in the range of 3 nm) and the samples were studied in 1 μm × 1 μm area per scans. The RMS roughness analysis was performed through the 3-D AFM scan according to the ISO 4287/1 standards.

X-ray diffraction (XRD) measurements were performed with a Rigaku Ultima IV diffractometer (Tokyo, Japan) with CuKα radiation ($\lambda = 1.5406 \text{ \AA}$, 40 kV at 40 mA). The thin films were studied in grazing-incidence diffraction geometry using PBA (parallel beam analyzer 0.112 deg.) soller slit. The angle between the film surface and the incident beam was fixed at 0.5°. The scintillation detector was used during the measurements. The measurements were carried out in 2 theta configurations with the 2 theta range of 20–50°, with a step of 0.02°. The MCS of thin films was calculated by the Scherrer method using the FWHM (full width at half maximum) of the (101) reflection of the TiO₂ anatase phase.

The total transmittance spectra of the TiO₂ films on borosilicate glass were measured in the wavelength range of 300–800 nm on a Jasco V-670 UV–VIS–NIR spectrophotometer equipped with a 40 nm integrating sphere.

XPS studies were performed on a Kratos Axis Ultra DLD (delayline detector) spectrometer in conjunction with a 165 mm hemispherical electron energy analyzer. The analysis was carried out with monochromatic Al Kα X-rays (1486.6 eV) operating at 15 kV and 225 W. All XPS spectra were recorded using an aperture slot of 300–700 mm and pass energy of 20 eV. The spectra were calibrated using C1s core level peak centered data at a binding energy of 285.0 eV. XPS measurements were carried out for the aged-TiO₂ thin films before and after UV treatment. UV treatment was applied for 12 hours to the aged-TiO₂ thin films in ambient air with an Actinic BL 15 W fluorescent lamp for removing contaminants from the TiO₂ thin film surface.

Wettability of the films was determined by water contact angle (WCA) measurements. DSA 25 (KRUSS Instrument) was carried out at room temperature. A sessile drop fitting method was applied for WCA measurements. Actinic BL 15 W fluorescent lamp (Philips), with max emission at 365 nm, was used to investigate the dependence of WCA of aged-TiO₂ films on UV irradiation under ambient conditions.

3.2. Photocatalytic Measurements

The photocatalytic activity of TiO₂ thin films was studied in a five-section plug-flow photocatalytic reactor with a section volume of 130 mL. Details of the reactor setup were reported in a previous

study [5]. MTBE ($C_2H_{12}O$), acetone (C_3H_6O), acetaldehyde (C_2H_4O), and heptane (C_7H_{16}) were used as model air pollutants (all reagents $\geq 99\%$ purity). The inlet concentrations of the gaseous pollutant were 5 and 10 ppm. The relative humidity was maintained at $6 \pm 1\%$ and $40 \pm 5\%$ for dry and humid air conditions, respectively. In the photocatalytic experimental setup, air flows of 0.5 and 1 L min^{-1} were used, which gave the residence time of 15.6 or 7.8 s per reactor section, respectively. The temperature in the reactor was not additionally regulated; equilibrium was reached between the surrounding temperature, heating by the UV-A lamps, and application of reflectors resulting in 33 ± 2 °C. The following lamps such as UV Philips Actinic BL 15 W with an average irradiance of 3.5 mW cm^{-2} with reflector (integrated in the range of 180–400 nm, with max emission at 365 nm, UV-B/UV-A ratio $< 0.2\%$), or VIS Philips TL-D 15 W, irradiance 3.3 mW cm^{-2} with reflector (integrated in the range of 180–700 nm, UV/UV VIS ratio $< 5\%$) were used as the UV and VIS sources. Irradiance from UV and VIS sources was measured by a fiber optic spectrometer (USB-2000 + UV-VIS, Ocean Optics).

MTBE, acetone, acetaldehyde, and heptane peaks were quantified by INTERSPEC 200-X FTIR spectrometer with a Specac Tornado 8-m gas cell at the IR bands of 1063–1124, 1172–1245, 2630–2910, and 2825–3010 cm^{-1} , respectively. The gas-phase intermediate products of MTBE and heptane, TBF and formic acid, respectively, were also quantitatively monitored by means of FTIR at the IR bands from 1138 to 1190 and from 1103 to 1107 cm^{-1} , respectively.

4. Conclusions

TiO₂ thin films were deposited by ultrasonic spray pyrolysis on borosilicate glass substrates at 350 and 450 °C, followed by annealing at 500 °C for 1 h in air. Photocatalytic activity of TiO₂ thin films were evaluated as a function of their morphological, structural, and optical properties. According to the SEM cross-sectional images, the thickness of TiO₂ films deposited at 350 and 450 °C were 190 and 330 nm, respectively. TiO₂ films possess smooth surface morphology, showing the RMS roughness in the range of 0.6–1 nm. The films consist of an anatase crystalline structure with the mean crystallite size in the range of 22–26 nm and indicate total transmittance of 80% in the visible spectral region. XPS study confirmed that UV-treatment was effective to reduce the amount of hydrocarbons on the film surface and to modify the surface chemical composition. It was confirmed that after UV-treatment, the surface of TiO₂ films deposited at 350 °C possessed higher amounts of oxygen vacancy defects and hydroxyl groups ((Vo)/(Ti–O) = 0.12, (OH)/(Ti–O) = 0.11) compared to the films deposited at 450 °C ((Vo)/(Ti–O) = 0.09, (OH)/(Ti–O) = 0.05). The rapid photoinduced hydrophilic to superhydrophilic conversion of TiO₂ thin film deposited at 350 °C revealed the importance of the high-level oxygen vacancy defects, related to the enhancement of hydroxyl groups on the film surface.

Photocatalytic activity tests of TiO₂ thin films revealed that the films deposited at 350 °C with surface area of 480 cm^2 effectually degraded 100% of the MTBE, whereas TiO₂ thin film deposited at 450 °C showed the MTBE conversion of ca. 75% with a surface area of 600 cm^2 . TiO₂ thin film deposited at 350 °C with surface area of 600 cm^2 effectually degraded, 90% of acetone and 75% of acetaldehyde vapor (inlet 10 ppm) under dry air (6% RH) conditions without the formation of gas-phase intermediate products. Complete degradation of MTBE as well as 80% conversion of acetaldehyde were also achieved under humid air (40% RH) conditions at residence time of 78 s. With the decrease in inlet concentration from 10 to 5 ppm the increase in conversion efficiency of heptane and acetaldehyde was obtained at residence time of 78 s, whereas complete degradation of 5 ppm of acetone and MTBE was obtained within ca. 62 and 47 s, respectively. TiO₂ thin films deposited at 350 °C were photocatalytically active under visible light degrading 60% of MTBE and 33% of acetone (inlet 5 ppm).

Based on the conducted analysis, it could be concluded that the amount of oxygen vacancy and hydroxyl groups on the TiO₂ surface highly influences the photocatalytic activity and wettability of sprayed TiO₂ thin films. This study demonstrated that TiO₂ thin films prepared by ultrasonic spray pyrolysis are sufficient to degrade different VOCs under different air conditions and irradiation sources and thereby are prospective coatings for self-cleaning and air purification applications.

Supplementary Materials: The following are available online at <http://www.mdpi.com/2073-4344/9/11/915/s1>, Table S1: Literature overview on photocatalytic decomposition of acetaldehyde acetone MTBE, and heptane on different TiO₂ thin films prepared by non-vacuum methods.

Author Contributions: I.D. carried out the thin film deposition and material characterizations (XRD, optical properties, and wettability test), attended data collection for the photocatalytic activity test, took part in the design of the all figures and tables, participated in the writing of the manuscript, and drafted the manuscript. M.K. (Marina Krichevskaya) carried out the photocatalytic activity test and interpretation of data, and participated in the writing of the manuscript. A.K. made the XPS data analysis. I.O.A. carried out the design of the study, participated in data analysis, and was associated with preparing of the manuscript. M.K. (Malle Krunks) participated in data analysis. All authors gave final approval for publication.

Funding: I.D. is supported by the Estonian Ministry of Education and Research, Estonian Research Council project IUT19-4, Estonian Centre of Excellence project TK141 and EU regional Fund project 2014-2020.4.01.16-0032. I.O.A., M.K. (Malle Krunks), and A.K. are supported by the Estonian Ministry of Education and Research, Estonian Research Council projects IUT19-4 and Estonian Centre of Excellence project TK141. M.K. (Marina Krichevskaya) is supported by the Estonian Ministry of Education and Research, Estonian Research Council projects IUT1-7. This work was partially supported by ASTRA 'TUT Institutional Development Programme for 2016–2022' Graduate School of Functional Materials and Technologies (2014-2020.4.01.16-0032).

Acknowledgments: The authors acknowledge V. Mikli for SEM, M. Danilson for XPS measurements, and A. O. Titilope for AFM measurements.

Conflicts of Interest: The authors declare no conflict of interest.

References

1. Wallace, L.A. *The Total Exposure Assessment Methodology (TEAM) Study Summary and Analysis*; U.S. Environmental Protection Agency: Washington, DC, USA, 1987; pp. 59–73.
2. Schmidt, M.C.; Buchbinder, A.M.; Weitz, E.; Geiger, M.F. Photochemistry of the indoor air pollutant acetone on Degussa P25 TiO₂ studied by chemical ionization mass spectrometry. *J. Phys. Chem. A* **2007**, *111*, 13023–13031. [[CrossRef](#)]
3. Chang, C.P.; Chen, J.N.; Lu, M.C. Heterogeneous photocatalytic oxidation of acetone for air purification by near UV-irradiated titanium dioxide. *J. Environ. Sci. Health A* **2003**, *38*, 1131–1143. [[CrossRef](#)]
4. FarLend, W.H.; United States Environmental Protection Agency. *Health and Environmental Effects Document for N-Heptane: Final Draft*; EPA: Washington, DC, USA, 1989; p. 5.
5. Dundar, I.; Krichevskaya, M.; Katerski, A.; Oja Acik, I. TiO₂ thin films by ultrasonic spray pyrolysis as photocatalytic material for air purification. *R. Soc. Open Sci.* **2019**, *6*, 181578. [[CrossRef](#)]
6. Schiewecka, A.; Uhdea, E.; Salthammer, T.; Salthammer, L.C.; Morawska, L.; Mazaheric, M.; Kumar, P. Smart homes and the control of indoor air quality. *Renew. Sustain. Energy Rev.* **2018**, *94*, 705–718. [[CrossRef](#)]
7. Degallaix, M.C. Air cleaning devices: A growing market polluted by confusing communication-certified performances for air cleaners. *J. Rehva* **2017**, *1*, 49–51.
8. Mamaghani, A.H.; Haghghat, F.; Lee, C.S. Photocatalytic oxidation technology for indoor environment air purification: The state-of-the-art. *Appl. Catal. B Environ.* **2017**, *203*, 247–269. [[CrossRef](#)]
9. Alonso-Telleza, A.; Massona, R.; Robert, D.; Kellera, N.; Keller, V. Comparison of Hombikat UV100 and P25 TiO₂ performance in gas-phase photocatalytic oxidation reactions. *J. Photochem. Photobiol. A Chem.* **2012**, *250*, 58–65. [[CrossRef](#)]
10. Bianchia, C.L.; Gatto, S.; Pirola, C.; Naldoni, A.; Michele Di, A.; Cerrato, G.; Crocellà, V.; Capucci, V. Photocatalytic degradation of acetone, acetaldehyde and toluene in gas-phase: Comparison between nano and micro-sized TiO₂. *Appl. Catal. B Environ.* **2014**, *146*, 123–130. [[CrossRef](#)]
11. Šuligoja, A.; Urška Lavrenčič Štangara, U.L.; Ristić, A.; Mazaj, M.; Verhovšek, D.; Tušar, N.N. TiO₂-SiO₂ films from organic-free colloidal TiO₂ anatase nanoparticles as photocatalyst for removal of volatile organic compounds from indoor air. *Appl. Catal. B Environ.* **2016**, *184*, 119–131. [[CrossRef](#)]
12. Shayegan, Z.; Lee, C.S.; Haghghat, F. TiO₂ photocatalyst for removal of volatile organic compounds in gas phase—A review. *Chem. Eng. J.* **2018**, *334*, 2408–2439. [[CrossRef](#)]
13. Verbruggen, S.W.; Deng, S.; Kurttepel, M.; Cott, D.J.; Vereecken, P.M.; Bals, S.; Detavernier, C.; Lenaerts, S. Photocatalytic acetaldehyde oxidation in air using spacious TiO₂ films prepared by atomic layer deposition on supported carbonaceous sacrificial templates. *Appl. Catal. B Environ.* **2014**, *160–161*, 204–210. [[CrossRef](#)]

14. Arabatzis, I.M.; Antonaraki, S.; Stergiopoulos, T.; Hiskia, A.; Papaconstantinou, E.; Bernard, M.C.; Falaras, P. Preparation, characterization and photocatalytic activity of nanocrystalline thin film TiO₂ catalysts towards 3,5-dichlorophenol degradation. *J. Photochem. Photobiol. A* **2012**, *149*, 237–245. [[CrossRef](#)]
15. Buchalska, M.; Surowska, M.; Hamalainen, J.; Livonen, T.; Leskela, M.; Macyk, W. Photocatalytic activity of TiO₂ films on Si support prepared by atomic layer deposition. *Catal. Today* **2015**, *252*, 14–19. [[CrossRef](#)]
16. Stefanov, B.I.; Niklasson, G.A.; Granqvist, C.G.; Österlund, L. Gas-phase photocatalytic activity of sputter-deposited anatase TiO₂ films: Effect of 001 preferential orientation, surface temperature and humidity. *J. Catal.* **2016**, *335*, 187–196. [[CrossRef](#)]
17. Tryba, B.; Jafari, S.; Sillanpää, M.; Nitta, A.; Ohtanic, B.; Morawski, A.W. Influence of TiO₂ structure on its photocatalytic activity towards acetaldehyde decomposition. *Appl. Surf. Sci.* **2019**, *470*, 376–385. [[CrossRef](#)]
18. Seo, H.O.; Woo, T.G.; Park, E.J.; Cha, B.J.; Kim, I.H.; Wook, H.S.; Kim, Y.D. Enhanced photocatalytic activity of TiO₂ films by removal of surface carbon impurities; the role of water vapor. *Appl. Surf. Sci.* **2017**, *420*, 808–816. [[CrossRef](#)]
19. Blount, C.M.; Kim, D.H.; Falconer, J.L. Transparent thin-film TiO₂ photocatalysts with high activity. *Environ. Sci. Technol.* **2001**, *35*, 2988–2994. [[CrossRef](#)]
20. Negishi, N.; Matsuzawa, S.; Takeuchi, K.; Pichat, P. Transparent Micrometer-Thick TiO₂ films on SiO₂-coated glass prepared by repeated dip-coating/calcination: Characteristics and photocatalytic activities for removing acetaldehyde or toluene in air. *Chem. Mater.* **2007**, *19*, 3808–3814. [[CrossRef](#)]
21. Watanabe, T.; Fukayama, S.; Masahiro, M.; Fujishima, A.; Hashimoto, K. Photocatalytic activity and photo-induced wettability conversion of TiO₂ thin film prepared by sol-gel process on a soda-lime glass. *J. Sol-Gel Sci. Technol.* **2000**, *19*, 71–76. [[CrossRef](#)]
22. Yao, N.; Yeung, K.L. Investigation of the performance of TiO₂ photocatalytic coatings. *Chem. Eng. J.* **2011**, *167*, 13–21. [[CrossRef](#)]
23. Kluson, P.; Luskova, H.; Cajthaml, T.; Solcova, O. Non thermal preparation of photoactive titanium (IV) oxide thin layers. *Thin Solid Films* **2006**, *495*, 18–23. [[CrossRef](#)]
24. Yu, J.C.; Yu, J.; Zhao, J. Enhanced photocatalytic activity of mesoporous and ordinary TiO₂ thin films by sulfuric acid treatment. *Appl. Catal. B Environ.* **2002**, *36*, 31–43. [[CrossRef](#)]
25. Yu, C.J.; Yu, J.; Ho, W.; Zhao, J. Light-induced super-hydrophilicity and photocatalytic activity of mesoporous TiO₂ thin films. *J. Photochem. Photobiol. A Chem.* **2002**, *148*, 331–339. [[CrossRef](#)]
26. Coronado, J.M.; Zorn, M.E.; Tejedor-Tejedor, I.; Anderson, M.A. Photocatalytic oxidation of ketones in the gas phase over TiO₂ thin films: A kinetic study on the influence of water vapor. *Appl. Catal. B Environ.* **2003**, *43*, 329–344. [[CrossRef](#)]
27. Maudhuit, A.; Raillard, C.; Héquet, V.; Le Coq, L.; Sablayrolles, J.; Molins, L. Adsorption phenomena in photocatalytic reactions: The case of toluene, acetone and heptane. *Chem. Eng. J.* **2011**, *170*, 464–470. [[CrossRef](#)]
28. Shang, J.; Du, Y.; Xu, Z. Photocatalytic oxidation of heptane in the gas-phase over TiO₂. *Chemosphere* **2002**, *46*, 93–99. [[CrossRef](#)]
29. Galanos, E.; Pouloupoulos, S.; Philippopoulos, C. Photocatalytic destruction of methyl tert butyl ether in the gas phase using titanium dioxide. *J. Environ. Sci. Health A* **2002**, *9*, 1665–1675. [[CrossRef](#)]
30. Park, W.E.; Joo, H.; Kang, J.W. Photodegradation of methyl tertiary butyl ether vapor with immobilized titanium dioxide. *Sol. Energy Mater. Sol. Cells* **2003**, *80*, 73–84. [[CrossRef](#)]
31. Preis, S.; Kachina, A.; Santiago, C.N.; Kallas, J. The dependence on temperature of gas-phase photocatalytic oxidation of methyl tert-butyl ether and tert-butyl alcohol. *Catal. Today* **2005**, *101*, 353–358. [[CrossRef](#)]
32. Oja Acik, I.; Mere, A.; Krunk, M.; Solterbeck, C.H.; Es-Souini, M. Properties of TiO₂ films prepared by the spray pyrolysis method. In *Solid State Phenomena*; Trans Tech Publications: Baech, Switzerland, 2004; Volume 99, pp. 259–264. [[CrossRef](#)]
33. Polivtseva, S.; Oja Acik, I.; Katerski, A.; Mere, A.; Mikli, V.; Krunk, M. Spray Pyrolysis deposition of Sn_xS_y thin films. *Energy Procedia* **2014**, *60*, 156–165. [[CrossRef](#)]
34. Perednis, D.; Gauckler, L.J. Thin film deposition using spray pyrolysis. *J. Electroceram.* **2005**, *14*, 103–111. [[CrossRef](#)]
35. Bang, J.H.; Didenko, Y.; Helmich, R.J.; Suslick, K.S. Nanostructured materials through ultrasonic spray pyrolysis. *Mater. Matters* **2012**, *7*, 15–20.

36. Raut, N.C.; Mathews, T.; Chandramohan, P.; Srinivasan, M.P.; Dash, S.; Tyagi, A.K. Effect of temperature on the growth of TiO₂ thin films synthesized by spray pyrolysis: Structural, compositional and optical properties. *Mater. Res. Bull.* **2011**, *46*, 2057–2063. [[CrossRef](#)]
37. Powder Diffraction File (PDF), (PDF-2/Release 2013 RDB) (01-070-6826) (archived on 1 November 2019).
38. Dupin, J.; Gonbeau, D.; Vinatier, P.; Lévassieur, A. Systematic XPS studies of metal oxides, hydroxides and peroxide. *Phys. Chem. Chem. Phys.* **2000**, *2*, 1319–1324. [[CrossRef](#)]
39. Bharti, B.; Kumar, S.; Lee, H.; Kumar, R. Formation of oxygen vacancies and Ti³⁺ state in TiO₂ thin film and enhanced optical properties by air plasma treatment. *Nat. Sci. Rep.* **2016**, *6*, 32355. [[CrossRef](#)]
40. Sarkar, A.; Khan, G. The formation and detection techniques of oxygen vacancies in titanium oxide-based nanostructures. *Nanoscale* **2019**, *11*, 3414–3444. [[CrossRef](#)]
41. Huang, Y.; Tien, H.; Ma, C.; Yang, S.; Wu, S.; Liu, H.; Mai, Y. Effect of extended polymer chains on properties of transparent graphene nanosheets conductive film. *J. Mater. Chem.* **2011**, *21*, 18236–18241. [[CrossRef](#)]
42. Amor, S.; Jacquet, M.; Fioux, P.; Nardin, M. XPS characterization of plasma treated and zinc oxide coated PET. *Appl. Surf. Sci.* **2009**, *255*, 5052–5061. [[CrossRef](#)]
43. Gromyko, I.; Krunks, M.; Dedova, T.; Katerski, A.; Klauson, D.; Oja Acik, I. Surface properties of sprayed and electrodeposited ZnO rod layers. *Appl. Surf. Sci.* **2017**, *405*, 521–528. [[CrossRef](#)]
44. Chen, W.; Koshy, P.; Christopher, S.C. Effects of film topology and contamination as a function of thickness on the photo-induced hydrophilicity of transparent TiO₂ thin films deposited on glass substrates by spin coating. *J. Mater. Sci.* **2016**, *51*, 2465–2480. [[CrossRef](#)]
45. Jimmy, C.; Yu, J.; Yuk, T.H.; Zhang, L. Effect of surface microstructure on the photoinduced hydrophilicity of porous TiO₂ thin films. *J. Mater. Chem.* **2002**, *12*, 81–85. [[CrossRef](#)]
46. McCafferty, E.; Wightman, J.P. Determination of the concentration of surface hydroxyl groups on metal oxide films by a quantitative XPS method. *Surf. Interface Anal.* **1998**, *26*, 549–564. [[CrossRef](#)]
47. Li, J.; Tang, S.; Lu, L.; Zeng, H.C. Preparation of nanocomposites of metals, metal oxides, and carbon nanotubes via self-assembly. *J. Am. Chem. Soc.* **2007**, *129*, 9401–9409. [[CrossRef](#)] [[PubMed](#)]
48. Zhang, L.; Zhang, J.; Jiu, H.; Ni, C.; Zhang, X.; Xu, M. Graphene-based hollow TiO₂ composites with enhanced photocatalytic activity for removal of pollutants. *J. Phys. Chem. Solids* **2015**, *86*, 82–89. [[CrossRef](#)]
49. Oja, I.; Mere, A.; Krunk, M.; Nisumaa, R.; Solterbeck, C.; Es-Souni, M. Structural and electrical characterization of TiO₂ films grown by spray pyrolysis. *Thin Solid Films* **2006**, *515*, 674–677. [[CrossRef](#)]
50. Simonsen, M.E.; Li, Z.; Søgaard, E.G. Influence of the OH⁻ groups on the photocatalytic activity and photoinduced hydrophilicity of microwave assisted sol–gel TiO₂ film. *Appl. Surf. Sci.* **2009**, *255*, 8054–8062. [[CrossRef](#)]
51. Ohtsu, N.; Masahashi, N.; Mizukoshi, Y.; Wagatsuma, K. Hydrocarbon decomposition on a hydrophilic TiO₂ surface by UV-irradiation: Spectral and quantitative analysis using in-situ XPS technique. *Langmuir* **2009**, *25*, 11586–11591. [[CrossRef](#)]
52. Holtzinger, C.; Rapenne, L.; Chaudouet, P.; Berthome, G.; Langlet, M. Thickness effects in naturally superhydrophilic TiO₂–SiO₂ nanocomposite films deposited via a multilayer sol–gel route. *J. Sol-Gel Sci. Technol.* **2012**, *64*, 465–479. [[CrossRef](#)]
53. Simonsen, M.E.; Sørensen, M.B.; Søgaard, E.G. Comparison of methods for evaluation of activity of photocatalytic films. *Environ. Sci. Pollut. Res.* **2012**, *19*, 3772–3781. [[CrossRef](#)]
54. Zheng, J.; Bao, S.; Guo, Y.; Jin, P. Natural hydrophobicity and reversible wettability conversion of flat anatase TiO₂ thin film. *ACS Appl. Mater. Interfaces* **2014**, *6*, 1351–1355. [[CrossRef](#)]
55. Chen, H.; Nanayakkara, E.C.; Grassian, V. Titanium dioxide photocatalysis in atmospheric chemistry. *Chem. Rev.* **2012**, *112*, 5919–5948. [[CrossRef](#)] [[PubMed](#)]
56. Sakai, N.; Fujishima, A.; Watanabe, T.; Hashimoto, K. Quantitative evaluation of the photoinduced hydrophilic conversion properties of TiO₂ thin film surfaces by the reciprocal of contact angle. *J. Phys. Chem. B* **2003**, *107*, 1028–1035. [[CrossRef](#)]
57. Jing, L.Q.; Qu, Y.C.; Wang, B.Q.; Li, S.D.; Jiang, B.J.; Yang, L.B.; Fu, W.; Fu, H.G.; Sun, J.Z. Review of photoluminescence performance of nano-sized semiconductor materials and its relationships with photocatalytic activity. *Sol. Energy Mater. Sol. Cells* **2006**, *90*, 1773–1787. [[CrossRef](#)]
58. Akbarzadeh, R.; Umbarkar, B.S.; Sonawane, S.R.; Takle, S.; Dongare, K.M. Vanadia–titania thin films for photocatalytic degradation of formaldehyde in sunlight. *Appl. Catal. A* **2010**, *374*, 103–109. [[CrossRef](#)]
59. Li, X.; Yu, J.; Jaroniec, M. Hierarchical photocatalysts. *Chem. Soc. Rev.* **2016**, *45*, 2603–2636. [[CrossRef](#)]

60. Rehman, S.; Ullah, R.; Butt, A.M.; Gohar, N.D. Strategies of making TiO₂ and ZnO visible light active. *J. Hazard. Mater.* **2009**, *170*, 560–569. [[CrossRef](#)]
61. Neti, N.R.; Parmar, G.R.; Bakardjieva, S.; Subrt, J. Thick film titania on glass supports for vapour phase photocatalytic degradation of toluene, acetone, and ethanol. *Chem. Eng. J.* **2010**, *163*, 219–229. [[CrossRef](#)]
62. Demeestere, K.; Dewulf, J.; Van Langenhove, H.; Sercu, B. Gas–solid adsorption of selected volatile organic compounds on titanium dioxide Degussa P25. *Chem. Eng. Sci.* **2003**, *58*, 2255–2267. [[CrossRef](#)]
63. Mamaghani, A.H.; Haghighat, F.; Lee, C. Photocatalytic degradation of VOCs on various commercial titanium dioxides: Impact of operating parameters on removal efficiency and by products generation. *Builld. Environ.* **2018**, *138*, 275–282. [[CrossRef](#)]
64. Ibrahim, H.; de Lasa, H. Kinetic Modeling of the Photocatalytic Degradation of Air-Borne Pollutants. *AIChE J.* **2004**, *50*, 1017–1027. [[CrossRef](#)]
65. Pelaez, M.; Nolan, N.T.; Pillai, S.C.; Seery, M.K.; Falaras, P.; Kontos, A.G.; Dunlop, P.S.M.; Hamilton, J.W.; Byrne, J.A.; O’Sheaf, K.; et al. A review on the visible light active titanium dioxide photocatalysts for environmental applications. *Appl. Catal. B Environ.* **2012**, *125*, 331–349. [[CrossRef](#)]
66. Valeeva, A.A.; Kozlova, E.A.; Vokhmintsev, A.S.; Kamalov, R.V.; Dorosheva, I.B.; Saraev, A.A.; Weinstein, I.A.; Rempel, A.A. Nonstoichiometric titanium dioxide nanotubes with enhanced catalytical activity under visible light. *Sci. Rep.* **2018**, *8*, 9607. [[CrossRef](#)] [[PubMed](#)]
67. Yu, J.; Maa, T.; Liu, S. Enhanced photocatalytic activity of mesoporous TiO₂ aggregates by embedding carbon nanotubes as electron-transfer channel. *Phys. Chem. Chem. Phys.* **2011**, *13*, 3491–3501. [[CrossRef](#)] [[PubMed](#)]
68. Krysa, J.; Novotna, P.; Kment, S.; Mills, A. Effect of glass substrate and deposition technique on the properties of sol-gel TiO₂ thin films. *J. Photochem. Photobiol. A* **2011**, *222*, 81–86. [[CrossRef](#)]



© 2019 by the authors. Licensee MDPI, Basel, Switzerland. This article is an open access article distributed under the terms and conditions of the Creative Commons Attribution (CC BY) license (<http://creativecommons.org/licenses/by/4.0/>).

Publication III

Dundar, A. Mere, V. Mikli, M. Krunk, I. Oja Acik. Thickness effect on photocatalytic activity of TiO₂ thin films fabricated by ultrasonic spray pyrolysis. *Catalysts*, 2020, 10, 1058.

Article

Thickness Effect on Photocatalytic Activity of TiO₂ Thin Films Fabricated by Ultrasonic Spray Pyrolysis

Ibrahim Dundar ^{1,*}, Arvo Mere ¹, Valdek Mikli ², Malle Krunks ¹ and Ilona Oja Acik ^{1,*}

¹ Department of Materials and Environmental Technology, Laboratory of Thin Film Chemical Technologies Tallinn University of Technology, Ehitajate tee 5, 19086 Tallinn, Estonia; arvo.mere@taltech.ee (A.M.); malle.krunks@taltech.ee (M.K.)

² Laboratory of Optoelectronic Materials Physics, Department of Materials and Environmental Technology, Tallinn University of Technology, Ehitajate tee 5, 19086 Tallinn, Estonia; valdek.mikli@taltech.ee

* Correspondence: ibrahim.dundar@taltech.ee (I.D.); ilona.oja@taltech.ee (I.O.A.)

Received: 31 July 2020; Accepted: 28 August 2020; Published: 14 September 2020



Abstract: In this study, TiO₂ thin films were deposited by ultrasonic spray pyrolysis from solutions with concentrations of 0.1 and 0.2 M. The deposition temperature was adjusted at 350 °C and all samples were annealed at 500 °C for 1 h in air. The thickness of TiO₂ films was changed in the range of 50 to ca. 800 nm by varying the number of spray cycles from 1 to 21 and the solution concentration. The results showed that the mean crystallite size of the anatase structure, the surface roughness, and light absorption increased with the film thickness. The effect of film thickness on the photocatalytic activity was investigated with the photodegradation of stearic acid under UV-A irradiation. The optimal thickness of TiO₂ films fabricated by ultrasonic spray pyrolysis for photocatalytic self-cleaning applications was in the range of 170–230 nm, indicating a ca. 2.6 times-higher photocatalytic self-cleaning activity compared to the reference sample, Pilkington Activ™. The photocatalytic results showed that the 190 nm-thick TiO₂ film deposited from the 0.1 M solution applying seven spray cycles exhibited the finest grain structure and maximum photocatalytic activity, leading to 94% of stearic acid degradation in 180 min under UV-A light with the reaction rate constant $k = 0.01648 \text{ min}^{-1}$.

Keywords: TiO₂; thin film; ultrasonic spray pyrolysis; thickness effect; precursor concentration; photocatalytic activity

1. Introduction

Highly active photocatalytic TiO₂ thin films are desired in several applications, especially in pollution treatment and self-cleaning technologies [1–3]. Among them, self-cleaning coatings have been the most rapidly developed technology during last decades targeting a wide range of applications from window glass and cement to textiles [3–5]. The market growth of photocatalytic coatings is expected to be achieved by their ever-growing demand in building construction, and growing concern over pollution and airborne virus outbreaks [4]. Therefore, the application of photocatalytic coatings on high-touch surfaces will be essential in public places such as hospitals, public transportation, athletic centers, schools, acute care facilities, airports, arenas, and other facilities to reduce the spread of airborne toxins and allergens, such as COVID-19 and other viruses [5].

Photocatalytic reaction is fundamentally a surface reaction; however, several studies have shown that the photocatalytic activity of thin films depends on the film thickness [6–8].

In the case of photocatalytic self-cleaning surfaces, it is important to define in which thickness the catalyst layer shows the highest photocatalytic activity and transparency in the visible spectral range in order to provide the required self-cleaning activity while retaining the visual appearance of the

coated surface. The effect of thickness on photocatalytic activity has been studied for nanocrystalline TiO₂ thin films, for example, obtained by atomic layer deposition (ALD) [9,10], sputtering [6,11,12], metal-organic chemical vapor deposition (MOCVD) [13,14], and sol-gel methods [15–19].

Kääriäinen et al. [10] studied the TiO₂ thin films in the thickness range of 2.6–260 nm deposited by ALD and reported the highest photocatalytic activity for 130 nm thick films. Blanco et al. [18] reported the highest photocatalytic activity for a 250 nm-thick sol-gel-deposited TiO₂ film. On the contrary, Xianyu et al. [19] reported, for sol-gel dip-coated TiO₂ films, an increase in photocatalytic activity within a thickness range of 70–670 nm. A similar increase in photocatalytic activity within the thickness range of 100 to 500 nm has also been reported for DC magnetron sputtered TiO₂ films [6]. However, Marcello et al. [13] reported an optimum thickness of 395 nm for MOCVD-deposited TiO₂ films, whereas Yong-Ick Cho et al. [14] reported, for MOCVD-deposited TiO₂ coatings, increases in photocatalytic activity between the thickness range of 110 nm to 5 µm, which remain constant for thicker films between 5 and 15 µm. According to these studies, the photocatalytic activity of the TiO₂ films improves with increasing film thickness until a limit, dominantly in the range of 130–500 nm, from which the degradation reaction remains almost constant or decreases. Some studies, on the other hand, confirm the increase in photocatalytic activity with film thickness up to several microns.

Based on the studies above, we could conclude that the photocatalytic activity of thin films is influenced by the film thickness; however, several other film parameters such as crystallinity and grain size, primarily conditioned by the thin-film preparation method, should also be taken into account.

In the wider photocatalytic self-cleaning coating application point of view, coating fabrication technologies must meet the requirements for rapid, robust, cost-effective, and resource-saving technologies, able to coat surfaces with different profiles and shapes. Chemical solution-based technologies provide the technological key for the production of cost-effective nanocrystalline transparent surface coatings. Among them, the ultrasonic spray pyrolysis (USP) method offers a possibility to fabricate nonplanar surfaces with a high uniformity [2,20]. Moreover, when processing a thin film by the chemical spray pyrolysis method, the key to engineering the film properties lays on the solution concentration [21] and deposition temperature [22], giving the fingerprint for the film properties, irrespective of the post-deposition treatment conditions [2,23]. Recently, we showed that the optimal deposition temperature of TiO₂ films by USP is 350 °C. These TiO₂ films with a material quantity of 0.2 mg/cm² effectively degraded volatile organic carbon species such as acetone, acetaldehyde, and heptane [2]. However, despite the many advantages, including the easy scale-up in industry and the possibility to promptly cover large areas, there are a limited number of studies about TiO₂ thin films deposited by the USP method as a photocatalytic material [2,20,24]. To the best of our knowledge, no comprehensive study has been reported focusing on the thickness effect on the photocatalytic activity of USP-prepared TiO₂ thin films.

The aim of the study was to find the optimal thickness range of TiO₂ thin films prepared by ultrasonic spray pyrolysis for photocatalytic applications. Therefore, we tested the effect of film thickness with different solution concentrations on the morphological, structural, and optical properties, and photocatalytic activity. In addition, the effect of solution concentration on the fingerprint properties of sprayed TiO₂ films was taken into account. The photocatalytic stearic acid degradation results were compared to the commercial Pilkington Active glass as a reference material for the photocatalyst thin films.

2. Results

2.1. Material Characterization

2.1.1. Surface Morphology

Figure 1 shows the SEM surface images of TiO₂ thin films deposited with 2, 6, and 15 spray cycles. All TiO₂ thin films showed plane-surface morphology regardless of the solution concentration and number of spray cycles. However, with the increase in the number of spray cycles, the formation of

nano-cracks become visible. The formation of nano-cracks in the thin films is usually determined by the development of compressive stress [25,26] and thermal expansion (coefficients) mismatch between the TiO₂ film ($8.4 \times 10^{-6} \text{ K}^{-1}$) and glass substrate ($3.3 \times 10^{-6} \text{ K}^{-1}$). The effect of cracks formed on the photocatalyst film surfaces is still open for discussion, whether it has a beneficial [27] or backward effect [27,28] on the photocatalytic performance.

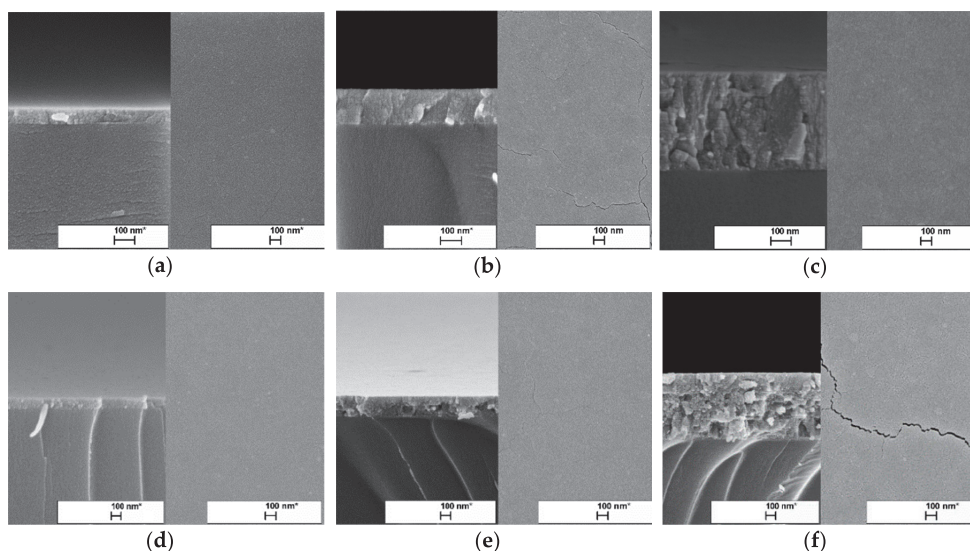


Figure 1. Surface and cross-sectional SEM images of TiO₂ thin films prepared from different solution concentrations and spray cycles. TiO₂ thin films deposited from 0.1 M solution with the number of spray cycles: (a) 2, (b) 6, and (c) 15. TiO₂ thin films deposited from 0.2 M solution with the number of cycles: (d) 2, (e) 6, and (f) 15.

The thickness of TiO₂ films was estimated from SEM cross-sectional images (Figure 1). The thicknesses of the TiO₂ films prepared from the 0.1 M solution were 65, 165, and 455 nm, while for the films from the 0.2 M solution, thicknesses of 50, 205, and 635 nm were shown with the increase in number of spray cycles from 2 to 15 (Table 1). In general, TiO₂ films deposited from the 0.2 M solution were thicker compared to those deposited from the 0.1 M solution. However, films deposited at two spray cycles showed similar thicknesses.

Table 1. Summary of the morphological and structural properties of TiO₂ thin films.

Cycle No.	TTIP Concentration in Solution (M)	Deposition Time (min)	Deposition Rate (nm min ⁻¹)	Thickness (nm)/SEM	RMS (nm)/AFM	Mean Crystallite Size (nm)/XRD
2	0.1	2.9	22.4	65	1.60	30
6	0.1	8.7	19.0	170	1.60	45
15	0.1	21.75	20.9	455	2.60	50
2	0.2	2.9	17.2	50	0.80	25
6	0.2	8.7	23.6	205	1.10	35
15	0.2	21.75	29.2	635	1.60	40

Figure 2 presents AFM images (scan area $2 \times 2 \mu\text{m}^2$) of the TiO₂ films sprayed from the 0.1 and 0.2 M solution applying 2, 6, and 15 spray cycles. The surface of TiO₂ films deposited from the 0.1 M solution at 2 and 6 spray cycles is characterized by fine grains with a size of ca. 20 nm and a low rate of agglomeration, as mainly agglomerates with a size of ca. 40 nm are visible. The characteristic

RMS roughness of both films is 1.6 nm, indicating that the TiO_2 films most probably tend to grow in the early stage of deposition following a layer-by-layer growth under these deposition conditions. By increasing the number of spray cycles to 15, the surface of the TiO_2 films reveals agglomerates with a size in the range of 40 to 150 nm, resulting in an increase in the RMS roughness to 2.6 nm. In addition, the nano-cracks on the surface could contribute to the increased RMS roughness values. TiO_2 films deposited from the 0.2 M solution show slightly different surface morphology. The characteristic grain size remains at ca. 20 nm; however, the size of agglomerates increases from ca. 50 to 100 nm by increasing the number of spray cycles from 2 to 15. This increase is also reflected in RMS roughness values, which increase from 0.8 to 1.6 nm with the spray cycles. These results are in correlation with our previous studies for TiO_2 films deposited from a 0.2 M solution by the pneumatic spray pyrolysis method, indicating that TiO_2 films, irrespective of the substrate, follow a 3-D growth profile, where, in the first stage, the formation of a separated island occurs, which, during further deposition, agglomerate to larger islands, retaining the characteristic grain size [29].

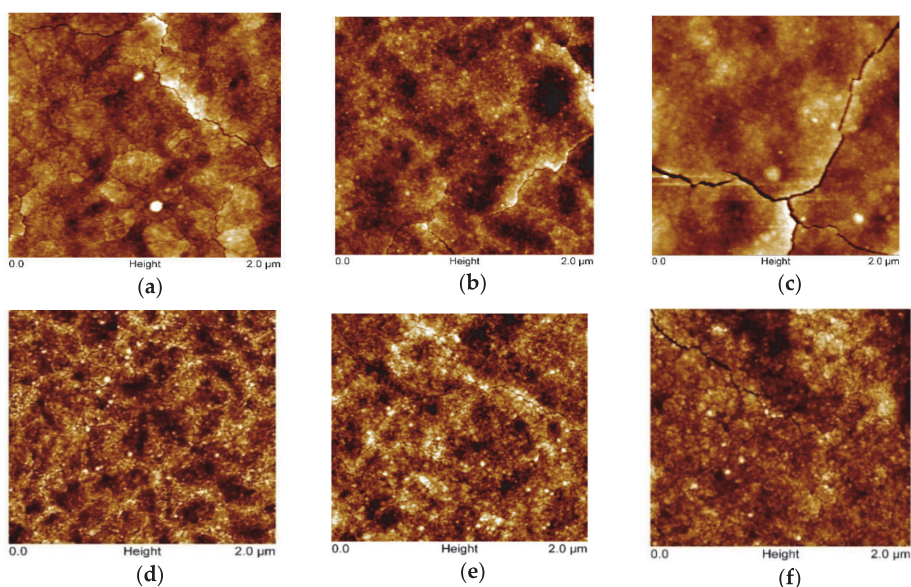


Figure 2. AFM images of TiO_2 thin films deposited from different solution concentrations and cycle numbers. TiO_2 thin films deposited from 0.1 M solution with the number of spray cycles: (a) 2, (b) 6, and (c) 15. TiO_2 thin films deposited from 0.2 M solution with the number of spray cycles: (d) 2, (e) 6, and (f) 15.

2.1.2. Structural Properties

Figure 3 displays XRD patterns of the TiO_2 films deposited from the 0.1 and 0.2 M solution by varying the number of spray cycles from 2 to 15. As it can be seen, all TiO_2 films, irrespective of the solution concentration and number of spray cycles, show anatase crystalline structure (JCPDS card No. 01-070-6826).

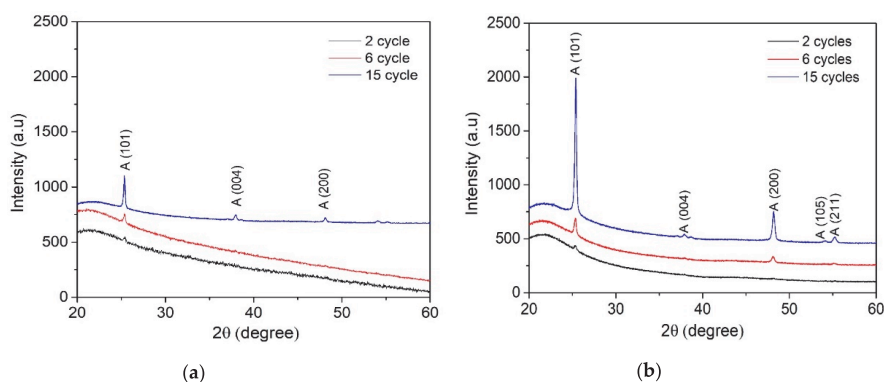


Figure 3. XRD patterns of TiO₂ films deposited from (a) 0.1 M solution with 2, 6, and 15 spray cycles and (b) 0.2 M solution with 2, 6, and 15 spray cycles.

The mean crystalline size of TiO₂ films (Table 1) was calculated from the (101) anatase diffraction peak using Scherrer's equation. It was observed that the mean crystallite size of TiO₂ thin films deposited from the 0.1 M solution increased from 30 to 50 nm and that of the 0.2 M solution increased from 25 to 40 nm with the number of spray cycles from 2 to 15. TiO₂ films deposited from the 0.1 M solution showed a larger mean crystallite size compared to the films deposited from the 0.2 M solution. This can be explained by the lower amount of organic residues on the film surface deposited from the 0.1 M solution compared to those deposited from the 0.2 M solution, taking into account the constant deposition time per cycle 87 s as the deposition time per cycle was kept constant at 87 s. In our previous study, we showed that sprayed TiO₂ films deposited at 315–435 °C contain organic residues originating from the decomposition of the titanium (IV) isopropoxide (TTIP):Acetylacetonate (AcacH) precursors system [30], and the further post-deposition treatment at 500 °C promotes the growth of crystalline structure. The presence of organic residues in the as-deposited films, which can be controlled by the deposition temperature, determines the structural properties. The results correlate with the AFM results, showing higher RMS surface roughness for the films deposited from the 0.1 M TTIP solution.

The deposition rate of the TiO₂ films from the 0.1 and 0.2 M solution was calculated, taking into account the constant spray cycle time of 87 s. The deposition rate (Table 1) of TiO₂ films deposited from the 0.1 M TTIP solution remains between 19 and 22 nm min⁻¹ and is not influenced by the number of spray cycles. In contrary to that, the films deposited from the 0.2 M TTIP solution show an increase in the deposition rate from 17 to 29 nm min⁻¹ with the number of spray cycles from 2 to 15.

Based on the morphological and structural studies of the TiO₂ films, we can conclude that the thickness of films is more precisely controlled by the number of spray cycles in the case of the 0.1 M solution, which leads to the formation of TiO₂ films with higher surface roughness and larger mean crystallite size compared to films deposited from the 0.2 M solution.

2.1.3. Optical Properties

The total transmittance spectra of TiO₂ films deposited from the 0.1 M (Figure 4a) and 0.2 M (Figure 4b) solutions indicate that the films are transparent in the visible spectral range, showing an average transmittance of 70–80%, irrespective of the solution concentration and the number of spray cycles. However, TiO₂ films deposited using two spray cycles most probably do not result in uniform coverage on the borosilicate substrate, possibly due to the formation of pinholes, as, in the low-wavelength side at 300 nm, the total transmittance spectrum does not cross the 0 point of the *y*-axis. The indirect bandgap of TiO₂ films was calculated by using the Tauc plot, and the obtained values for films remained at 3.40 ± 0.05 eV. The optical bandgap value of bulk anatase-TiO₂ was 3.20 eV.

A higher bandgap value than that of the bulk TiO_2 has also been observed in the different studies of TiO_2 thin films deposited by chemical spray pyrolysis methods [31,32].

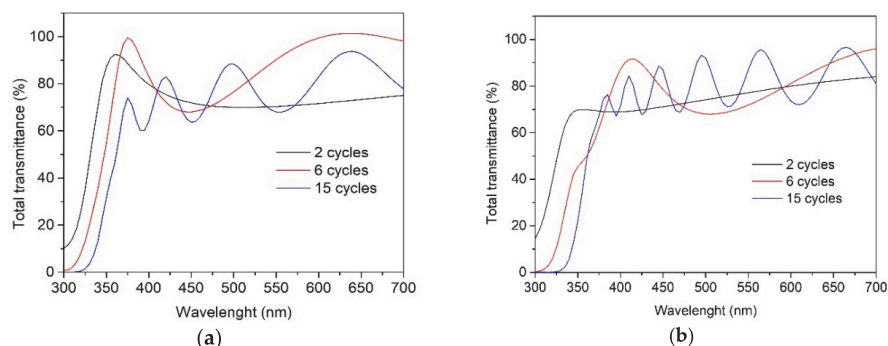


Figure 4. Total transmittance spectra of the TiO_2 films deposited from solution with the concentrations of (a) 0.1 M and (b) 0.2 M onto borosilicate substrate and varying the number of spray cycles from 2 to 15.

The thickness of TiO_2 films (Figure 5) as a function of the number of spray cycles was determined from total transmittance spectra interference fringes using an effective refractive index of 2.8 by the Fizeau fringe method. The refractive index was estimated by taking into account the average thickness of the TiO_2 film deposited at six spray cycles from SEM cross-sectional images. The film thickness obtained from SEM cross-sectional images is presented for comparison (Figure 5). Some discrepancies in thickness values obtained from SEM cross-sectional images and total transmittance spectra, especially for films from the 0.2 M solution, can originate from the local thickness from SEM and average thickness obtained by UV-VIS.

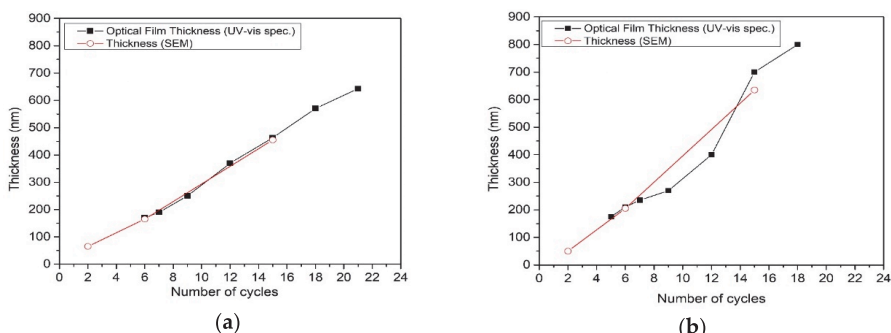


Figure 5. TiO_2 thin film thickness dependence on number of spray cycles and solution concentration (a) 0.1 M and (b) 0.2 M. Film thickness values obtained from SEM cross-sectional images and UV-Vis spectroscopy using Fizeau method.

In the case of TiO_2 films deposited from the 0.1 M solution, the film thickness dependence on the number of spray cycles (Figure 5a) shows almost linear behavior, indicating a similar growth rate within the studied thickness range (Table 1). On the other hand, the thickness of TiO_2 films, deposited from the 0.2 M solution, shows exponential behavior on the number of spray cycles and rapid increase in the deposition rate (Table 1), confirming the 3D film growth. In the case of the 0.2 M solution, the rapid film growth rate with the number of spray cycles hinders the formation of films without organic residues, thereby retarding the formation of crystalline material, which is reflected by the lower mean crystallite size of the anatase phase in films deposited from the 0.2 M solution compared to those deposited from the 0.1 M solution (Table 1).

The absorbance spectra of the TiO₂ films obtained from 0.1 M solution (Figure 6a) and 0.2 M solution (Figure 6b) show similar tendency. All TiO₂ films absorbed light in the UV-A region (a wavelength of 380 nm and below) and showed variation in the degree of absorbance with increasing the number of spray cycles and thereby the film thickness. The absorption edge of TiO₂ films is red shifted for thicker films deposited at 6 and 15 cycles, which can be attributed to larger crystallite size of the thicker films, correlating with XRD results (Table 1).

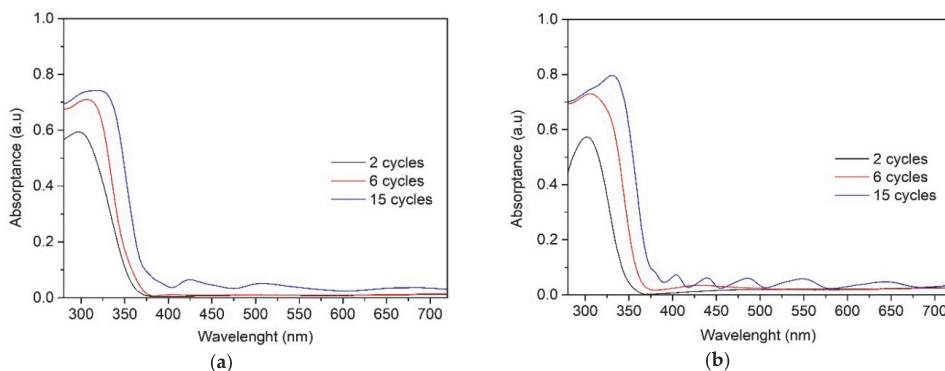


Figure 6. UV-Vis absorption spectra of the TiO₂ films deposited with solutions of (a) 0.1 M and (b) 0.2 M and varying the number of spray cycles from 2 to 15.

2.2. Photocatalytic Activity

The effect of film thickness on the photocatalytic activity was evaluated for TiO₂ thin films prepared using 0.1 and 0.2 M solutions. Self-cleaning performance was investigated by spin-coated stearic acid degradation on the surface of TiO₂ thin films under UV-A light irradiation. This is a widely applied method for assessing the activity of self-cleaning materials as stearic acid is an adequate model compound for organic fouling [33,34]. Stearic acid absorbs strongly in the region 2700–3000 cm⁻¹, with bands at 2958, 2923, and 2853 cm⁻¹ due to asymmetric in-plane C–H stretching in the CH₃ group and asymmetric and symmetric C–H stretching in the CH₂ groups, respectively [20]. The degradation of stearic acid was determined by using the integrated area of characteristic bands of stearic acid in the wavenumber range of 2700–3000 cm⁻¹ (Figure 7). The decrease in the specific stearic acid band intensity was monitored using FT-IR spectroscopy as a function of irradiation time. FTIR spectra were measured before the UV-A irradiation and after every 60 min for three hours.

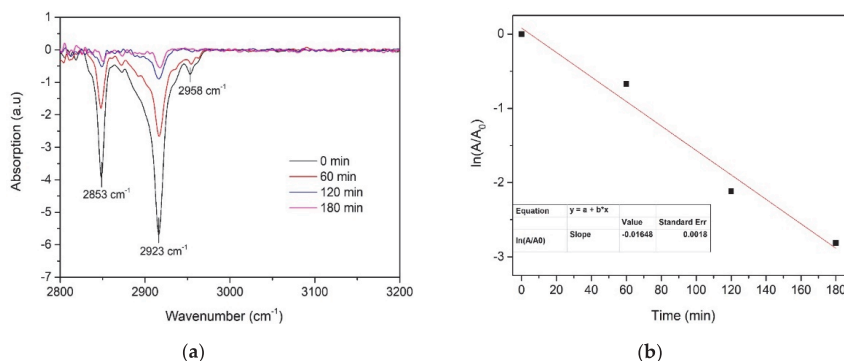


Figure 7. (a) FTIR spectra of stearic acid on the surface of TiO₂ thin-film-deposited 0.1 M solution using 7 spray cycles and (b) the determination of the photodegradation rate constant (k).

Stearic acid degradation under UV-A light is known to follow first-order kinetics, i.e., the integrated band area (A) depends on time as follows:

$$A(t) = A_0 e^{-k} \quad (1)$$

where k is the photodegradation rate constant. The photodegradation rate constant is the slope value of the linear fit of the plot $\ln(A/A_0)$ versus time. Photodegradation of stearic acid on the surface of the TiO_2 film (thickness ca. 210 nm) and determination of the photodegradation rate constant are presented in Figure 7.

TiO_2 thin films were treated with UV-A light for 60 min to make the film surface photo-induced and superhydrophilic prior to coating the surface of the films with stearic acid. After UV-A treatment for 60 min, the water contact angle of all samples drops below 10° , indicating superhydrophilic behavior. It has been observed by several authors that the thin film surface structure and wettability properties of the films affect the growth of the stearic acid layer on the surface of a photocatalytic material [20,35]. It has been reported that the samples having similar structural and wettability properties show the same initial integrated area of stearic acid [35]. Therefore, it can be assumed that the initial integrated area of stearic acid is approximately the same for all samples in the current study.

Photodegradation of stearic acid layer as a function of irradiation time, and the photodegradation rate constants (k) for TiO_2 thin films deposited with variable solution concentrations and different cycle numbers are presented in Figures 8 and 9, respectively.

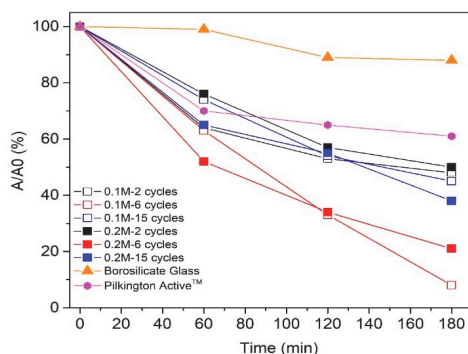


Figure 8. The degradation of stearic acid as a function of ultraviolet (UV-A) irradiation time on TiO_2 films deposited from 0.1 and 0.2 M solution applying 2, 6, and 15 spray cycles.

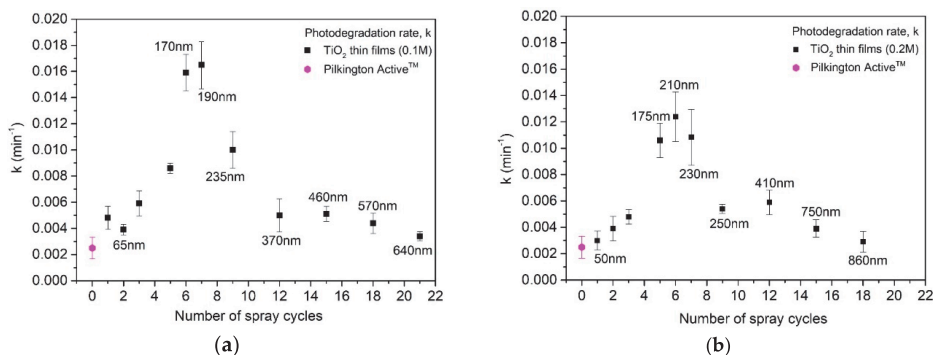


Figure 9. Photodegradation rate constant (k) values (standard errors shown by error bars) for the TiO_2 films deposited from solution with a concentration of (a) 0.1 M and (b) 0.2 M as a function of the number of spray cycles and film thicknesses. Film thicknesses are obtained by UV-Vis spectroscopy (Figure 5).

Photocatalytic degradation of stearic acid layer on TiO₂ films deposited by employing 2 (thickness ca. 50–65 nm) and 15 spray cycles (thickness 450 nm (0.1 M) and 635 nm (0.2 M)) was ca. 50% after 180 min exposure to UV-A irradiation (Figure 8). TiO₂ films deposited employing 6 cycles with thicknesses of ca. 170 nm (0.1 M) and 210 nm (0.2 M) indicate almost complete degradation (92%) of stearic acid after 180 min of UV-A irradiation. For comparison, the degradation of the stearic acid layer on the commercial Pilkington Active™ glass was 1.5 times lower (35%) compared to the sprayed TiO₂ films within the same thickness range (50–60 nm) and under the same measurement conditions. According to the SEM cross-sectional image (not shown), the Pilkington Active glass consists of a double-layer structure with a total thickness of ca. 60 nm, comprising a 25 nm-thick TiO₂ layer and 35 nm SiO₂ barrier layer, similar to the literature [34].

Figure 9 presents the photocatalytic reaction rate constant of the sprayed TiO₂ films from 0.1 and 0.2 M solutions compared to the commercial Pilkington Active™ as a reference. The photocatalytic reaction rate constant increases with the film thickness from ca. 50 nm (2 cycles) to ca. 200 +/- 30 nm (5–7 cycles) and decreases with the further increase in film thickness, viz. the number of spray cycles. TiO₂ films deposited from both 0.1 and 0.2 M solutions employing six and seven spray cycles indicate ca. 3.5 times-higher photocatalytic reaction rate constant compared to the films with other thicknesses in both series. Furthermore, TiO₂ films deposited from the 0.1 M solution (Figure 9a) indicate a slightly higher photocatalytic reaction rate constant compared to the films with similar thicknesses or cycle numbers deposited from the 0.2 M solution.

The lower activity of the TiO₂ films deposited employing one to three spray cycles (Figure 9), with a thickness below 100 nm, compared to the 200 +/- 30 nm TiO₂ is related to their lower absorption of UV-A light (Figure 6). When the film is very thin, only a small portion of incident light is absorbed in the catalyst. Thus, the films with low thickness are incapable of high photocatalytic performance [13,17]. The photocatalytic activity increases with the film thickness from 50 to 200 +/- 30 nm, which can be attributable to the increase in the amount of TiO₂, and thus higher light absorption (Figure 6), providing more photogenerated carriers for the reaction. However, thicker TiO₂ films deposited at a higher number of spray cycles than nine, irrespective of solution concentration, show a decrease in their photocatalytic activity. This phenomenon is characteristic for thin films, observed by other authors as well [17,36], and has been explained by a higher recombination rate of photocarriers [17,34].

TiO₂ films deposited employing seven spray cycles from the 0.1 M solution (Figure 9a) show a higher photocatalytic reaction rate constant of 0.01648 min⁻¹ compared to the films with similar thicknesses from the 0.2 M solution of 0.01094 min⁻¹. A similar solution concentration effect on photocatalytic activity has been reported for spin-coated TiO₂ films deposited from 0.1 and 0.3 M solutions. However, in their studies, the higher photocatalytic activity of films from the 0.1 M solution was attributed to significantly higher surface roughness compared to 0.3 M, viz. 7.6 and 1.5 nm [17]. In our studies, however, the surface roughness of films deposited from 0.1 and 0.2 M does not differ in such a high level. Therefore, we can conclude that, in this study, the combination of several film properties such as higher mean crystallite size (45 nm vs. 35 nm), finer grain structure with a smaller size of agglomerates (20–40 vs. 70 nm), and higher surface RMS roughness (1.6 nm vs. 1.1 nm) favors the photocatalytic self-cleaning activity of TiO₂ films deposited from the 0.1 M solution compared to those from 0.2 M solutions. Furthermore, after the maximum photocatalytic activity (Figure 9), the *k* value decreases, irrespective of the solution concentration, and not resulting in a plateau as could be expected. We could speculate that the maximum photocatalytic activity of films with a thickness of 200 +/- 30 nm is induced by the reflectance-assisted absorptance, being enhanced by the internal borosilicate glass/TiO₂ interface. This phenomenon could promote the additional generation of carriers, which migrates to the film surface and increases the photocatalytic activity of films.

Our study confirms that in the case of the solution-based chemical methods, not only the film thickness but also the solution concentration-derived effect on film properties shall be taken into account when optimizing the deposition protocol for the TiO₂ thin films.

As the decomposition rate of stearic acid could depend on many factors, including UV illumination conditions. Thus, it is difficult to directly compare stearic acid decomposition rate values obtained for TiO₂ films in the literature. Our results coincide with the ones obtained by Cedillo-Gonzalez et al. [37]. In their study, they have shown that spin-coated TiO₂ film with a thickness of 150 nm exhibit stearic acid degradation rate constant of 0.0017 min⁻¹ under UV-A irradiation.

3. Materials and Methods

3.1. Thin-Film Synthesis and Materials Characterization

Thin films were deposited onto 2 × 2 cm² borosilicate glass substrates at 350 °C by using the ultrasonic spray pyrolysis method. All films were annealed at 500 °C for 1 h in air on a hotplate. The spray solution consisted of titanium (IV) isopropoxide (TTIP) and acetylacetone (AcacH) in a molar ratio of 1:4 in ethanol. The TTIP concentration in spray solution was fixed at 0.1 and 0.2 mol L⁻¹. Compressed air was applied as the carrier gas with a flow rate of 5 L min⁻¹, and the corresponding solutions are named in the text as 0.1 M and 0.2 M solutions. The spraying rate was set up to 2.5 mL min⁻¹. In the current study, the film thickness was controlled by altering the number of spray cycles, adjusted to 1, 2, 3, 6, 9, 12, 15, 18, and 21.

Scanning electron microscopy (SEM) and atomic force microscopy (AFM) were operated to investigate surface morphology. The surface morphology and the film thickness of the films were obtained with the help of Zeiss HR FESEM Ultra 55 scanning electron microscopes with an acceleration voltage of 4.0 kV. The surface morphology of the films was studied using a NT-MDT Solver 47 Pro system, and measurement was carried out in the non-contact mode and the investigated area was 2000 × 2000 nm² per scan. Surface roughness analysis was carried out through the two-dimensional AFM scan, which was in accordance with the ISO 4287/1 standard. The root mean square (RMS) roughness was calculated over a 2000 × 2000 nm² scanned surface area with an accuracy of ± 0.5 nm.

The crystalline structure and phases were investigated using an X-ray diffractometer (XRD). XRD patterns were recorded on a Rigaku Ultima IV diffractometer with Cu K α radiation ($\lambda = 1.5406$ Å, 40 kV at 40 mA). The XRD patterns were performed in 2 theta configurations with the 2 theta range of 20–60°, with a scanning speed of 2 min⁻¹ and with a step size of 0.02°. The Scherrer method was used to calculate the mean crystallite size, using the FWHM (full-width at half-maximum) of the (101) reflection of the TiO₂ anatase phase.

The total transmittance and reflectance of the TiO₂ films on borosilicate glass was measured in the wavelength range of 250–800 nm using a Jasco V-670 UV-VIS-NIR spectrophotometer equipped with a 40 nm integrating sphere. Absorption spectra were calculated by using total transmittance and reflectance spectra of TiO₂ films, with the following equation:

$$A = 1 - T - R \quad (2)$$

Wettability of the films was determined by water contact angle (WCA) measurement. DSA 25 (KRÜSS Instrument) was carried out at room temperature. A sessile drop-fitting method was applied for WCA measurements. An Actinic BL 15 W fluorescent lamp (Philips), with max emission at 365 nm, was used to investigate the dependence of the WCA of aged-TiO₂ films on UV-irradiation under ambient conditions.

3.2. Photocatalytic Measurements

The photocatalytic activity was evaluated using stearic acid as a model compound, in which a thin layer of stearic acid is deposited onto 2 × 2 cm² TiO₂ samples and the photocatalytic decomposition of stearic acid is observed as a function of UV-A irradiation time.

Stearic acid coating was performed from a solution of 8.8 mM stearic acid in methanol. In addition, 100 μ L of stearic acid solution in methanol was dropped onto the center of the sample and deposited

using the sol-gel spin-coating method with a rotation speed of 1000 rpm for 30 s. Samples were then dried at 80 °C in air for 10 min.

Fourier-transform infrared spectroscopy (FTIR) was performed to examine the photocatalytic destruction of stearic acid in a transmission mode as a function of UV irradiation time. FTIR spectra were measured before the UV-A irradiation and every 60 min for three hours. The degradation of stearic acid was determined by using the integrated area of the bands [20].

The following parameters were set-up for FTIR measurement: Wavenumber region 3200–2500 cm^{-1} , number of scans 32, resolution 4 cm^{-1} . The UV Philips Actinic BL 15 W with maximum emission at 365 nm and incident light intensity of 3.5 mW cm^{-2} was used as an irradiation source. A TiO_2 sample without a stearic acid layer on it was used as a reference during the measurements [20].

4. Conclusions

TiO_2 thin films were fabricated on a borosilicate glass substrate by using ultrasonic spray pyrolysis. The solution concentrations of 0.1 and 0.2 M and various deposition cycles were used. The deposition temperature was adjusted at 350 °C and the process was followed by annealing at 500 °C for 1 h in air. The results showed that the TiO_2 film thickness increases from 50 to 800 nm with the increase in precursor concentration from 0.1 to 0.2 M and the number of spray cycles from 1 to 21. TiO_2 films possess smooth surface morphology, showing an RMS roughness in the range of 1.60–2.60 and 0.80–1.60 nm for films deposited from 0.1 and 0.2 M solutions, respectively. XRD analysis showed that the mean crystallite size increases with the number of spray cycles, remaining in the range of 30–50 and 25–40 nm for films deposited from 0.1 and 0.2 M solutions, respectively. All TiO_2 films indicate a total transmittance of 70–80% in the visible spectral region.

Photocatalytic activity of the TiO_2 thin films was studied by the stearic acid test under UV-A light. The photodegradation rate of stearic acid increases with film thickness from 50 to 200 \pm 30 nm and decreases at higher film thicknesses. A maximum photocatalytic activity of 200 \pm 30 nm thick TiO_2 films could be induced by the reflectance-assisted absorptance, supported by the borosilicate glass/ TiO_2 interface, which could promote additional generation of charge carriers.

The TiO_2 thin film from the 0.1 M solution with a thickness of ca. 190 nm showed the highest activity in stearic acid degradation under UV-A with a reaction rate constant $k = 0.01648 \text{ min}^{-1}$, and a 6 times higher photocatalytic reaction rate constant than Pilkington Active™ self-cleaning glass ($k = 0.0025 \text{ min}^{-1}$).

This study revealed that the 150–250 nm-thick TiO_2 thin film prepared by ultrasonic spray pyrolysis could be of particular interest for the development of self-cleaning windows providing a low manufacturing cost due to the higher photocatalytic performance obtained from the lower precursor concentration (0.1 M TTIP) without the need of further film thickness.

Author Contributions: I.D. carried out the thin-film deposition and material characterizations (XRD, optical properties, and wettability test), carried out data collection for a photocatalytic activity test by FTIR, took part in the design of all the figures and tables, and participated in the writing of the manuscript and drafted the manuscript. A.M. participated in data analysis and associated preparation of the manuscript. V.M. carried out SEM and AFM measurements. I.O.A. carried out the design of the study and participated in data analysis and associated preparation of the manuscript. M.K. participated in data analysis. All authors have read and agree to the published version of the manuscript.

Funding: I.D. is supported by the Estonian Ministry of Education and Research, Estonian Research Council projects IUT19-4 and PRG627, Estonian Centre of Excellence project TK141, and EU regional Fund project 2014-2020.4.01.16-0032. I.O.A., M.K and A.M. are supported by the Estonian Ministry of Education and Research, Estonian Research Council projects IUT19-4 and PRG627, and Estonian Centre of Excellence project TK141. V.M. is supported by the Estonian Centre of Excellence project TK141. This work has been partially supported by ASTRA ‘TUT Institutional Development Program for 2016–2022’ Graduate School of Functional Materials and Technologies (2014-2020.4.01.16-0032).

Conflicts of Interest: The authors declare no conflict of interest.

References

1. Dedova, T.; Oja Acik, I.; Chen, Z.; Katerski, A.; Balmassov, K.; Gromyko, I.; Nagyne-Kovacs, T.; Szilagyai, I.M.; Krunk, M. Enhanced photocatalytic activity of ZnO nanorods by surface treatment with H₂AuCl₄: Synergic effects through an electron scavenging, plasmon resonance and surface hydroxylation. *Mater. Chem. Phys.* **2020**, *245*, 122767. [CrossRef]
2. Dundar, I.; Krichevskaya, M.; Katerski, A.; Oja Acik, I. TiO₂ thin films by ultrasonic spray pyrolysis as photocatalytic material for air purification. *R. Soc. Open Sci.* **2019**, *6*, 181578. [CrossRef] [PubMed]
3. Banerjee, S.; Dionysiou, D.D.; Pillai, S.C. Self-cleaning applications of TiO₂ by photo-induced hydrophilicity and photocatalysis. *Appl. Catal. B* **2015**, *176–177*, 396–428. [CrossRef]
4. Chen, J.; Poon, C. Photocatalytic construction and building materials: From fundamentals to applications. *Build Environ.* **2009**, *44*, 1899–1906. [CrossRef]
5. Future Markets. Available online: www.futuremarketsinc.com/the-global-market-for-photocatalytic-nanocoatings (accessed on 22 July 2020).
6. Daviðsdóttira, S.; Shabadi, R.; Galcaci, A.C.; Andersson, I.H.; Dirscherle, K.; Ambat, R. Investigation of DC magnetron-sputtered TiO₂ coatings: Effect of coating thickness, structure, and morphology on photocatalytic activity. *Appl. Surf. Sci.* **2014**, *313*, 677–686. [CrossRef]
7. Kenanakisa, G.; Vernardoua, D.; Dalamagkasa, A.; Katsarakis, N. Photocatalytic and electrooxidation properties of TiO₂ thin films deposited by sol–gel. *Catal. Today* **2015**, *240*, 146–152. [CrossRef]
8. Quici, N.; Vera, L.M.; Choi, H.; Puma, G.L.; Dionysiou, D.D.; Litter, I.M.; Destailats, H. Effect of key parameters on the photocatalytic oxidation of toluene at low concentrations in air under 254 + 185 nm UV irradiation. *Appl. Catal. B Environ.* **2010**, *95*, 312–319. [CrossRef]
9. Heikkilä, M.; Puukilainen, E.; Ritala, M.; Leskelä, M. Effect of thickness of ALD grown TiO₂ films on photoelectrocatalysis. *J. Photoch. Photobiol. A Chem.* **2009**, *204*, 200–208. [CrossRef]
10. Kääriäinen, M.-L.; Kääriäinen, T.O.; Cameron, D.C. Titanium dioxide thin films, their structure and its effect on their photoactivity and photocatalytic properties. *Thin Solid Films* **2009**, *517*, 6666–6670. [CrossRef]
11. Guillén, C.; Herrero, J. TiO₂ coatings obtained by reactive sputtering at room temperature: Physical properties as a function of the sputtering pressure and film thickness. *Thin Solid Films* **2017**, *636*, 193–199. [CrossRef]
12. Sheng, J.; Karasawa, J.; Fukami, T. Thickness dependence of photocatalytic activity of anatase film by magnetron sputtering. *J. Mater. Sci.* **1997**, *16*, 1709–1711.
13. Marcello, A.B.; Correa, V.O.; Bento, T.R.; Pillis, F.M. Effect of growth parameters on the photocatalytic performance of TiO₂ films prepared by MOCVD. *J. Braz. Chem. Soc.* **2020**, *31*, 1270–1283. [CrossRef]
14. Jung, S.; Kim, S.; Imaishi, N.; Cho, Y. Effect of TiO₂ thin film thickness and specific surface area by low-pressure metal–organic chemical vapor deposition on photocatalytic activities. *Appl. Catal. B Environ.* **2005**, *55*, 253–257. [CrossRef]
15. Yu, J.; Zhao, X.; Zhao, Q. Effect of film thickness on the grain size and photocatalytic activity of the sol-gel derived nanometer TiO₂ thin films. *J. Mater. Sci.* **2000**, *19*, 1015–1017.
16. Tada, H.; Tanaka, M. Dependence of TiO₂ photocatalytic activity upon its film thickness. *Langmuir* **1997**, *13*, 360–364. [CrossRef]
17. Wu, C.; Lee, Y.; Lo, Y.; Lin, C.; Wu, C. Thickness-dependent photocatalytic performance of nanocrystalline TiO₂ thin films prepared by sol–gel spin coating. *Appl. Surf. Sci.* **2013**, *280*, 737–744. [CrossRef]
18. Blanco, E.; Gonzalez-Leal, M.J.; Solar, R. Photocatalytic TiO₂ sol–gel thin films: Optical and morphological characterization. *Sol. Energy* **2015**, *122*, 11–23. [CrossRef]
19. Xianyu, X.W.; Park, K.M.; Lee, I.W. Thickness effect in the photocatalytic activity of TiO₂ thin films derived from sol-gel process. *Korean Chem. Eng.* **2001**, *18*, 903–907. [CrossRef]
20. Spiridonova, J.; Katerski, A.; Danilson, M.; Krichevskaya, M.; Krunk, M.; Oja Acik, I. Effect of the titanium isopropoxide: Acetylacetone molar ratio on the photocatalytic activity of TiO₂ thin films. *Molecules* **2019**, *24*, 4326. [CrossRef]
21. Perednis, D.; Gauckler, G.L. Thin film deposition using spray pyrolysis. *J. Electroceram.* **2005**, *14*, 103–111. [CrossRef]
22. Nakaruk, A.; Sorrell, C.C. Conceptual model for spray pyrolysis mechanism: Fabrication and annealing of titania thin films. *J. Coat. Technol. Res.* **2010**, *7*, 665–676. [CrossRef]

23. Oja, I.; Mere, A.; Krunk, M.; Nisuma, R.; Solterbeck, C.-H.; Es-Sounic, M. Structural and electrical characterization of TiO₂ films grown by spray pyrolysis. *Thin Solid Films* **2006**, *515*, 664–677. [[CrossRef](#)]
24. Dundar, I.; Krichevskaya, M.; Katerski, A.; Krunk, M.; Oja Acik, I. Photocatalytic degradation of different VOCs in the gas-phase over TiO₂ thin films prepared by ultrasonic spray pyrolysis. *Catalysts* **2019**, *9*, 915. [[CrossRef](#)]
25. Spalatu, N.; Hiie, J.; Kaupmees, R.; Volobujeva, O.; Krustok, J.; Oja Acik, I.; Krunk, M. Postdeposition processing of thin films and solar cells: Prospective strategy to obtain large, sintered, and doped SnS grains by recrystallization in the presence of a metal halide flux. *ACS Appl. Mater. Interfaces* **2019**, *11*, 17539–17554. [[CrossRef](#)] [[PubMed](#)]
26. Spalatu, N.; Krunk, M.; Hiie, J. Structural and optoelectronic properties of CdCl₂ activated CdTe thin films modified by multiple thermal annealing. *Thin Solid Films* **2017**, *633*, 106–111. [[CrossRef](#)]
27. Vahl, A.; Veziroglu, S.; Henkel, B.; Strunskus, T.; Polonskyi, O.; Aktas, C.O.; Faupel, F. Pathways to tailor photocatalytic performance of TiO₂ thin films deposited by reactive magnetron sputtering. *Materials* **2019**, *12*, 2840. [[CrossRef](#)] [[PubMed](#)]
28. Yazid, A.S.; Rosli, M.Z.; Juoi, M.J. Effect of titanium (IV) isopropoxide molarity on the crystallinity and photocatalytic activity of titanium dioxide thin film deposited via green sol-gel route. *J. Mater. Res. Technol.* **2019**, *8*, 1434–1439. [[CrossRef](#)]
29. Oja Acik, I.; Junolainen, A.; Mikli, V.; Danilson, M.; Krunk, M. Growth of ultra-thin TiO₂ films by spray pyrolysis on different substrates. *Appl. Surf. Sci.* **2009**, *256*, 1391–1394. [[CrossRef](#)]
30. Oja Acik, I.; Mere, A.; Krunk, M.; Solterbeck, C.H.; Es-Souini, M. Properties of TiO₂ films prepared by the spray pyrolysis method. *Solid State Phenom.* **2004**, *99*, 259–264.
31. Rauta, N.C.; Mathews, T.; Chandramohan, P.; Srinivasan, M.P.; Dasha, S.; Tyagi, A.K. Effect of temperature on the growth of TiO₂ thin films synthesized by spray pyrolysis: Structural, compositional and optical properties. *Mater. Res. Bull.* **2011**, *46*, 2057–2063. [[CrossRef](#)]
32. Deshmukh, H.P.; Shinde, P.S.; Patil, P.S. Structural, optical and electrical characterization of spray deposited TiO₂ thin films. *Mater. Sci. Eng. B* **2006**, *130*, 220–227. [[CrossRef](#)]
33. Paz, Y.; Luo, Z. Photooxidative self-cleaning transparent titanium dioxide films on glass. *J. Mater. Res.* **1995**, *10*, 2842–2848. [[CrossRef](#)]
34. Mills, A.; Lepre, A.; Elliott, N.; Bhopal, S.; Parkin, P.I.; O'Neill, S.A. Characterisation of the photocatalyst Pilkington Activ TM a reference film photocatalyst? *J. Photoch. Photobiol. A. Chem.* **2003**, *160*, 213–224. [[CrossRef](#)]
35. Smirnova, N.; Fesenko, T.; Zhukovsky, M.; Goworek, J.; Eremenko, A. Photodegradation of Stearic Acid Adsorbed on Superhydrophilic TiO₂ Surface: In Situ FTIR and LDI Study. *Nanoscale Res. Lett.* **2015**, *10*, 7. [[CrossRef](#)]
36. Kumar, J.K.; Raju, R.C.N.; Subrahmanyam, A. Thickness dependent physical and photocatalytic properties of ITO thin films prepared by reactive DC magnetron sputtering. *Appl. Surf. Sci.* **2011**, *257*, 3075–3080. [[CrossRef](#)]
37. Cedillo-Gonzalez, I.E.; Hernandez-Lopez, M.J.; Ruiz-Valdez, J.J.; Barbieri, V.; Siligardi, C. Self-cleaning TiO₂ coatings for building materials: The influence of morphology and humidity in the stain removal performance. *Constr. Build. Mater.* **2020**, *237*, 117692. [[CrossRef](#)]



Appendix 2

Table 1.1 Selected studies on photocatalytic decomposition of different VOCs on TiO₂ thin films prepared by wet-chemical methods.

Ref.	Dep. Method	Material Properties							Photocatalytic activity					
		Subs.	Specific Quantity of Material	Ti-source	D, nm	RMS, nm	MCS, nm	TT, %	Measurement Parameters				Degradation reaction rate/degraded amount	
									Pollutant	Inlet concent.	Photocat. surface area, cm ²	UV light intensity, mW cm ⁻²		RH, %
104	Sol-gel	Glass tube	NA	TTIP	200	NA	NA	NA	Acetaldehyde Toluene Acidic acid	1 µl	26	2.5	NA	1.9 µmol ⁻¹ s ⁻¹ g ⁻¹ 0.1 µmol ⁻¹ s ⁻¹ g ⁻¹
105	Sol-gel dip coating	Glass	NA	TTIP	1000	NA	NA	80	Methyl ethyl ketone	1-6 g m ⁻³	NA	NA	0%, 30%	0.006 min ⁻¹ (0%RH) 0.004 min ⁻¹ (30%)
106	Sol-gel dip coating	SLG	NA	TPOT	900-5300	NA	16	70	Acetaldehyde, Toluene	1, 3.25 ppm	50	1.0	50	80-90% removal 53-60% removal
107	Sol-gel dip coating	SLG	NA	TTIP	500-2100	NA	NA	70-80	Acetaldehyde	1350 ppm	50	1.2	NA	0.1-0.4 µmol ⁻¹ min ⁻¹ reaction rate
	Spray Pyrolysis	Quartz, SL Glass	NA	TTIP	2100	NA	NA	70-80	Acetaldehyde	1350 ppm	50	1.2	NA	33-48% conversion
108	Spray Pyrolysis	Glass	NA	Nano-X	110	NA	30	NA	Acetone	3 µl	25	2.3	25	NA
109	Sol-gel dip coating	Glass cylinder	NA	TTIP	300-2000	NA	4-35	NA	Acetone	0.017-0.02 g h ⁻¹	67.2	NA	45	67-98% conversion
110	Sol-gel dip coating	Glass cylinders	0.25 mg cm ⁻²	TTIP	NA	NA	NA	NA	Acetone, MIBK	450 ppm	NA	2.7	20	9.40x10 ⁷ mol s ⁻¹ g ⁻¹ reaction rate
111	Sol-gel reverse micellar	SLG, Al SS, quartz	NA	TTIP	NA	NA	13	NA	Acetone	400 ppm	140	0.54	80	4.4, 9.5 x10 ⁻⁴ min ⁻¹ 1.9, 2.3 x10 ⁻³ min ⁻¹
	Sol-gel dip coating	Al	NA	TTIP	NA	NA	13	NA	Acetone	400 ppm	140	0.54	80	7.8-9.5x10 ⁻⁴ min ⁻¹

Ref.	Dep. Method	Material Properties							Photocatalytic activity					
		Subs.	Specific Quantity of Material	Ti-source	D, nm	RMS, nm	MCS, nm	TT, %	Pollutant	Measurement Parameters				Degradation reaction rate/degraded amount
										Inlet concen.	Photocat. surface area, cm ²	UV light intensity, mW cm ⁻²	RH, %	
112	Sol-gel dip-coating	Glass rings	20-120 mg cm ⁻²	TTIP	130-690	NA	NA	NA	Toluene	0.01-0.5 ppm	NA	NA	0-66	60-80% conversion
113	Sol-gel dip-coating	Glass tube	NA	TTIP	1300	NA	8	NA	Toluene	0.5-8 ppm	NA	NA	NA	22-48% removal
114	Sol-gel dip-coating	Glass	NA	TTIP	200-350	NA	25	70-80	2-propanol	80 μM	19	1.3	NA	100% conversion
115	Sol-gel dip coating	Glass	3.5 mg cm ⁻²	TTIP	5500	NA	NA	NA	MTBE	500 ppm	NA	NA	NA	90% conversion
116	Sol-gel dip coating	Glass	NA	TBOT	200-250	6-9	12-14	70	Methanol	5 μl	16.8	Visible light	NA	80% conversion
117	Sol-gel	Borosilicate glass tube	NA	TTIP	NA	NA	NA	NA	Formaldehyde	100-500 ppm	60	0-1.56	NA	0.148 min ⁻¹ 0.170 min ⁻¹ reaction rate
118	Sol-gel dip coating	Stainless steel	NA	Ti(OBu) ₄	40-342	NA	6	NA	Formaldehyde	145 μmol l ⁻¹	13.75	0.113, 1.84	NA	35%, 89% conversion
119	Spray pyrolysis	Glass tube	NA	Titanyl-acetyl acetone	350	NA	35	80	Butane	3.03 mol dm ⁻³	187	1.0	NA	90% conversion
120	Spray pyrolysis	Glass fibre	NA	TTIP	NA	NA	NA	NA	Trimethyl amine, Methanethiol, Dimethyl sulfide	5 ppb	54	2.0	NA	100% conversion

Ref.	Dep. Method	Material Properties							Photocatalytic activity					
		Substrate	Specific Quantity of Material	Ti-source	D, nm	RMS, nm	MCS, nm	TT, %	Pollutant	Measurement Parameters				Degradation reaction rate/degraded amount
										Inlet concen.	Photocat. surface area, cm ²	UV light intensity, mW cm ⁻²	RH, %	
121	Sol-gel spin-coating	Glass	NA	TTIP	98, 106	0.7, 1.0	NA	80	n-hexane	50 ppm	25	7.0	NA	100% conversion
122	Sol-gel spin-coating	Silica glass	NA	TTIP	70-670	1	NA	NA	2-propanol	NA	6.25	NA	NA	33% (70 nm), 88% (670nm) conversion

Curriculum vitae

Personal data

Name: Ibrahim Dündar
Date of birth: 20.07.1988
Place of birth: Adana, Turkey
Citizenship: Turkish

Contact data

E-mail: ibrahim.dundar114@gmail.com

Experience

2016–2021 Laboratory of Thin Film Chemical Technologies, Tallinn
Early-stage University of Technology
researcher

Education

2016–2021 Tallinn University of Technology, Chemical and Materials
Technology, PhD
2014–2016 Tallinn University of Technology, Materials and Sustainable
Energetics, MSc.
2007–2012 Dumlupinar University, Ceramics Engineering, BSc
2010–2011 AGH University of Science and Technology, Materials Science
and Ceramics Engineering
2003–2007 Mehmetcik Lisesi

Language competence

Turkish Fluent
English Advance
German Beginner
Estonian Beginner

Participation in conferences

2016–2020 Graduate school “Functional materials and technologies
FMDTDK”, Tallinn University of Technology, Estonia. (Oral and
poster presentations)
2018 Solar chemistry and photocatalysis: Environmental applications
(SPEA) Meeting, Almeria, Spain (Poster presentation)
2017 European materials research society (E-MRS) Spring meeting,
Strasbourg, France (Poster presentation)
2016 Conference of young scientist on energy issues, Kaunas,
Lithuania (Oral presentation)

Defended dissertations

2016 Master`s Niobium doped titanium dioxide thin films by chemical spray
degree: pyrolysis, Supervisors: Ilona Oja Acik, Atanas Katerski

Research projects

PRG627 Antimony chalcogenide thin films for next-generation semi-transparent solar cells applicable in electricity producing windows.

TK141 Centre of Excellent: "Advanced materials and high technology devices for sustainable energetics, sensorics, and nanoelectronics".

IUT19-4 "Thin films and nanomaterials by wet chemical methods for next generation photovoltaics".

B24 "Metal oxide thin films by wet chemical methods for electronic devices".

Supervised dissertation

Zengjun Chen, Master's Degree, 2018, (sup) Ilona Oja Acik; Ibrahim Dündar, TiO₂ thin films fabricated by using ultrasonic spray pyrolysis, Tallinn University of Technology School of Engineering, Department of Materials and Environmental Technology. (Student now PhD student in Tallinn University of Technology).

List of publications

1. **Dundar, I.**; Mere, A.; Mikli, V.; Krunks, M.; Oja Acik, I. (2020). Thickness Effect on Photocatalytic Activity of TiO₂ Thin Films Fabricated by Ultrasonic Spray Pyrolysis. *Catalysts*, 10, 1058. 10.3390/catal10091058.
2. **Dundar, I.**; Krichevskaya, M.; Katerski, A.; Krunks, M.; Oja Acik, I. (2019). Photocatalytic Degradation of Different VOCs in the Gas-Phase over TiO₂ Thin Films Prepared by Ultrasonic Spray Pyrolysis, *Catalysts* 9, 915. 10.3390/catal9110915.
3. **Dundar, I.**; Krichevskaya, M.; Katerski, A.; Oja Acik, I. (2019). TiO₂ thin films by ultrasonic spray pyrolysis as photocatalytic material for air purification. *Royal Society open science*, 6, 181578. 10.1098/rsos.181578.
4. Chen, Z.; **Dundar I.**; Oja Acik I. (2019) TiO₂ thin films by ultrasonic spray pyrolysis. *IOP Conference Series: Materials Science and Engineering*, 503, 012006. 10.1088/1757-899X/503/1/012006
5. **Dundar I.**; Oja Acik I.; Mere A.; Katerski A.; Krunks M.; Mikli V. (2016). Niobium doped TiO₂ layers by chemical spray pyrolysis. *Proceedings 13th International Conference of Young Scientists on Energy Issues*, May 26-27, 2016, Kaunas, Lithuania.
6. Patent application: EE201800012A: "A method of making a transparent visual light activated photocatalytic superhydrophilic glass material", January 15, 2020.

Elulookirjeldus

Isikuandmed

Nimi: Ibrahim Dündar
Sünniaeg: 20.07.1988
Sünnikoht: Türgi
Kodakondsus: Türgi
ORCID: 0000-0002-4519-7009

Kontaktandmed

E-post: ibrahim.dundar114@gmail.com

Hariduskäik

2016–2021 Tallinna Tehnikaülikool – PhD, keemia- ja materjalitehnoloogia
2014–2016 Tallinna Tehnikaülikool – MSc, Materjalid ja protsessid
jätkusuutlikus energeetikas (Cum laude)
2007–2012 Dumlupinar University, Keraamikateadused ja tehnika, BSc
2010–2011 AGH University of Science and Technology, Materials Science
and Ceramics Engineering
2003–2007 Mehmetcik Lisesi

Keelteoskus

Türgi keel Emakeel
Inglise keel Kõrgtase
Saksa keel Algtase
Eesti keel Algtase

Osalemine teaduskonverentsidel

2016–2020 Funktsionaalsete materjalide ja tehnoloogiate doktorikool,
Tallinna Tehnikaülikool, Eesti
2018 Solar chemistry and photocatalysis: Environmental
applications (SPEA) Meeting, Almeria, Spain
2017 European materials research society (E-MRS) Spring meeting,
Strasbourg, France
2016 Conference of young scientist on energy issues, Kaunas,
Lithuania

Teaduskraadid

2016, magistrikraad, Nb-legeeritud TiO₂ õhukesed kiled pihustuspürolüüsi meetodil,
Tallinna Tehnikaülikool, juhendajad: Ilona Oja Acik; Atanas Katerski.

Teadusprojektid

PRG627 “Antimon-kalkogeniid õhukesed kiled järgmise põlvkonna pool-
läbipaistvatele päikeseelementidele kasutamiseks elektrit
tootvates akendes”.
TK141 “Tippkeskused: Uudsed materjalid ja kõrgtehnoloogilised seadmed energia
salvestamise ja muundamise süsteemidele”.
IUT19-4 “Õhukesed kiled ja nanomaterjalid keemilistel
vedeliksadestusmeetoditel uue põlvkonna fotovoltseadistele”.

B24 “Keemilistel meetoditel kasvatatud metalli oksiidide õhukesed kiled elektroonikaseadistele”.

Juhendatud väitekirjad

Zengjun Chen, Magistrikraad, 2018, (juhendajad) Ilona Oja Açık; Ibrahim Dündar, TiO₂ thin films by ultrasonic spray pyrolysis, Tallinna Tehnikaülikool, Inseneriteaduskond, Materjali- ja keskkonnatehnoloogia instituut.

Publikatsioonid

1. **Dundar, I.**; Mere, A.; Mikli, V.; Krunks, M.; Oja Acik, I. (2020). Thickness Effect on Photocatalytic Activity of TiO₂ Thin Films Fabricated by Ultrasonic Spray Pyrolysis. *Catalysts*, 10, 1058. 10.3390/catal10091058.
2. **Dundar, I.**; Krichevskaya, M.; Katerski, A.; Krunks, M.; Oja Acik, I. (2019). Photocatalytic Degradation of Different VOCs in the Gas-Phase over TiO₂ Thin Films Prepared by Ultrasonic Spray Pyrolysis, *Catalysts* 9, 915. 10.3390/catal9110915.
3. **Dundar, I.**; Krichevskaya, M.; Katerski, A.; Oja Acik, I. (2019). TiO₂ thin films by ultrasonic spray pyrolysis as photocatalytic material for air purification. *Royal Society open science*, 6, 181578. 10.1098/rsos.181578.
4. Chen, Z.; **Dundar I.**; Oja Acik I. (2019) TiO₂ thin films by ultrasonic spray pyrolysis. *IOP Conference Series: Materials Science and Engineering*, 503, 012006. 10.1088/1757-899X/503/1/012006
5. **Dundar I.**; Oja Acik I.; Mere A.; Katerski A.; Krunks M.; Mikli V. (2016). Niobium doped TiO₂ layers by chemical spray pyrolysis. *Proceedings 13th International Conference of Young Scientists on Energy Issues*, May 26-27, 2016, Kaunas, Lithuania.
6. Patent application: EE201800012A: “A method of making a transparent visual light activated photocatalytic superhydrophilic glass material”, January 15, 2020.

ISSN 2585-6901 (PDF)
ISBN 978-9949-83-675-8 (PDF)